CEA-N-2232
NEANDC-(E) 224
INDC-(FR) 51/L

- Note CEA-N-2232 -

Centre d'Etudes de Limeil

SOME ASPECTS OF NUCLEAR FISSION

par

André MICHAUDON

Invited talk given at the Neutron Interlab Seminar
Oxford - July 1-3, 1981

- Décembre 1981 -

- Note CEA-N-2232 -

Centre d'Etudes de Limeil

SOME ASPECTS OF NUCLEAR FISSION

par

André MICHAUDON

Invited talk given at the Neutron Interlab Seminar
Oxford - July 1-3, 1981

CEA-N-2232 NEANDC (E) 224 INDC (FR) 51/L - André MICHAUDON

QUELQUES ASPECTS DU PROCESSUS DE FISSION

Sommaire.- La fission est toujours activement étudiée du point de vue expérimental et théorique en vue de mieux connaître les aspects statiques et dynamiques de ce phénomène. Une bonne détermination de la barrière de fission a été obtenue en utilisant la méthode de Strutinsky. Un bon accord est maintenant atteint entre les hauteurs de barrières calculées et mesurées, sauf pour les actinides légers pour lesquels la bosse intérieure calculée est trop basse pour expliquer les résultats expérimentaux. Un examen plus approfondi des calculs et des meilleures données relatives à la fission induite par neutrons dans ^{230}Th, ^{231}Pa et ^{232}Th montre que la barrière de fission pour ^{231}Th présente trois bosses, tandis que les résultats relatifs à ^{231}Pa et ^{232}Th, quoique compatibles avec une barrière à trois bosses, n'apportent pas la preuve indiscutable de son existence. La dynamique, contrairement à la statique, est mal connue. Des résultats détaillés ont été obtenus à partir des mesures des propriétés des fragments de la fission induite par neutrons thermiques dans ^{235}U. Ces résultats peuvent être interprétés comme dus à une dissipation d'importance moyenne entre le point-selle et la scission. Cependant, d'autres résultats relatifs à la "fission froide" induite par neutrons thermiques dans ^{233}U et ^{235}U ne

./.

CEA-N-2232 NEANDC (E) 224 INDC (FR) 51/L - André MICHAUDON

SOME ASPECTS OF NUCLEAR FISSION.

Summary.-Fission is still actively studied both from the theoretical and experimental points of view in order to know better the statics and the dynamics of the process. A good knowledge of the fission barrier has been obtained by using the Strutinsky procedure. Good agreement is now reached between double-humped fission barrier heights and experiments, except for light actinides for which the calculated inner hump is too low to explain the fission data. Closer examination of the calculations together with the analysis of the best fission data for ^{230}Th, ^{231}Pa and ^{232}Th neutron-induced fission lead to the conclusion that the fission barrier for ^{231}Th is triple-humped whereas the data for ^{231}Pa and ^{232}Th, though consistent with a triple-humped barrier, do not provide indisputable evidence for its existence. The dynamics, in contrast to the statics, are poorly known. Detailed results have been obtained from the measurements of fragment properties for thermal-neutron induced fission of ^{235}U. These results can be interpreted as moderate dissipation between saddle point and scission. Yet, other recent results obtained from "cold fragmentation" in thermal-neutron induced fission in ^{233}U and ^{235}U are not consistent with this hypothesis. Rather, according to recent microscopic calculations of the potential energy surface, cold fragmentation seems to stem from a

./.

sont pas compatibles avec cette hypothèse. En fait, d'après de récents calculs microscopiques de la surface d'énergie potentielle, la fission froide semble due à un nouveau mécanisme suivant lequel le noyau fissionnant subit une soudaine transition de forme entre la vallée de fission et celle de fusion. A cet égard, la fission froide serait similaire au processus inverse de la fusion par ions lourds.

1981 81 p.

Commissariat à l'Energie Atomique - France

---

new mechanism whereby the fissioning nucleus undergoes a sudden shape transition from the fission to the fusion valley. In this respect, cold fragmentation would be similar to the inverse process for heavy-ion fusion.

1981 81 p.

Commissariat à l'Energie Atomique - France

TABLE OF CONTENTS

I - INTRODUCTION

It is customary to say that the understanding of the fission process requires two problems to be solved and only two : the statics and the dynamics of the phenomenon.

I.A - The statics consist in the determination of the potential energy of the fissioning system as a function of its shape between the initial state (which is nearly spherical) and the final state which is the scission point composed of two touching fragments. The great variety of shapes between these two extremes is defined by a set {s} of shape parameters in number n :

$$\{s\} = s_1, s_2, \ldots s_n \qquad (I.1)$$

At small deformations, the nuclear shape is fairly simple and n has a small value whereas at large deformations the shape is more complex and needs a greater number of parameters to be reproduced or another parameterization.

The potential energy V({s}) at deformation {s} can be calculated with various methods.

A method used since the very early studies of fission is called macroscopic because it assumes that the nucleus is a bulk of matter without internal structure and the calculations can be made with simple and conventional hypotheses. In this respect, the liquid drop model (LDM) which considers the nucleus as a drop of charged and incompressible matter has been used and is still used extensively. This model has been quite successful in predicting the gross properties of the fission process but failed to explain more sophisticated aspects discovered in the mid 60's such as : fission isomers, vibrational resonances, intermediate structure in subthreshold fission cross-sections, etc...

At the other extreme, the microscopic models aim at describing the detailed motion of all the nucleons in the nucleus. In the Hartree-Fock (H.F.) or Hartree-Fock Bogolyubov (H.F.B.) methods which use self-consistent fields, a very accurate and thorough picture of the nuclear properties can be obtained, in principle. These methods have made great progress recently and encouraging results have been obtained. But the quality of these results require the knowledge of a good "effective nucleon-nucleon interaction". Such an interaction cannot be derived as yet from basic principles but rather is determined phenomenologically and is tested only at small deformations. Moreover, the single-particle state basis used in the calculations needs to be large to cover the whole range of deformations and this leads to very long computer times.

An intermediate approach, called the macroscopic-microscopic method, invented by Strutinsky [Str 67] uses the macroscopic energy together with a microscopic correction. More specifically, the potential energy at deformation {s} can be written in the following form :

$$V(\{s\}) = V_M(\{s\}) + \Delta E_{sh}(\{s\}) \qquad (1.2)$$

in which $V_M(\{s\})$ is the macroscopic energy, as obtained for example with the LDM

and $\Delta E_{sh}(\{s\})$ is the "shell-energy correction" which is closely linked to the density of single-particle states at the Fermi surface.

The most interesting feature of this method is that a double-humped fission barrier is obtained for actinide nuclei when combining the single-humped shape of $V_M(\{s\})$ with the oscillatory behaviour of $\Delta E_{sh}(\{s\})$ as a function of elongation (see fig. 1). Such a barrier shape proved immediately successful in explaining several puzzling fission results, already mentioned, namely : fission isomers, vibrational resonances, intermediate structure in subthreshold fission cross-sections, etc...

The description of the fission process in terms of the double-humped fission barrier is extremely interesting and has been covered in several review papers (see for example [Bra+ 72], [Nix 72], [Mic 73]). The most recent and comprehensive paper is that by Björnholm and Lynn [BL 80].

In the present talk, I will not review the double-humped fission barrier situation since this has been done previously on several occasions. Rather, I shall focus attention on the light actinide region (Th and Pa isotopes) where the double-humped barrier fails to explain quantitatively the data. But a triple-humped barrier, already predicted by the theorists, can probably explain the results in that mass region. This aspect of fission is reviewed in chapter II.

I.B - The dynamics play also an important role in the understanding of the fission process because it describes the manner the fissioning system crosses (or passes over) the fission barrier and behaves during its descent from the saddle point down to scission. Two aspects of dynamics need to be considered :

- the mass inertia parameter $B(\{s\})$ which probably varies with deformation. This variation of $B(\{s\})$ brings about a change in the fission path which would be obtained with a constant B value.

- viscosity or dissipation. This aspect controls the coupling of the collective degrees of freedom in the fission mode to the other degrees of freedom. If the coupling is weak, then there is no transfer of kinetic energy to excitation energy of the fissioning system and the system is said to be fluid. If, on the contrary, the coupling is strong, then there is some kinetic energy converted into excitation energy and the system is said to be viscous. Models have been invented to treat such cases. The adiabatic model, for example, assumes that there is no kinetic energy transfer into excitation and therefore that all the available energy at scission appears as pre-scission kinetic energy. At the other extreme, the statistical model assumed that the energy at scission is shared among all degrees of freedom, whether collective or intrinsic, according to the laws of thermal equilibrium. Intermediate models are also used (see Section III.A).

Very little is known about dissipation though this nuclear process is studied through both heavy-ion and fission reactions. A review of the whole subject would be by far beyond the scope of this talk. Rather, in chapter III, I shall present some recent results about ^{234}U and ^{236}U "cold fragmentation" which may shed some light to the motion between the saddle-point and scission and which may be explained thanks to a new fission mechanism.

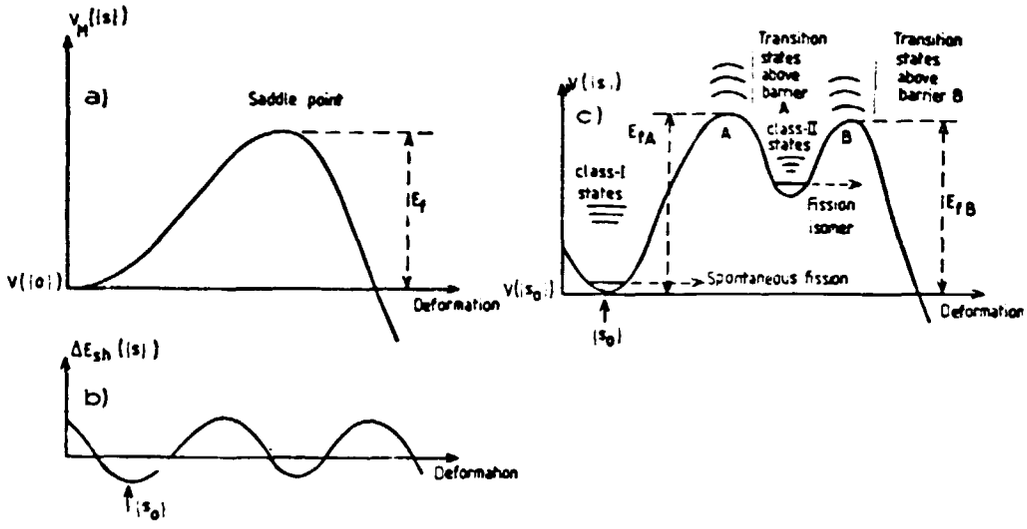

Figure 1

Illustration, in the one-dimensional representation, of the results obtained with the macroscopic-microscopic method for the calculation of the fission barrier for a typical actinide nucleus

a) Macroscopic energy $V_M(\{s\})$

b) Shell-energy correction $\Delta E_{sh}(\{s\})$

c) Double-hump fission barrier obtained when combining the macroscopic energy with the shell-energy correction.

In b) and c) the ground-state deformation $\{s_0\}$ is indicated by a vertical arrow.

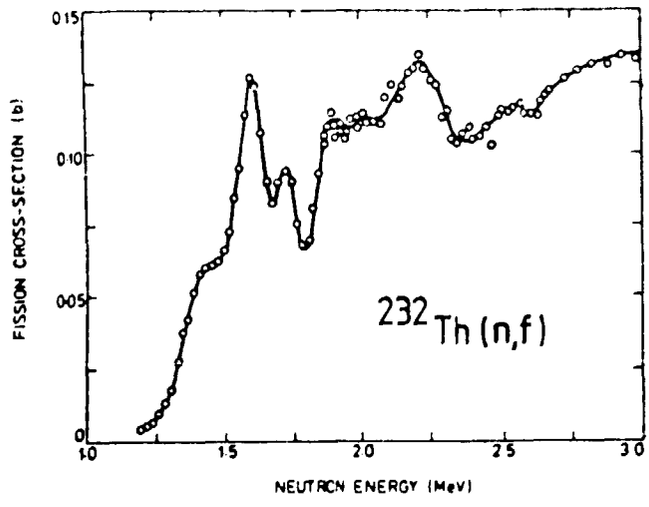

Figure 2

Neutron-induced fission cross-section for ^{232}Th [HS 55].

II - POSSIBLE EXISTENCE OF A THIRD WELL IN THE FISSION BARRIER.

II.A - History and general background.

The important success of the double-humped fission barrier in explaining many different fission data is now well established. Quantitative analysis of these data gives consistent fission barrier parameters for most of actinide nuclei. Yet, there is a range of nuclei for which agreement has not been reached between calculations and experiments. This discrepancy occurs for light actinides, such as thorium isotopes for which the calculated inner hump of the fission barrier is too low to explain the data. This disagreement persists even if various kinds of realistic models are used to calculate the barrier. This is the so-called "thorium anomaly" which is discussed in this chapter. Since the fission data considered in this respect are the vibrational resonances, they are briefly discussed below (see also [Mic 78]).

It has been known for a long time, that the fission mode was not completely damped in neutron-induced fission. For example, structure in the near-threshold fission cross-section appeared in measurements as early as 1955 for ^{232}Th [HS 55] (see fig. 2) and 1965 for ^{230}Th [EJ 65] (see fig. 3). This structure consists in one peak, as in σ_{nf} for ^{230}Th, or several peaks, as in σ_{nf} for ^{232}Th. These peaks cannot be explained by conventional models, for example by assuming rapid changes in the number of neutron inelastic and fission exit channels. On the other hand, it is a well-known fact that vibrational levels are fully damped at the excitation energies (in the compound nuclei), roughly equal to 6 MeV, corresponding to the occurence of structure in the cross-section. Therefore, these levels cannot cause any structure in the cross-sections.

The advent of the double-humped fission barrier provided a straight forward explanation of this phenomenon in terms of vibrational levels in the second well of this barrier. Such states are called class-II states as compared to class-I states in the first well. For a given total energy of the nuclear system, less excitation energy is available for class-II states than for class-I states. If the second well is shallow, the damping of the vibrational class-II states is weak and the width of these states is small. As a consequence, the fission probability presents a sharp peak in the vicinity of the vibrational state, and this peak shows up in the fission cross-section in the form of a resonance called "vibrational resonance" (fig. 4).

Quantitative analysis of the observed vibrational resonances can be made and reasonably good fits to the data can be obtained. As an illustration, fig. 5 shows the experimental data measured by James et al. [JLE 72]. Various fits to these data using different sets of model parameters are displayed in fig. 6.

It must be noted that these fits take into account, not only the class-II level responsible for the "vibrational resonance", but also the associated sequence of rotational levels. The energy sequence E_{JK} of such a rotational set of levels is given by the following formula :

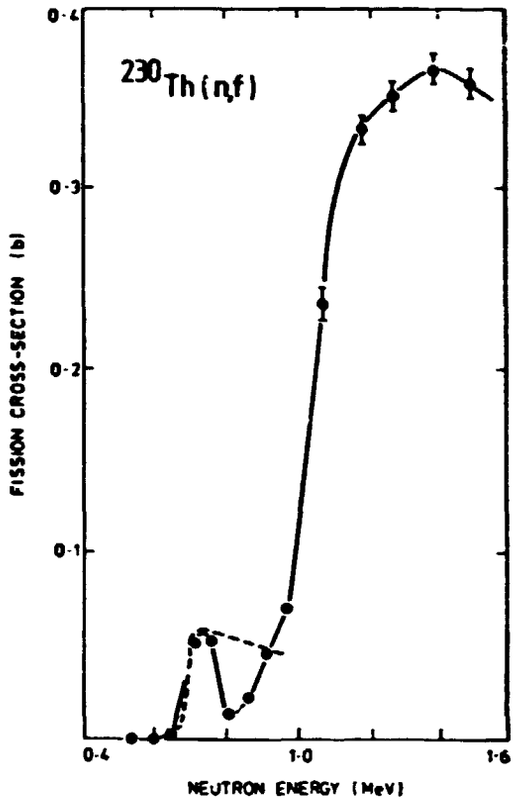

Figure 3 : Neutron-induced fission cross-section for ^{230}Th (Black dots are experimental data points [EJ 65]. Solid and dashed curves are calculations assuming one single-hump barrier [BL 80]).

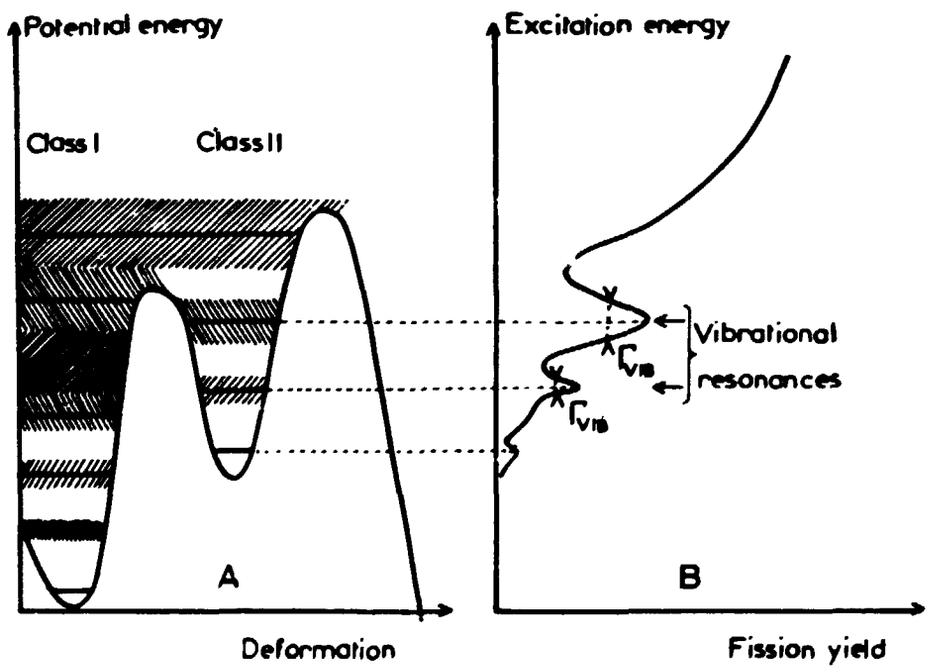

Figure 4 : Mechanism for the occurrence of big peaks called "vibrational resonances" in near-threshold fission cross-sections. On the left (fig. A) class-I and class-II vibrational states are shown as horizontal lines ; the damping of these states (hatched areas) increases with excitation energy. On the right (fig. B), resonances appear in the fission yield (or cross-section) as an effect of these vibrational states.

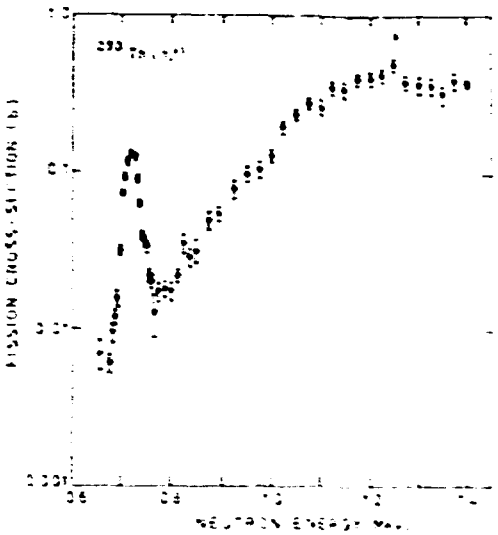

Figure 5 : Neutron-induced fission cross-section for ^{230}Th (JLE 72).

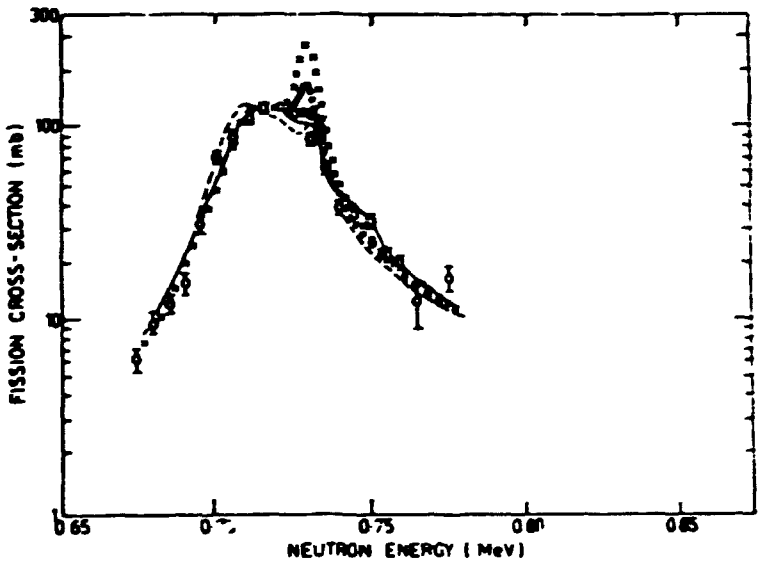

Figure 6 : Vibrational resonance around 715 keV in the neutron-induced fission cross-section for ^{230}Th. The experimental points (open circles) are those of fig. 5. The curves (—— and ---) as well as the other points (x.. and .) are various fits to the data (JLE 72).

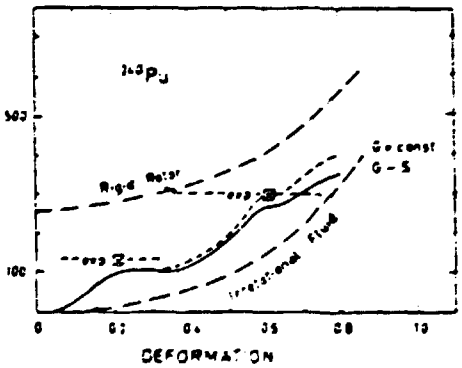

Figure 7 : Comparison of theoretical and experimental values (x) of the moment of inertia for ^{240}Pu as a function of deformation. The two experimental points are for the ^{240}Pu ground and isomeric states (SBP 73). (The ordinate gives the value of $\frac{2\mathcal{J}}{\hbar^2}$ in MeV^{-1})

$$E_{JK} = E_K^0 + \frac{\hbar^2}{2\mathcal{J}}\left[J(J+1) - K(K+1) + \delta_{K,1/2}\ a_{1/2}(-)^{J+1/2}(J+\frac{1}{2})\right] \qquad \text{(II.1)}$$

in which J is the spin of the rotational level

K is the spin projection number of the vibrational level

$\mathcal{J}$ is the moment of inertia of the nuclear system

and $a_{1/2}$ is the decoupling parameter which plays a role for K = 1/2 levels only.

In the case of the 715 keV peak for ^{230}Th, measurement of the angular distribution of the fission fragments across the peak clearly indicates forward peaking, which is evidence for the presence of K = 1/2 components (see fig. 14). Among the parameters needed to fit the data, $\mathcal{J}$ and $a_{1/2}$ are of special interest for the determination of the properties of the class-II states. Good fits to the data are obtained with

$$1.8 \text{ keV} < \frac{\hbar^2}{2\mathcal{J}} < 2.7 \text{ keV}$$

$$-2.3 < a_{1/2} < -2.0 \qquad \text{(II.2)}$$

The inertia parameter $\hbar^2/2\mathcal{J}$ thus obtained can be compared to the value $\hbar^2/2\mathcal{J} \approx 6$ keV for the ground state, as deduced from the energies of the low-energy sequence of rotational levels for ^{231}Th. The states responsible for the ^{230}Th vibrational resonance around 715 keV neutron energy have therefore a moment of inertia more than twice the value for the ground state.

There is no precise relation between the deformation and the moment of inertia of a nucleus. Inertia increases with deformation but in a way which depends on the model used in the calculation, as illustrated in fig. 7. It is clear however that the states causing the vibrational resonance have a deformation greater than that of the ground state, in qualitative agreement with the double-hump barrier hypothesis.

Similar considerations hold for the ^{240}Pu fission isomer which has a value of $\hbar^2/2\mathcal{J}$ equal to 3.343 keV as compared to 7.156 keV for the ground state.

But this interpretation, to be correct, implies that both barriers are high enough for the vibrational level to have a small total width. This is in contradiction with all calculations which show that the inner barrier is below the neutron separation energy, therefore preventing a vibrational resonance to exist at 715 keV incident neutron energy. This is one example of the "Thorium anomaly" mentioned earlier.

A possible explanation for this anomaly gradually came out from progress made both in calculations and experiments.

More complete calculations of the fission barrier, in the region of the second saddle-point, were carried out by Möller and Nix [MN 74] taking into account mass-asymmetry deformations. The calculated results showed that, for light actinides, the second saddle point becomes more elongated and the potential energy surface presents a shallow depression, like a lake (fig. 8).

Measurements of the ^{232}Th fission cross-section carried out with a better resolution in the region of the vibrational resonances discovered earlier (fig. 2), revealed the presence of a fine structure composed of sharp peaks in each big vibrational resonance [BMP 75] (fig. 9). Preliminary analysis of the positions of these sharp peaks was consistent with sequences of rotational levels and with an inertia parameter equal to 2.46 keV and 2.73 keV for the two vibrational resonances at 1.5 and 1.6 MeV. It must be noticed that the interpretation of the energy spacings between the sharp peaks, in terms of rotational levels, was easier for ^{232}Th (as compared to ^{230}Th) because the analysed ^{232}Th vibrational resonances have K = 3/2 (instead of K = 1/2 for ^{230}Th) thus eliminating the decoupling parameter $a_{1/2}$.

It is interesting to remark that the value of the inertia parameter deduced from the analysis of the fine structure for ^{232}Th is within the range of values needed to fit the Th^{230} data, confirming that the moment of inertia of the vibrational resonances for Th isotopes is, not only much greater than that for the ground state but also above the values obtained for some U and Pu fission isomers. (Table 1).

These results obtained from both calculations and experiments suggest a more refined mechanism, illustrated in fig. 10, for the interpretation of the known Thorium vibrational resonances. The excitation energy in the compound nucleus (≈ 6 MeV) corresponding to the observation of vibrational resonances, is above the inner barrier where the class-I and class-II states are completely mixed and cannot be distinguished one from another. Moreover, the vibrational states at this energy (whether class-I or class-II) are fully damped and therefore cannot, as such, cause any structure in the data. But the vibrational resonances may be caused by levels in the third well (called class-III states) with a fine structure coming from the associated sequence of rotational levels.

It must be remembered that the class-I compound nucleus states, as observed in the low-energy neutron resonances, cannot be seen in the data at about 1 MeV neutron energy because, independently of their overlap, their spacing is several orders of magnitude smaller than the width of the resolution function.

These ^{232}Th results stimulated a renewed interest in the vibrational resonances in fission cross-sections of light actinides, in order to find indisputable evidence for the existence of a third well in the fission barrier and for the fission mechanism proposed above. Much progress has been made since then in obtaining more accurate data and in having a clearer understanding of the mechanism which appears more complicated than was first anticipated (see for example [Pay 80]).

In the following part of this presentation, the above fission mechanism is described in more detail with its implications for the data obtained for ^{230}Th, ^{232}Th and also ^{231}Pa.

II.B - Consequences for the fission process of a third well in the fission barrier.

Examination of the potential energy surface (fig. 8) shows that it is symmetric with respect to the s_3 degree of freedom. Therefore, there are in fact two third wells with minima of the potential energy surface at (s_2^0, s_3^0) and $(s_2^0, -s_3^0)$ and with symmetric properties relative to s_3 (fig. 11). Coupling through the barrier between these two wells modifies the properties of their vibrational levels. For each wave function $\psi_0(s_3)$ (with eigenvalue E_0) in either well, considered separately,

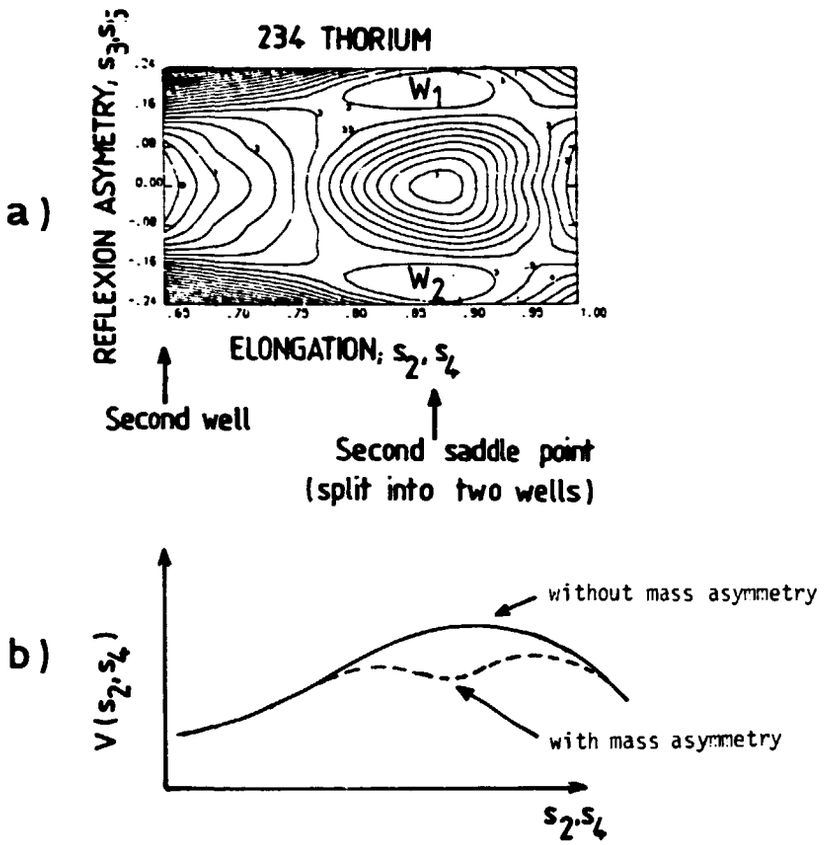

Figure 8

a) Contour plot of the potential energy surface for ^{234}Th in the region of the second saddle point. The inclusion of reflection asymmetry causes two wells W1 and W2 to appear in this surface.

b) Fission barrier in the region of the second saddle-point without mass asymmetry (solid curve) and with mass asymmetry (dashed curve).

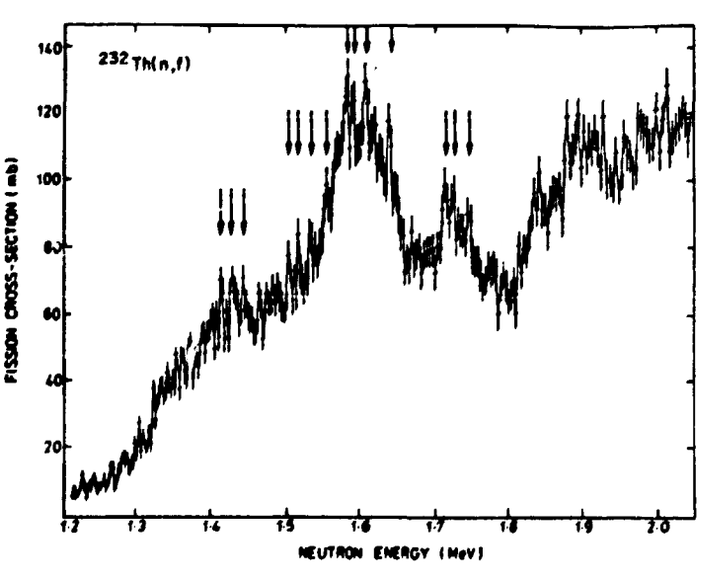

Figure 9 : First evidence of fine structure superimposed on the gross structure in the ^{232}Th fission cross-section. Arrows indicate the presence of some of the sharp peaks of this fine structure |BMP 75|.

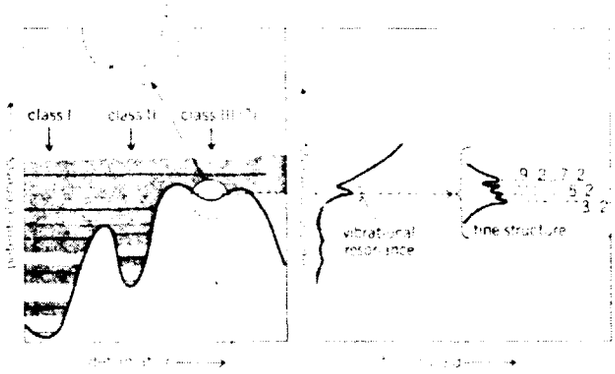

Figure 10 : A possible explanation of the thorium anomaly in terms of third well in the fission barrier. The mechanism is illustrated for a $K^{\pi} = 3/2^{-}$ rotational band, as measured in the broad peaks at 1.5 and 1.6 MeV incident neutron energy for the ^{232}Th fission cross-section. In the case of two "third wells", the mechanism is more complicated, as explained in the text.

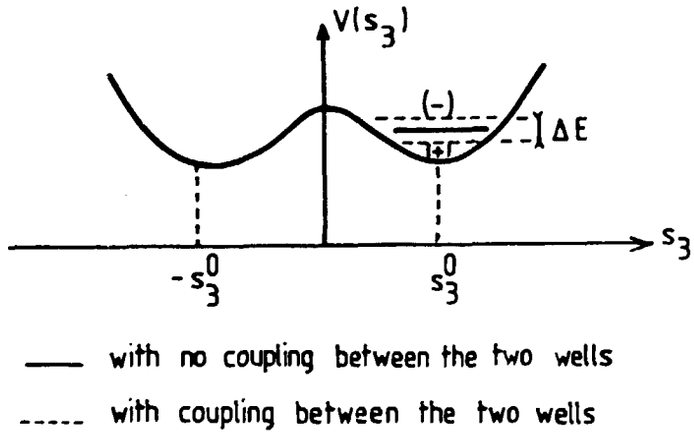

Figure 11 : Cut of the potential energy surface along the s_3 (mass asymmetry) shape parameter. Two minima appear at s_3^0 and $-s_3^0$. Degeneracy of a vibrational level (solid line) is lifted (dashed lines) if coupling between the two wells is taken into account.

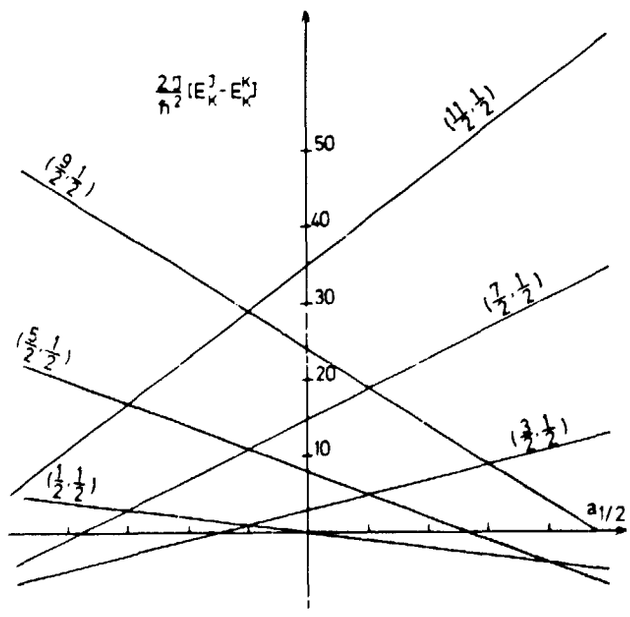

Figure 12 : Energies of rotational levels having K = 1/2 as a function of the decoupling parameter $a_{1/2}$. Levels are labelled according to their (J,K) value.

this coupling leads to a pair of wave-functions φ_0^+ and φ_0^- (with opposite parities and eigenvalues E_0^+ and E_0^- respectively). From text books, we can find the following expressions :

$$\varphi_0^+ = \frac{1}{\sqrt{2}}\left[\varphi_0(s_3) + \varphi_0(-s_3)\right]$$
$$\varphi_0^- = \frac{1}{\sqrt{2}}\left[\varphi_0(s_3) - \varphi_0(-s_3)\right] \qquad \text{(II.3)}$$

$$\text{and } \Delta E = E_0^- - E_0^+ = C \exp\left| -\frac{1}{\hbar}\int_{-s_3^0}^{+s_3^0} \sqrt{2\mu(V(s_3) - E_0)}\, ds_3 \right| \qquad \text{(II.4)}$$

where $V(s_3)$ is the potential energy across the barrier, along the s_3 degree of freedom.

The parities of the wave functions φ_0^+ and φ_0^- against s_3 inversion apply in the same manner to space reflection.

Therefore, for interpreting the fine structure data in the vibrational resonances, one has to consider not one but <u>two sequences of rotational levels of opposite parities</u> and with bandheads separated by an energy ΔE. In fact, detection of sharp peaks corresponding to these two sequences is evidence that the process is cause by two "third wells" in the fission barrier. This criterion obviously was not considered in earlier analyses of the data.

The relative positions of the rotational levels having the same (J,K) quantum numbers but opposite parities greatly depend on whether the K quantum number is equal to or different from 1/2.

For K > 1/2, one parity sequence is approximately shifted, as a whole, by ΔE compared to the other parity sequence. This is because $a_{1/2} = a_{-1/2} = 0$ and ΔE is supposed to be spin independent.

For K < 1/2, the situation is more complicated because the decoupling parameters $a_{1/2}$ and $a_{-1/2}$ need to be taken into account. As may be seen from expression (II.1) and fig. 12, the influence of $a_{1/2}$ (or $a_{-1/2}$) can, not only modify the regularity of the rotational pattern as a function of J (for small values of $a_{1/2}$), but also lead to level inversion (for large values $a_{1/2}$).

Though the two values $a_{1/2}$ and $a_{-1/2}$ were considered as independent parameters in some early analyses, it was soon realized that, according to basic considerations, one has :

$$a_{1/2} = -a_{-1/2} \qquad \text{(II.5)}$$

This simple relation has the advantage of reducing by one the number of adjustable parameters in fitting the data but, on the other hand, if the value of $|a_{1/2}|$ is large, then one can have different spin inversion in the two parity sequences as is illustrated in fig. 13.

Evidence for the existence of a third well requires a very good resolution to identify all (or most of) the levels of these <u>two</u> rotational sequences.

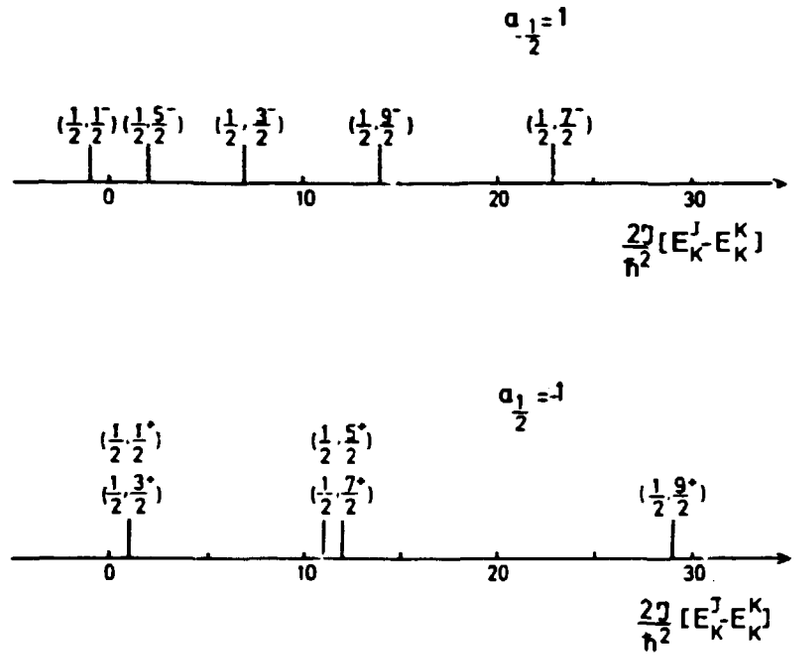

Figure 13 : Sequences of K = 1/2 rotational levels for both negative and positive parities and for $a_{-1,2} = -a_{1,2} = 1$, as deduced from fig. 12.

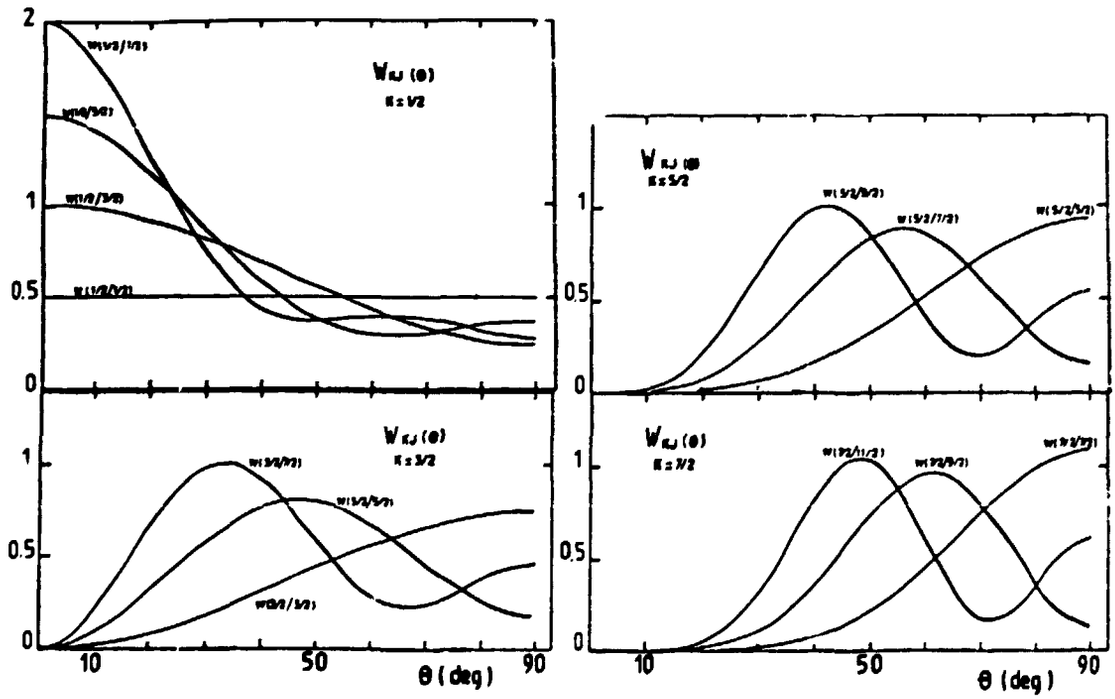

Figure 14 : Angular distribution $W_{KJ}(\theta)$ of fission fragments for states having various (K, J) values, as calculated using formula II.16 in the text.

In addition to these high resolution measurements, the direct spin (and possibly parity) determination of the sharp peaks would be very valuable. This would help removing the ambiguities associated with an analysis based solely on energy spacings.

Spin determination is made through angular distribution $W(\theta)$ of the fission fragments assuming conservation of the K-quantum number from saddle point to scission. One obtains for a spin I = 0 target nucleus

$$W(\theta) = \sum_{JK\pi} \sigma_{nf}(JK\pi)\, W_K^J(\theta)$$

$$W_K^J(\theta) = \frac{2J+1}{4} \left[|d^J_{1/2K}(\theta)|^2 + |d^J_{-1/2K}(\theta)|^2 \right] \qquad \text{(II.6)}$$

$$\text{with } \int_0^\pi W_K^J(\theta) \sin\theta \, d\theta = 1$$

where $\sigma_{nf}(JK\pi)$ is the partial fission cross-section for quantum numbers $JK\pi$.

$W_K^J(\theta)$ is the angular distribution of the fission products, for the channel having quantum numbers JK, at angle θ relative to the incident neutron beam.

and $d_{\frac{1}{2}K}(\theta)$ is the reduced wave function for a symmetric top

The expressions for the fission fragment angular distributions in the case of non-zero target nuclei are more complicated and are discussed for the specific case of Pa^{231} in Section II.D.

It can be noted that $W_K^J(\theta)$ is parity independent for spin-0 target nuclei. Parity may play a role for the overall angular distribution through the parity dependence of σ_{nf}, if several fission channels are involved.

Graphs of $W_K^J(\theta)$ as a function of θ are displayed in fig. 14 for various sets of KJ values. The angular distribution is of course symmetric relative to $\theta = 90°$.

Forward peaking is predicted for K = 1/2 and J > 1/2, and is more pronounced for larger J-values. Sideways peaking is obtained for the K > 1/2 values, and is more pronounced for larger K-values. Therefore, a K = 1/2 component can be easily identified through a crude anisotropy measurement. But the determination of the J-values for a set of levels having the same K quantum number (whether K is equal to or different from 1/2), is much more difficult because the differences in W_K^J are much smaller and can be detected only through very precise measurements.

The techniques used for measurement of the angular distributions depend on whether the neutron source delivers monoenergetic neutrons or bursts of neutrons with a wide spectrum used in conjunction with the time-of-flight method.

- With monoenergetic neutrons, the fission fragments can be detected with a plastic foil (Makrofol) placed around the sample and using well-known etching techniques. Though the solid angle covered by the plastic detectors is relatively large, there is nevertheless a loss of fission fragments in the detection system compared to fission cross-section measurements. Also, since the peaks are very sharp, it is very difficult to set the incident neutron energy exactly on each peak.

- With time-of-flight techniques, the detection of fission fragments cannot be made with plastic foils. The angle of fission fragment emission can be selected either with grid ionisation chambers in which fission fragments are counted when they are emitted at angles between 0 and θ_M (the maximum angle determined by the geometry of the chamber) or with solid-state detectors set at chosen angle θ.

In both cases, there is a loss of count rate and, to compensate for this, measurements must be made with poorer resolution. By time of flight, it is relatively easy to identify the peaks and the fission yields in each peak for angles $0 < \theta < \theta_M$, in contrast to measurements made with monoenergetic neutrons.

Both techniques have been widely used and are discussed for ^{230}Th, ^{231}Pa and ^{232}Th in Sections II.C, II.D and II.E respectively.

If measurements of fission cross-sections and angular distributions were both carried out with sufficient precision to resolve the sharp peaks, then these data could be analysed independently one from each other because apart from a background cross-section the fission contribution in each peak would come from one single state having well-defined $J^{\pi}K$ quantum numbers. But this is not the case and, especially in the angular distribution data, contribution from several states are found in the data points. Therefore, to be meaningful, <u>the analysis must be made simultaneously on both types of data (fission cross-section and angular distribution)</u>.

II.C - <u>The (^{230}Th+n) system</u>.

This nucleus is certainly the best studied case for finding evidence of the existence of "third wells" in the fission barrier, because :

i) it is a spin-zero target nucleus and, therefore, the expressions for angular distributions are relatively simple.

ii) it presents, as already discussed, a well separated vibrational resonance at 715 keV with a peak cross-section of about 100 mb.

iii) Forward peaking of the fission fragments across this resonance clearly indicates that K = 1/2. Despite the additional complexity brought about by the decoupling parameter, this K-value is an advantage for the identification of two rotational bands of opposite parities. (See Section II.B).

iv) The energy of this vibrational resonance is lower than for ^{232}Th. Therefore, fine structure components can be better separated, especially by time of flight since it is well known that

resolution improves with decreasing energy. Also, at lower energy, the analysis of the data is rendered easier because fewer values of the orbital angular momentum contribute to the cross-section, as an effect of the centrifugal barrier.

The renewed interest in the (^{230}Th+n) system stimulated not only new and more accurate measurements but also closer examination of old data which had been overlooked. This was the case for the Los Alamos results measured with a nuclear detonation as a pulsed neutron source, using the time of flight method [MV 71]. These data recorded on film reveal in fact "wiggles" across the 715 keV peak for fission fragments detected at 100° and 125° relative to the incident neutron beam [Mic 78].

These results have recently been reported on several occasions and an updated version [VM 81] is given in fig. 15. Fine structure components are clearly present in both data sets with an amplitude exceeding the statistical uncertainty estimated to ± 5 % at the maximum of the cross-section (a systematic error of ± 20 % which was combined with the statistical uncertainty in earlier analyses plays in fact a different role and must be treated separately).

Unfortunately, this experiment was aimed at the measurement of the cross-section only with minimisation of possible anisotropy effects. This is the reason why the fragment detection angles were chosen close to 90° where the differences in the various $W^J_{1/2}$ contributions are small (see fig. 14). Nevertheless, this measurement presents the advantage of data measured at two different angles with a very good energy resolution because of the very high neutron intensity of a nuclear detonation. Therefore, the ratio $\sigma_{nf}(100°)/\sigma_{nf}(125°)$ (plotted in fig. 15) is of great value for interpreting the data.

In order to confirm these old results, several measurements of both σ_{nf} and $W(\theta)$ were made which are summarized in Table II.

Using the Geel linac as a pulsed neutron source, Blons et al [Blo+ 78a] carried out an angle-integrated fission cross-section measurement, using a gas scintillator as a fission detector, with a resolution of 1.7 keV. These results were obtained with a resolution comparable to that of L.A.N.L. but with a better statistical accuracy, and they clearly confirm the presence of a fine structure. (See fig. 16).

Despite the difficulties encountered in this type of measurements, fission cross-section data were also obtained with a good energy resolution (2.5 keV) using monoenergetic neutron beams [Bru 80] but the resolution is still too broad to clearly resolve the fine structure (fig. 17).

However, the use of monoenergetic neutron proves superior for measurements of angular distributions. Two data sets are of very good quality :

i) using the Makrofol technique, the Bordeaux team was able to obtain data with an energy resolution of 2.5 keV, as for the fission cross-section measurement [Bru 80] (fig. 18).

The anisotropy thus measured can be compared to previous data obtained with the same technique by Yuen et al. [Yue+ 71] with a resolution of ± 5 keV and James et al. [JLE 72] with a resolution of 10 keV to 20 keV (fig. 19).

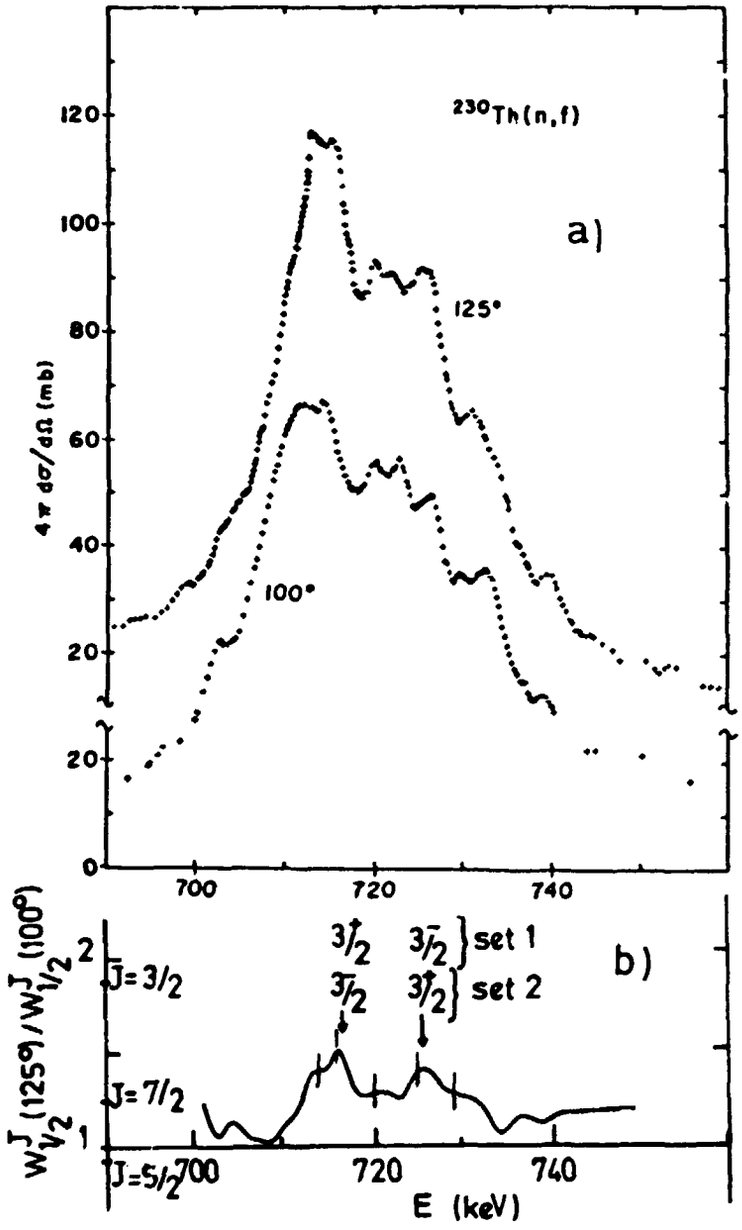

Figure 15

a) Neutron-induced fission cross-sections for ^{230}Th and for fragments emitted at $\theta = 100°$ and $\theta = 125°$ [VM 81].

b) Ratio of the above cross-sections. The calculated values of this ratio for states having different J values (but K = 1/2) are indicated on the abscissa.

The sets 1 and 2 are discussed in the text.

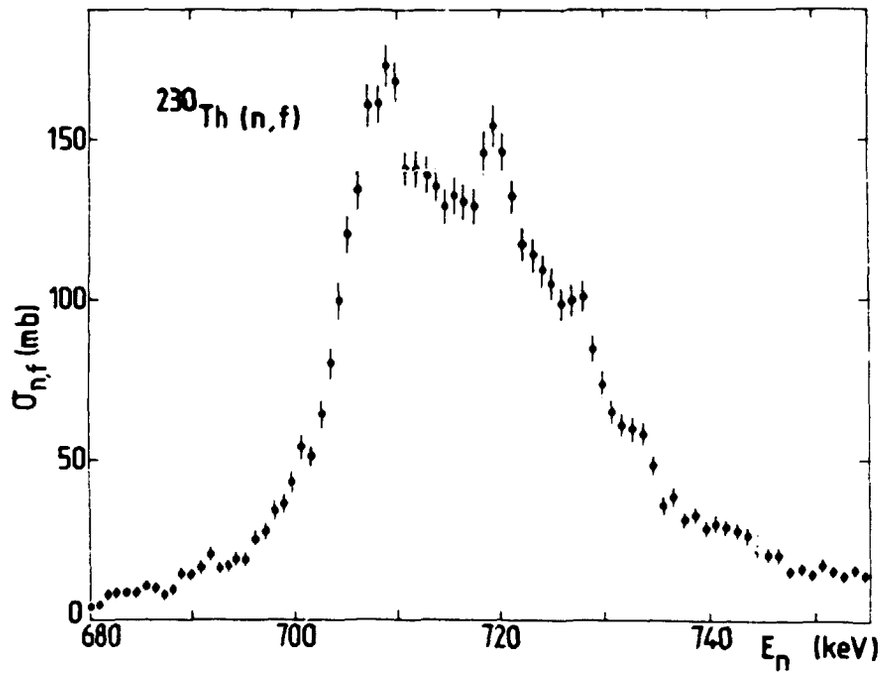

Figure 16

Neutron-induced fission cross-section for ^{230}Th measured by time of flight with a resolution of about 1.7 keV (FWHM) [Blo+ 78a].

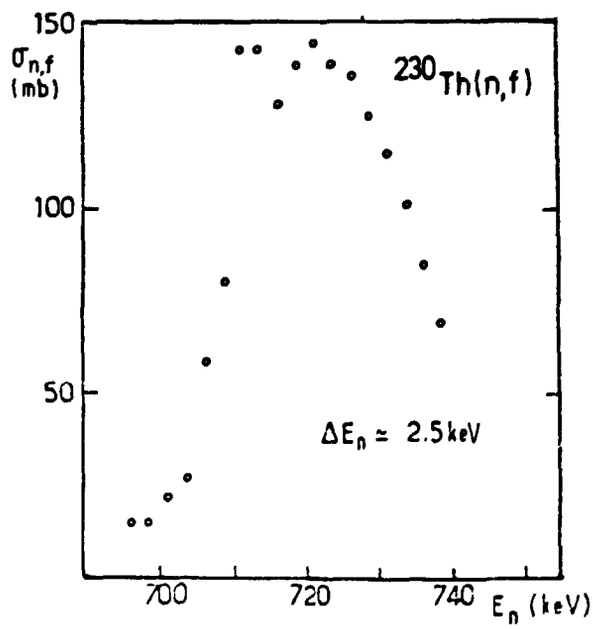

Figure 17 : Neutron-induced fission cross-section for ^{230}Th, measured with monoenergetic neutrons and a resolution of 2.5 keV (FWHM) [Bru 80].

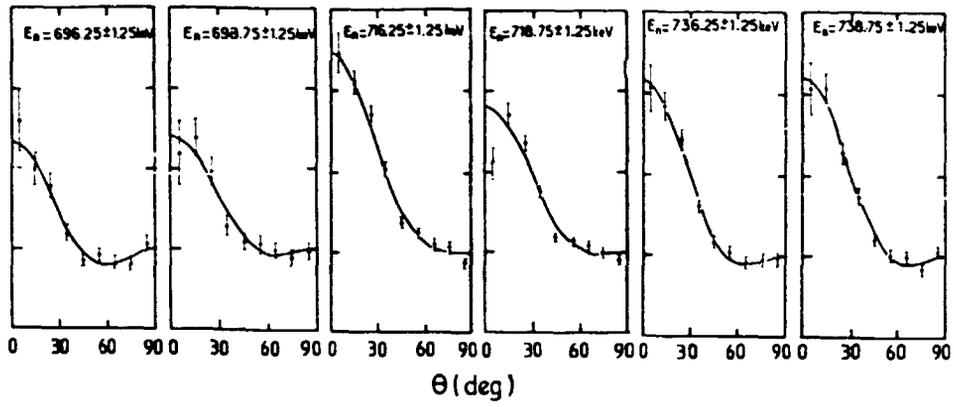

Figure 18

Angular distribution of fission fragments emitted in the neutron-induced fission of ^{230}Th at various incident neutron energies [Bru 80].

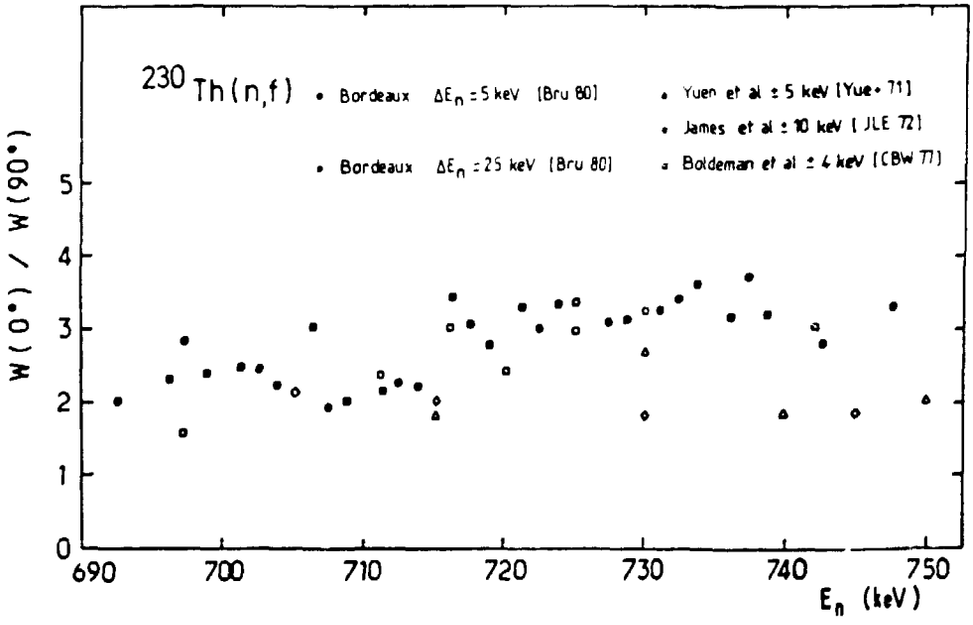

Figure 19

Comparison of various data for the anisotropy of fission fragments emitted in the neutron-induced fission for ^{230}Th [Bru 80].

ii) Solid-state detectors were used by Caruana et al. to measure the angular distribution at 6 fixed angles with a resolution of ± 4 keV [CBW 77] (See fig. 19).

A summary of these experimental data is given in Table II.

The validity of the theory can be verified by fitting simultaneously both fission cross-section and anisotropy data. Several attempts have been made with various hypotheses and are reviewed in what follows. These hypotheses fall into two categories :

i) one rotational band only having a well-defined parity (this is consistent with a second well in the fission barrier) (See II.C.1).

ii) two rotational bands of opposite parities and having two opposite values of the decoupling parameter ($a_{1/2} = - a_{-1/2}$) (This is consistent with two "third wells" in the fission barrier). (See II.C.2).

II.C.1 - <u>One single-parity rotational band hypothesis</u>.

The old data measured by James et al. could be fitted with one parity sequence of levels only [JLE 72] as already noticed. But it is not possible to fit the more accurate data with one single band of rotational levels (having either $K = 1/2^+$ or $K = 1/2^-$). Attempts made with this hypothesis are reviewed below :

$K = 1/2^+$ (fig. 20) and $K = 1/2^-$ (fig. 21) in [Bru 80]

$K = 1/2^+$ (fig. 22) and $K = 1/2^-$ (fig. 23) in [Blo+ 80]

$K = 1/2^+$ (fig. 24) in [Bol+ 81]

The parameters used in these calculations are given in Table III. The $K = 1/2^-$ option (used previously by the Harwell Group [JLE 72]) was ignored in [Bol+ 81] as unable to give a good fit to the new data sets.

In fact, as can be verified in fig. 20 through 24, none of the calculations can satisfactorily fit the data though various parameter sets were used (see Table III). Therefore, one can conclude that the data are not in agreement with one-single-parity-band in the second well of the barrier and that two-parity bands must be considered.

II.C.2 - <u>Two-parity rotational band hypothesis</u>.

The number of parameters is the same as in the one-parity sequence since $a_{1/2} = - a_{-1/2}$, as noted above.

Several attempts to fit the same data were also made by the same groups (calculations made with independent $a_{1/2}$ and $a_{-1/2}$ parameters are not considered here).

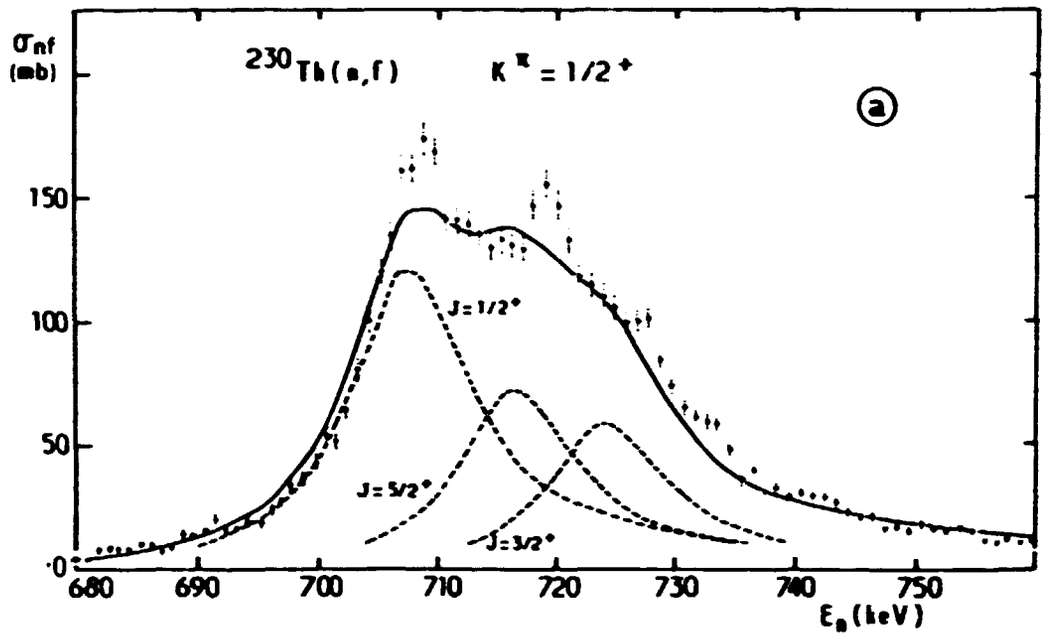

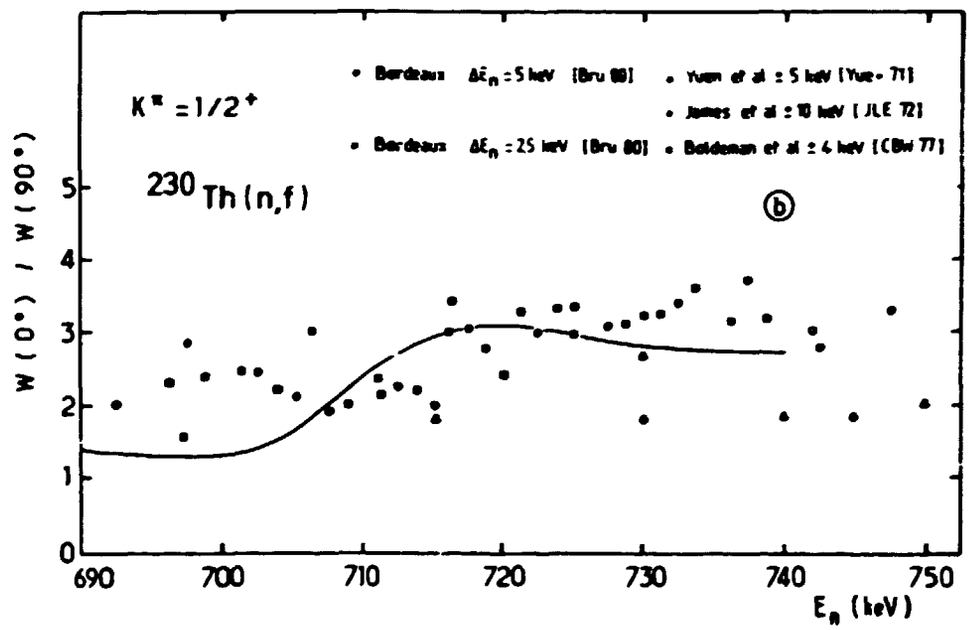

Figure 20

Attempt to fit simultaneously both the cross-section (a) and the fission fragment anisotropy (b) for ^{230}Th neutron-induced fission, assuming one single vibrational level ($K^{\pi} = 1/2^{+}$) with its associated rotational band [Bru 80].

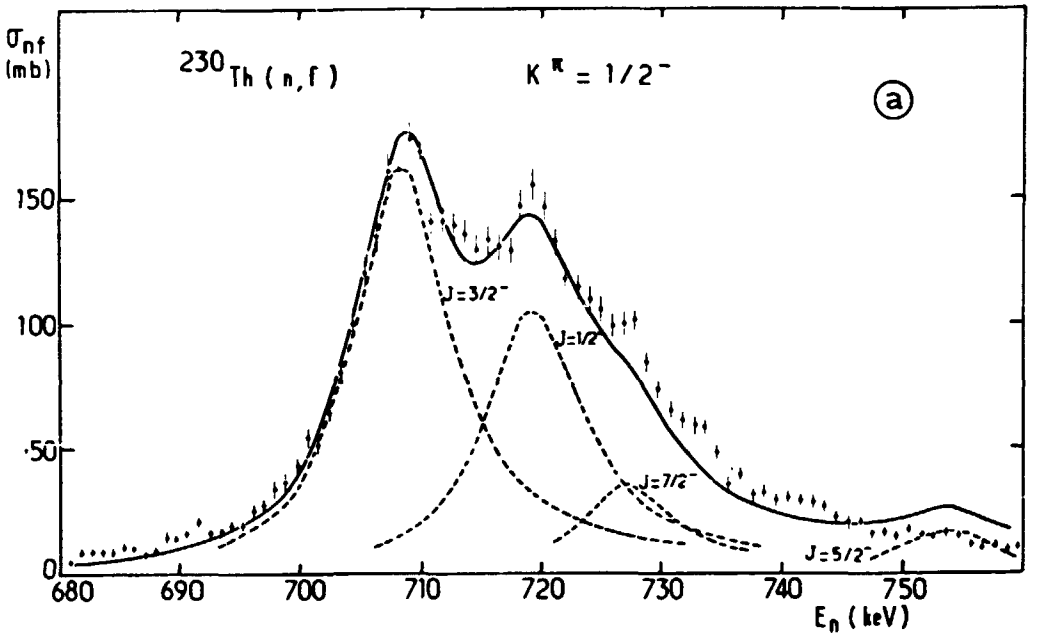

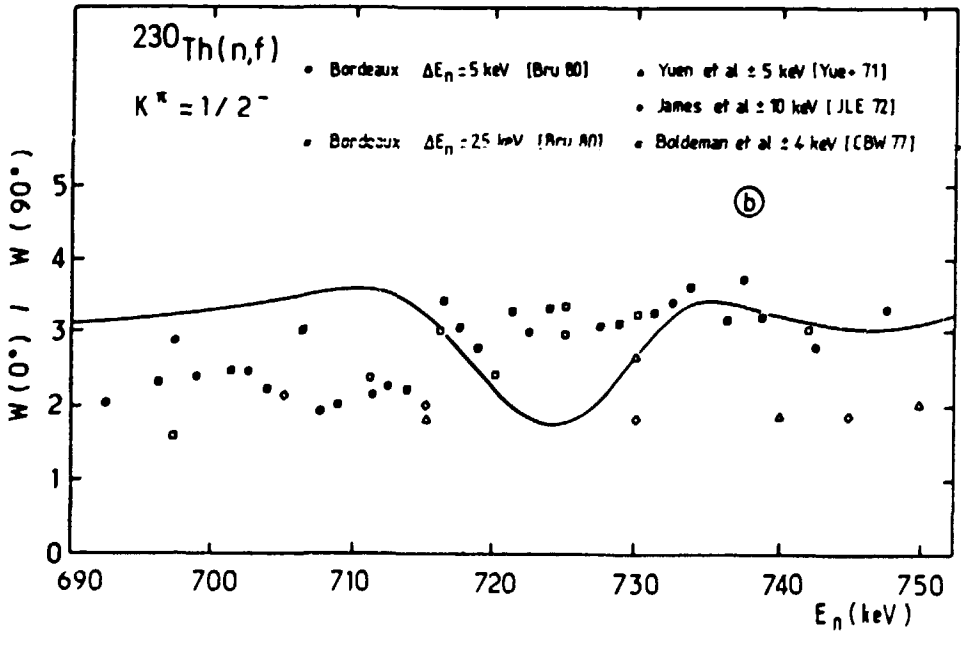

Figure 21

Same attempt as in fig. 20 but with $K^{\pi} = 1/2^{-}$ [Bru 80].

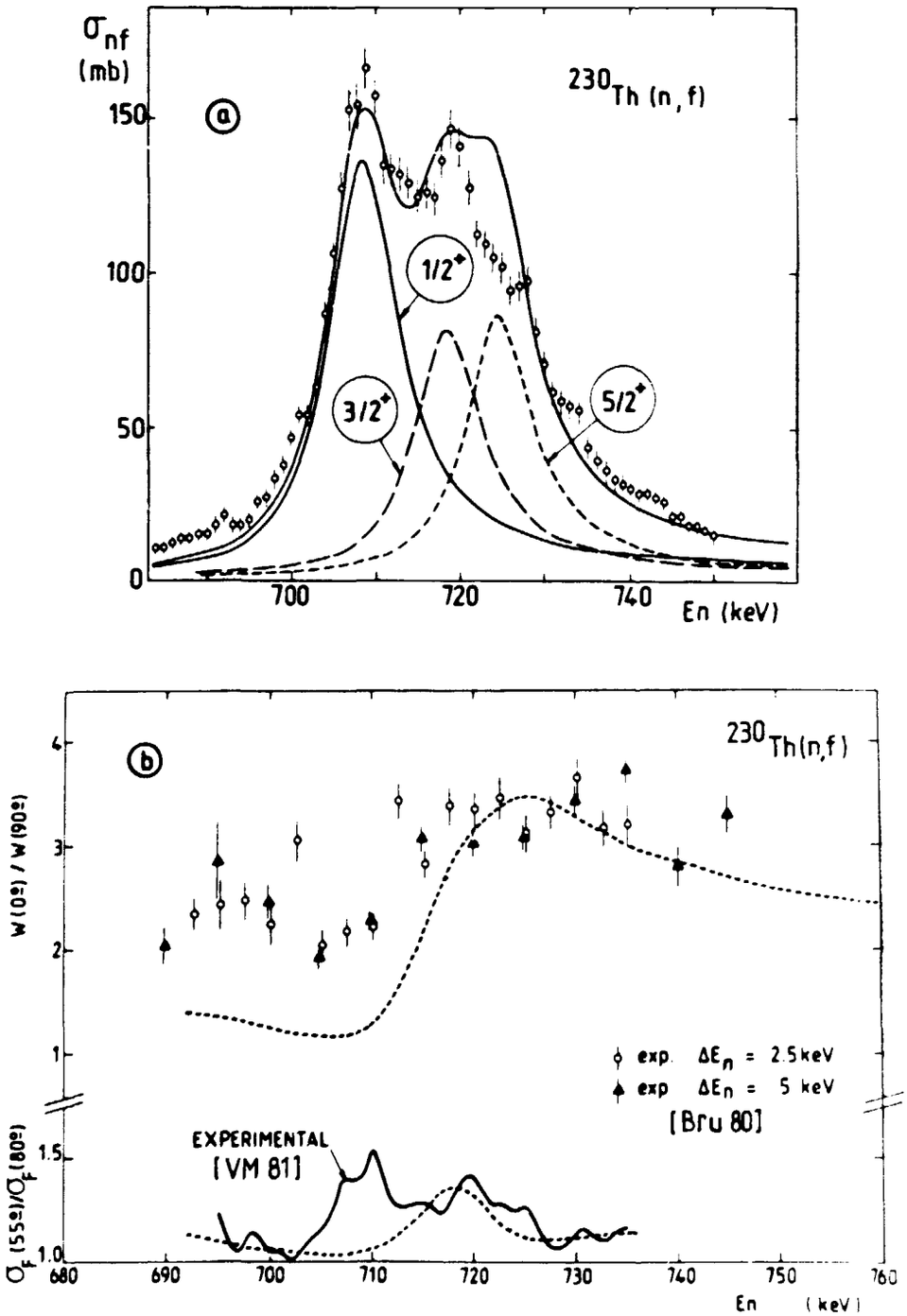

Figure 22

Same attempt as in fig. 20, with $K^{\pi} = 1/2^{+}$, as described in [Blo+ 80]

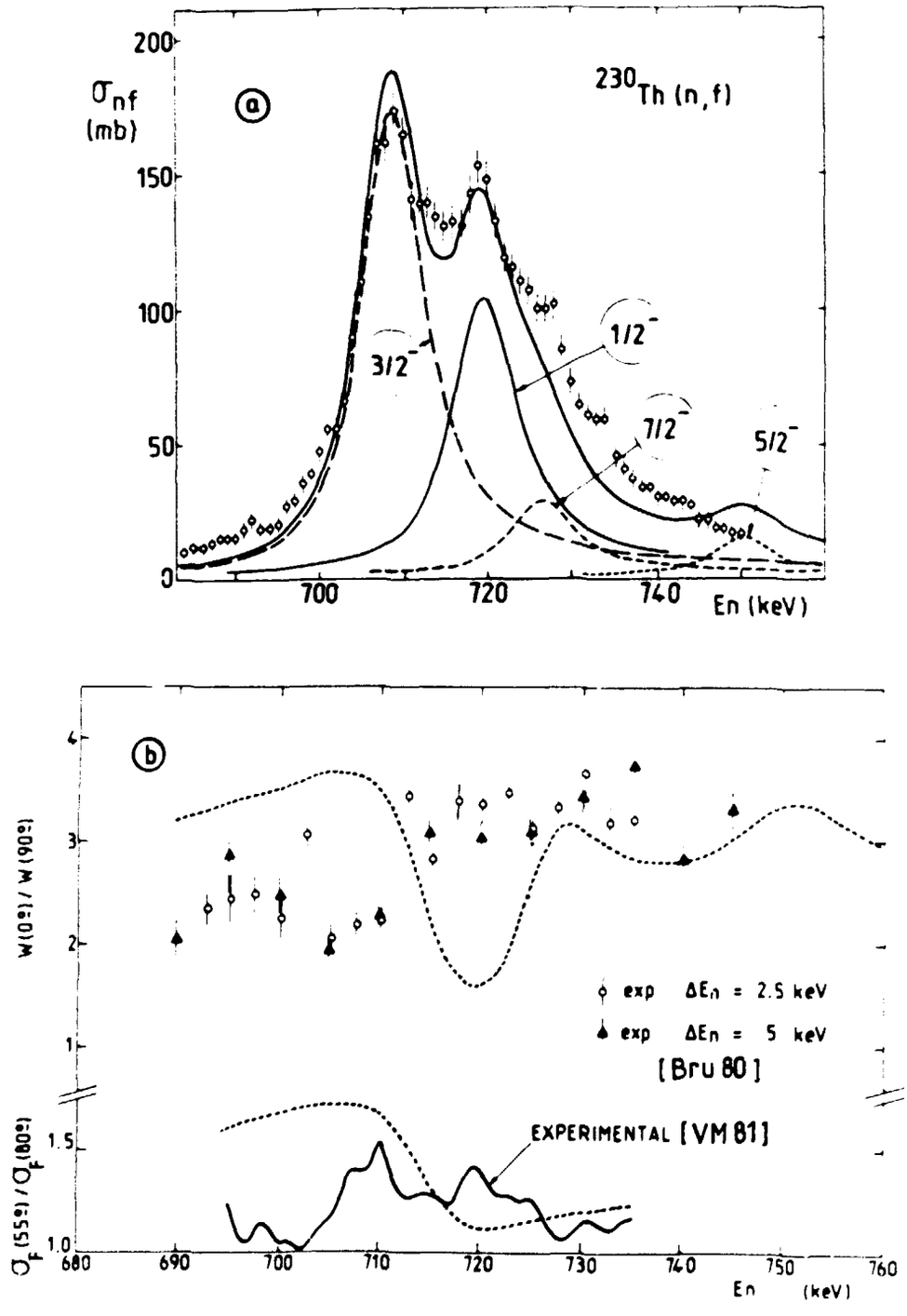

Figure 23

Same attempt as in fig. 22 but with $K^{\pi} = 1/2^{-}$ [Blo+ 80].

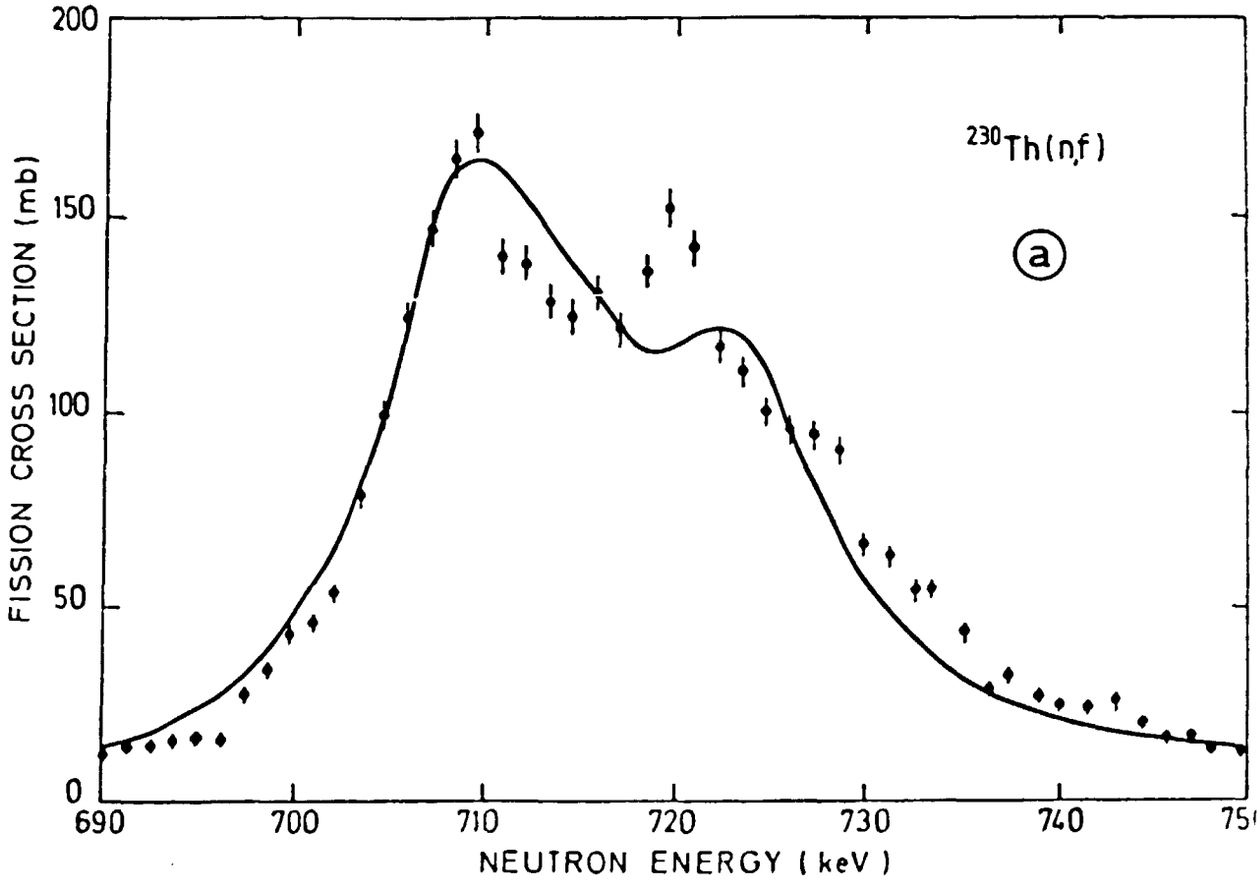

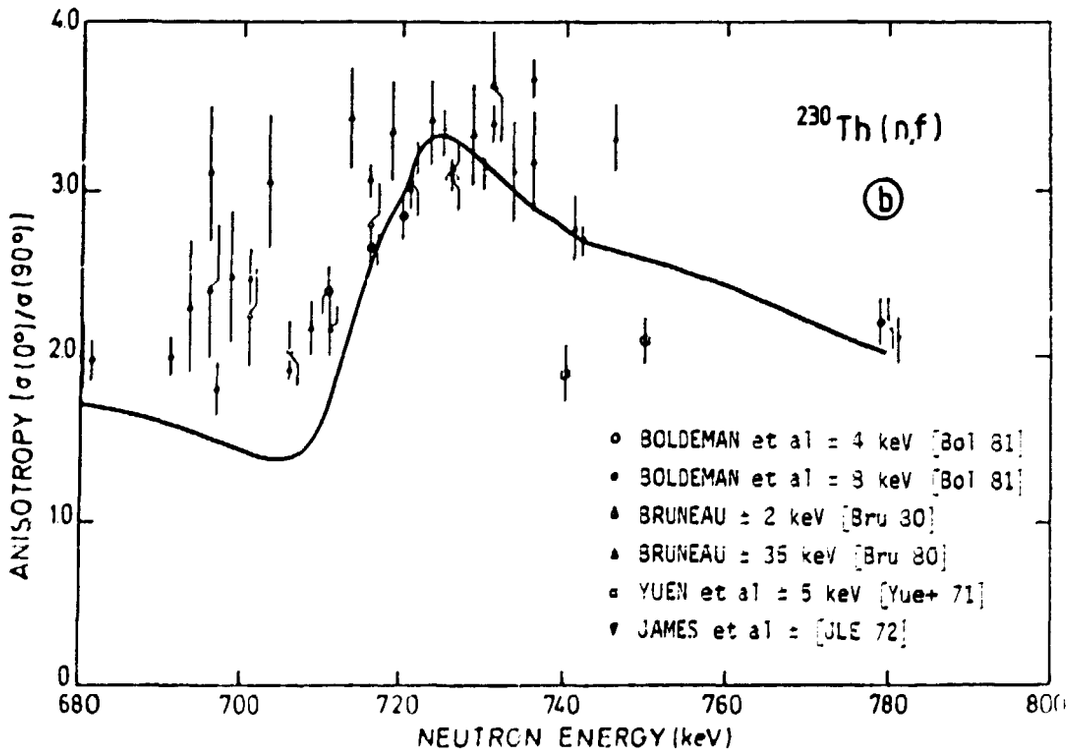

Figure 24

Same attempt as in fig. 20, with $K^{\pi} = 1/2^{+}$, as described in [Bol+ 81]

The results of the best fits obtained are given in :

Fig. 25 from [Bru 80]

Fig. 26 from [Blo+ 80] (version B)

Fig. 27 from [Bol+ 81]

Fig. 28 from [Blo 81] (version C)

The main parameters used in these fits are given in Table IV.

The clue to the understanding of the determination of these parameters is given by examining the LANL $\sigma_{nf}(125°)/\sigma_{nf}(100°)$ data plotted in fig. 15. These data present two peaks around 716 keV and 725 keV which can be reached only by J = 3/2 states. The exact predicted value is not obtained in the experiments probably because of resolution effects. Therefore, two main parameter sets can be considered depending on the parity assignments for the two postulated J = 3/2 states :

Set 1 : $3/2^+$ state at 716 keV and $3/2^-$ state at 725 keV

Set 2 : $3/2^-$ state at 716 keV and $3/2^+$ state at 725 keV

All the fits made using the two-parity band hypothesis belong to one or the other of these two sets, as given below :

Set 1 : [Bru 80], [Blo+ 80] version B, [Bol+ 81],

Set 2 : [Blo 81] version C.

Therefore, it is natural that all the fits of set 1 have very close parameters. The difference in the parity assignments for the two J = 3/2 levels is compensated by different $a_{1/2}$ and ΔE values. It is interesting to remark that whatever the parameter set is, the inertia parameter remains close to 2 keV, probably because it is mainly determined by the overall width of the vibrational resonance.

The comparison between these two parameter sets is given in fig. 28 where the fits of J. Blons, versions B and C, are plotted. One can see that set 2 gives a slightly better fit to the cross-section. But, what is still more in favor of set 2, is the fit to the anisotropy data. The calculated W(0°)/W(90°) and especially $\sigma_{nf}(125°)/\sigma_{nf}(100°)$ values are much more in agreement with the measurements than those calculated with set 1. Therefore, good agreement is obtained with the version C of [Blo 81] which is preferred to the other option.

In conclusion, one can say that the ^{230}Th vibrational resonance at 715 keV provides a good evidence for the existence of a triple-humped barrier in ^{231}Th because the data cannot be reproduced by a one-parity sequence of rotational levels (typical of a second well) but need two sequences of rotational levels to be explained, in accord with the third well hypothesis. Also the inertia parameter obtained from the fits is about 2 keV, far below the ~ 3.3 keV value corresponding to measured U and Pu fission isomers. This, in itself, implies that the vibrational levels responsible for the 715 keV resonance have a deformation substantially greater than that of the second well where the fission isomers take place, hence giving additional weight to the third well hypothesis.

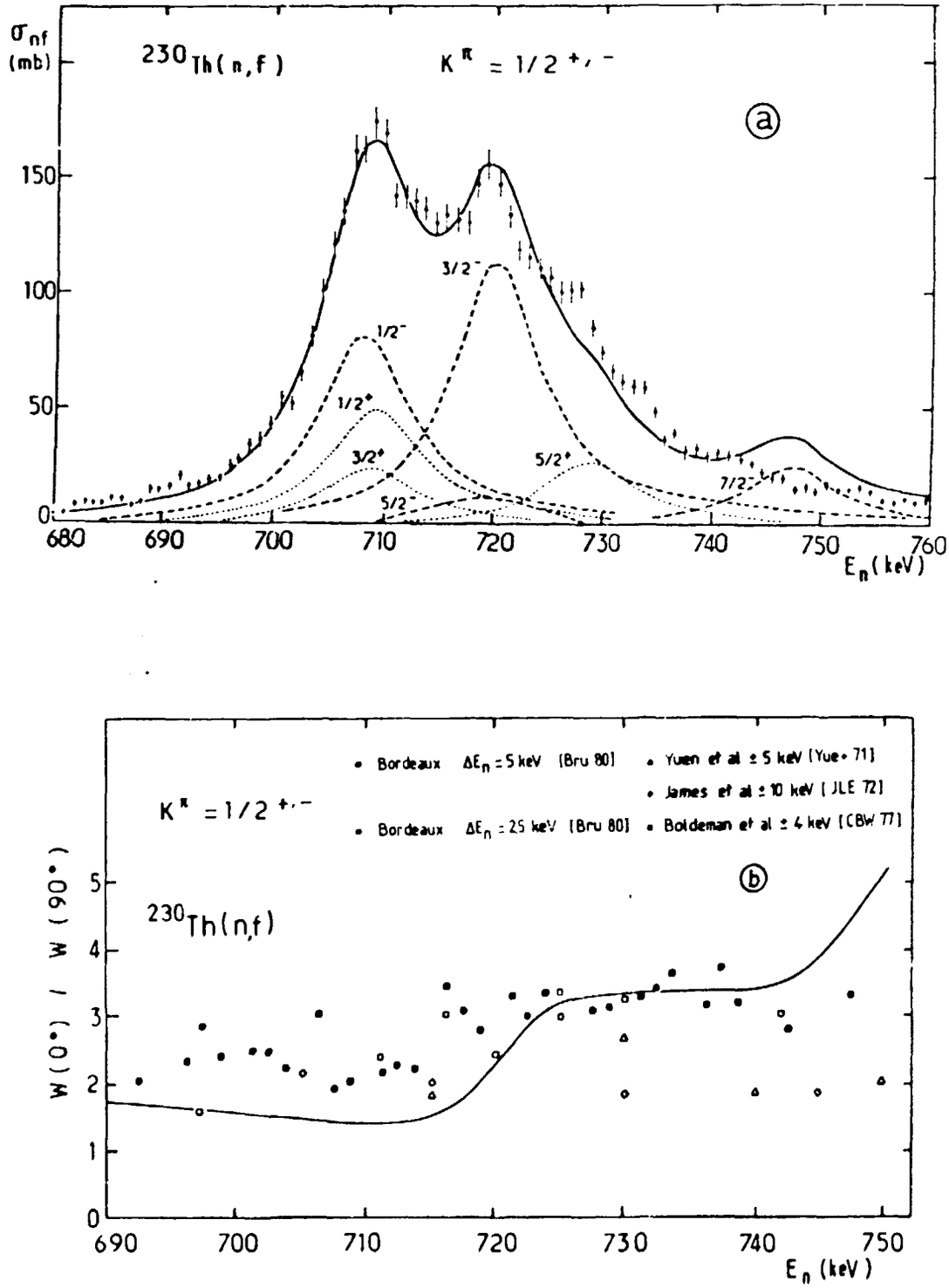

Figure 25

Attempt to fit simultaneously both the cross-section (a) and the fission fragment angular distribution (b) for ^{230}Th neutron-induced fission, assuming two-parity sequences of rotational levels (K^{π} = $1/2^+$ and $1/2^-$) [Bru 80]. For further details, see text and Table IV.

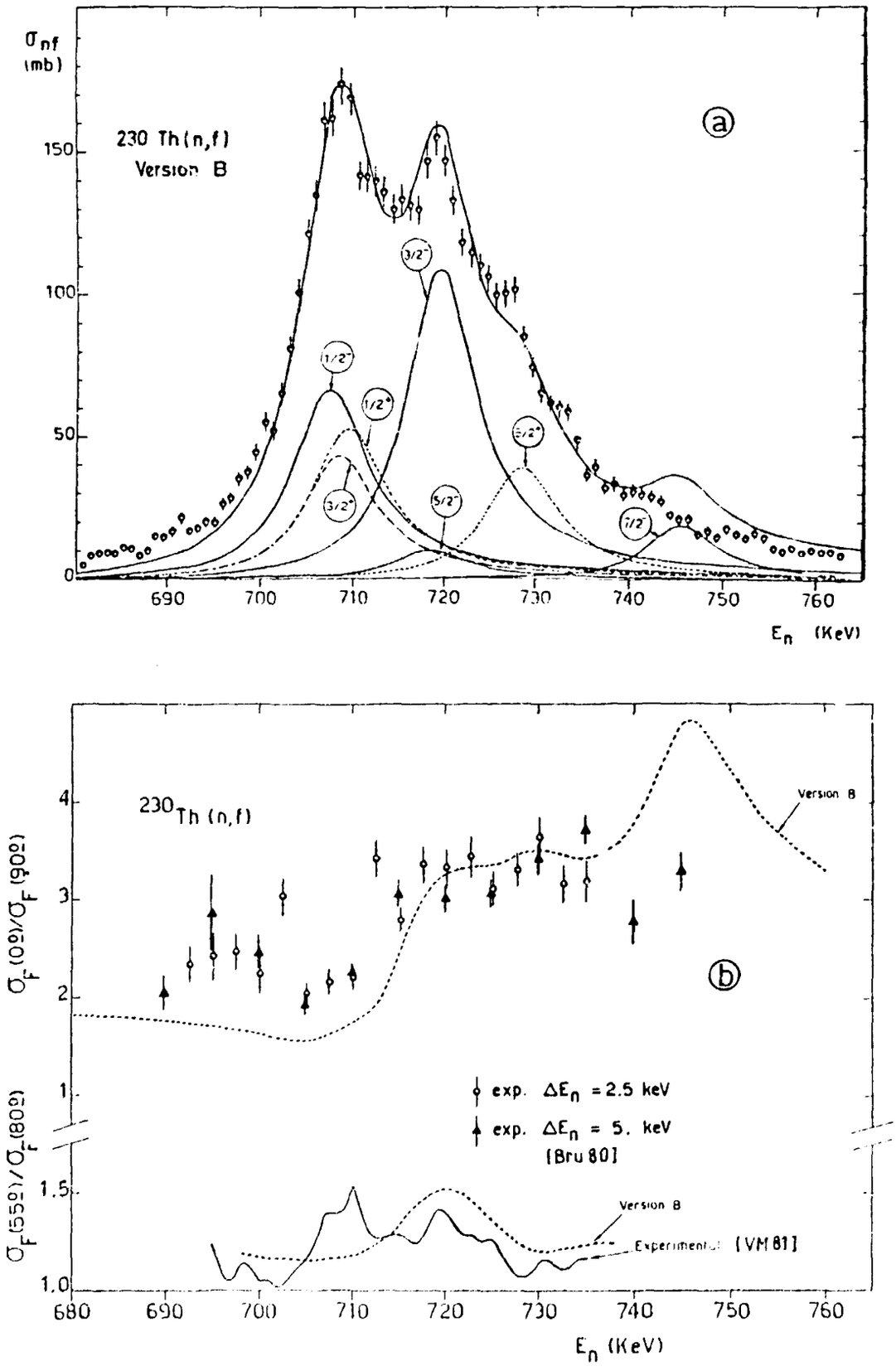

Figure 26

Same as in fig. 25 but the fit is from [Blo+ 80] (version B). For further details, see text and Table IV.

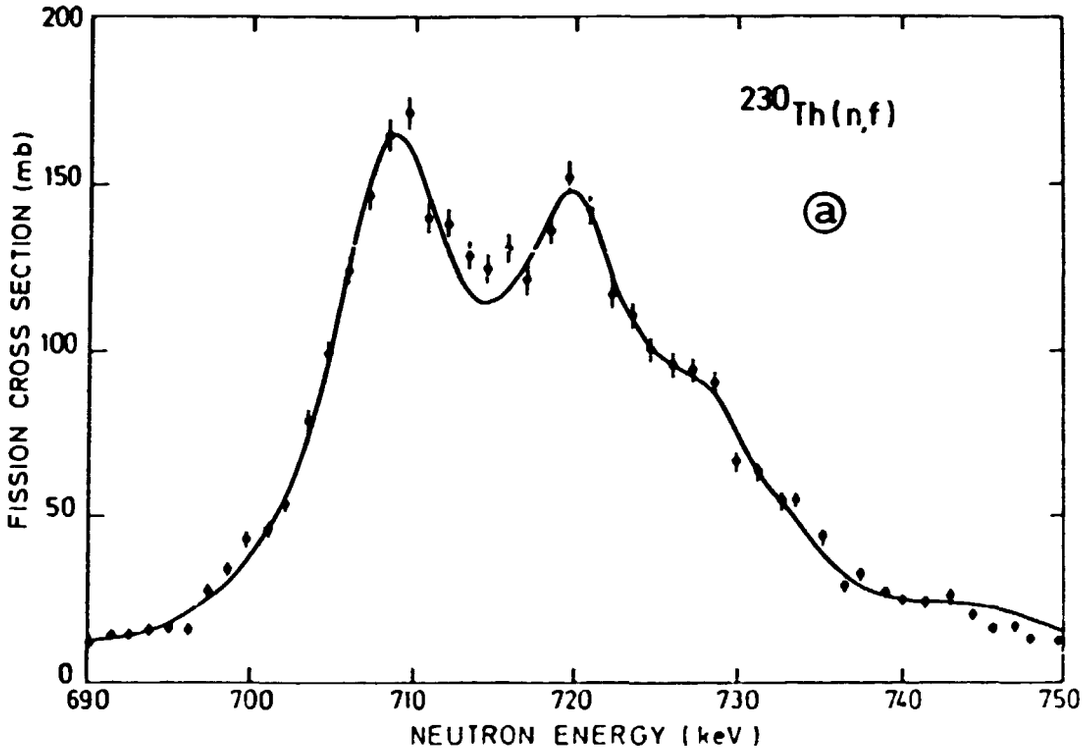

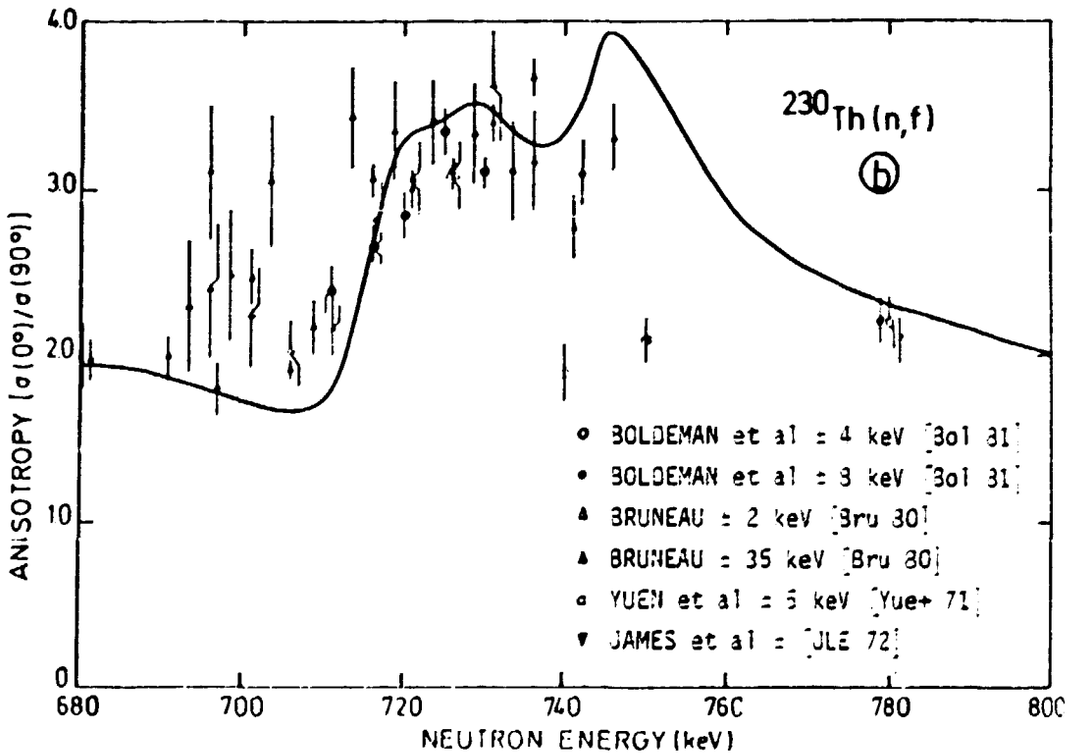

Figure 27

Same as in fig. 25 but the fit is from [Bol+ 81]. For further details, see text and Table IV.

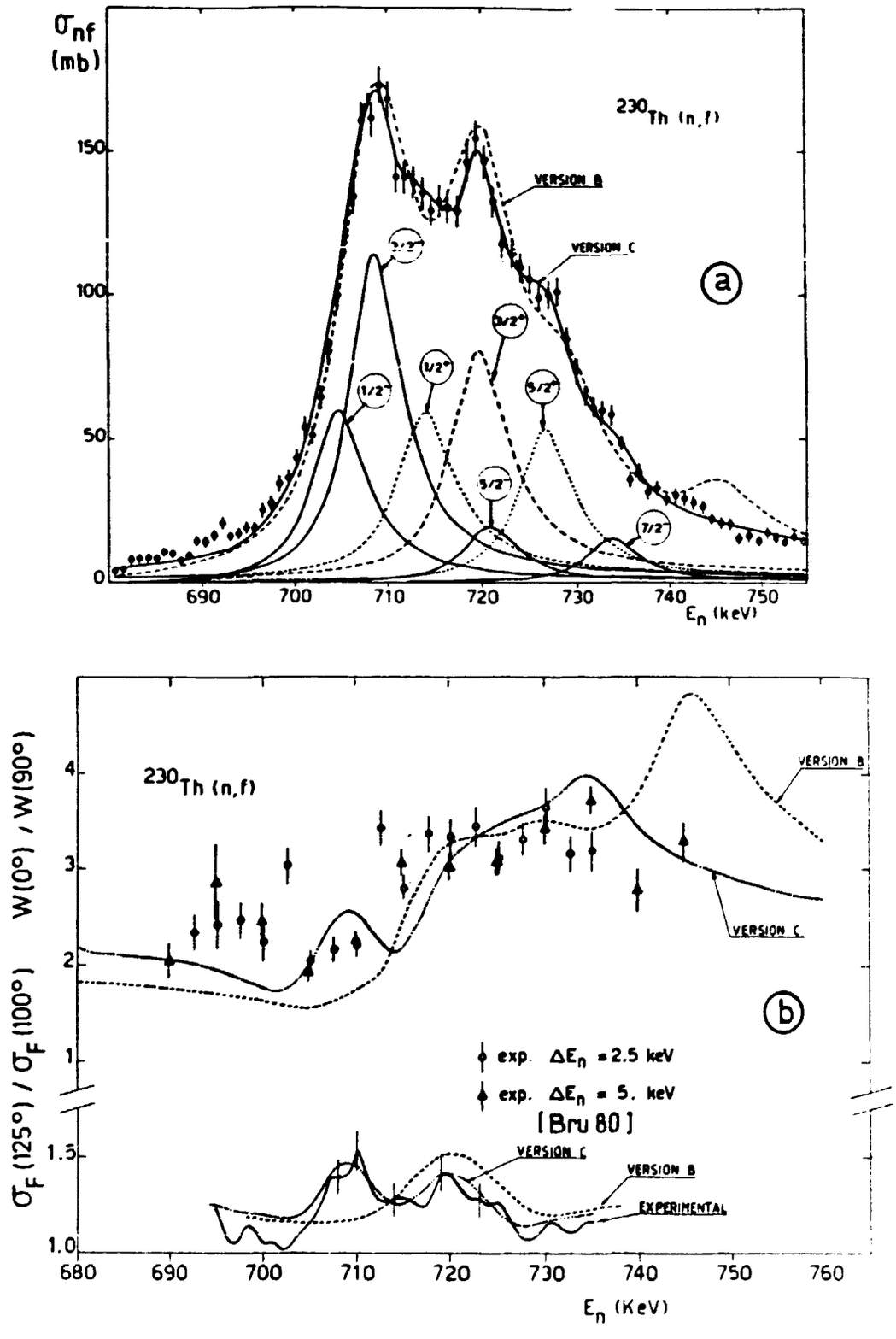

Figure 28

Same as in fig. 25 but the fit is from [Blo 81] (version C). For further details, see text and Table IV. Results from [Blo+ 80] (version B) (---) are also shown for comparison.

II.D - The (^{231}Pa+n) system

^{231}Pa is a non-fissile nucleus presenting also some structure in its near-threshold fission cross-section. Interpretation of the data is rendered more difficult because the compound nucleus ^{232}Pa is odd-odd with a more complicated structure than the odd thorium isotopes. The spin and its projections can take only integer values thus excluding the K = 1/2 case which, though adding some complexity, provides the possibility for a better identification of two-parity bands in the fine structure of the vibrational resonances. Also, the spin of ^{231}Pa is different from zero ($I^{\pi} = 3/2^{-}$) with the consequence that the angular distribution is parity dependent, in contrast to the ^{230}Th and ^{232}Th cases. Examples of this parity dependence are given in fig. 29. This feature could be of interest for the identification of two rotational bands of opposite parities and slightly shifted in energy.

A summary of the ^{231}Pa fission data is given in Table V.

Structure in the ^{231}Pa fission cross-section was detected as early as 1964 by Dubrovina and Shigin [DS 64] and confirmed by Muir and Veeser [MV 71] using a nuclear detonation as a pulsed neutron source associated with the time of flight technique. In this last measurement, a sharp resonance appeared at E_n = 158 keV with a natural width smaller than the width of the resolution function (4 keV). The same resonance also appeared, even more sharply, in measurements carried out with monoenergetic neutrons and a resolution of about $\Delta E_n \simeq$ 2 to 5 keV around E_n = 160 keV. This resonance is so narrow that it sticks out in the data in one point only with an observed peak cross-section of 25 mb (at ΔE_n = 5 keV) and of 39 mb (at ΔE_n = 2 keV) (see fig. 30). Such a resonance with a width of about 2 keV is due to a pure vibrational state, with quantum numbers (K,J^{π}) equal to ($3,3^{+}$) as determined from an angular distribution measurement (fig. 31), that can exist only in a shallow well of the fission barrier, not compatible with the calculated properties of the second well, but possibly consistent with the postulated third well.

The interesting features of the ^{231}Pa fission cross-section stimulated a joint effort from three laboratories (Bruyères-le-Chatel, Los Alamos and Oak Ridge) to undertake the "best possible measurement" of this cross-section with presently-available techniques. It was hoped that these measurements would reveal the details of the fine structure and clarify the third well situation by showing, for example, that the 158 keV resonance is in fact a doublet.

The results obtained with the time of flight technique and a nominal resolution of 0.19 ns/m represented a substantial improvement compared to previous measurements (resolution width of 0.4 keV compared to 2 keV around 160 keV). The fission cross-section thus obtained is plotted between 0.12 MeV and 0.45 MeV in fig. 32. The gross structure already observed in previous experiments at about 200 keV and 330 keV is reproduced but, in addition, a fine structure also appears superimposed onto it. The sharp peak at 158 keV, still shows up as a single peak, but defined this time by several points and with an observed peak cross-section of 89 mb (more than twice the highest value measured before). The energies of all the sharp peaks observed in this energy range are given in Table VI. Above 450 keV, the fine structure cannot be resolved because of the deterioration of the resolution with energy.

Analysis of the gross structure at 200 keV and 330 keV is possible in terms of vibrational levels having $K^{\pi} = 0^{+}$ (almost pure) and $K^{\pi} = 0^{-}$ (slightly damped) respectively [Sic+ 79].

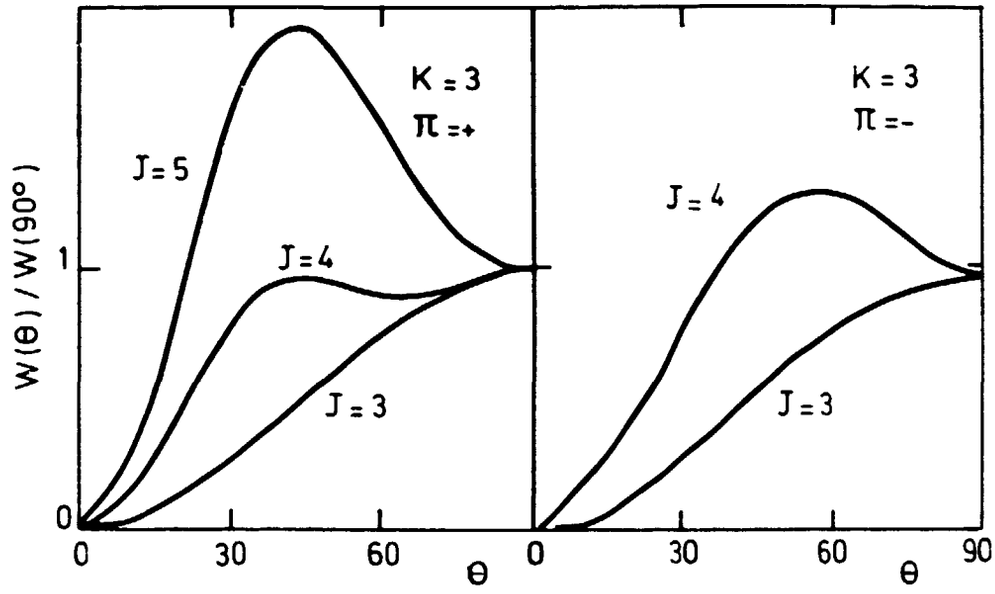

Figure 29

Calculated fission fragment angular distribution for several J values and for $K^{\pi} = 3^{+}$ and 3^{-} [Sic+ 79].

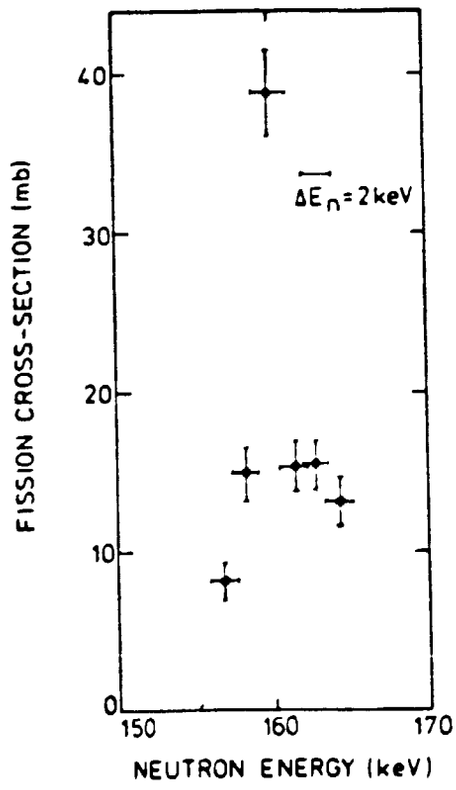

Figure 30

Vibrational resonance around E_n = 160 keV in the ^{231}Pa neutron-induced fission cross-section [Sic+ 79]

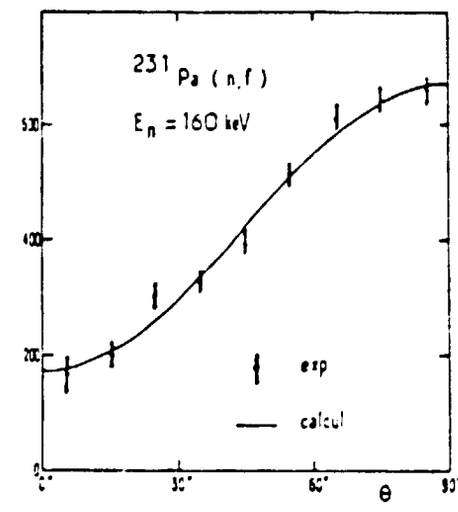

Figure 31

Measured and calculated (with $KJ^{\pi} = 33^{+}$) fission fragment angular distribution in the ^{231}Pa vibrational resonance around E_n = 160 keV (see fig. 30) [Sic+ 79]

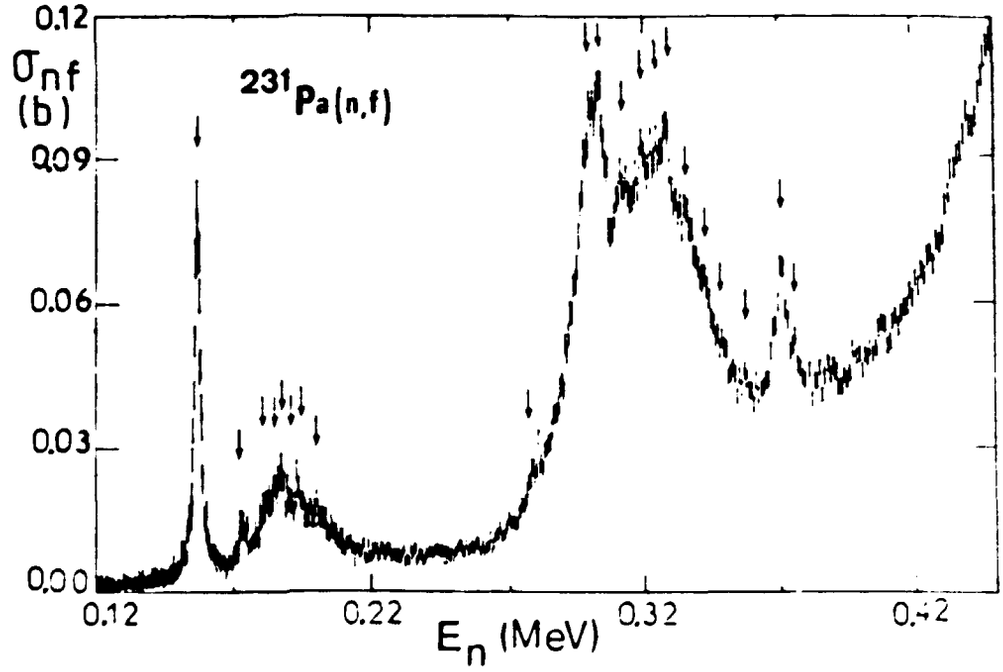

Figure 32

Neutron-induced fission cross-section for ^{231}Pa measured by time of flight with an energy resolution of 400 eV at E_n = 160 keV. The arrows indicate the presence of sharp peaks in the fine structure [Pla+ 81].

An attempt to find some evidence for the existence of a third well was made by a combined analysis of the sharp peaks in the fission cross-section and the FFAD* by Sicre et al [Sic+ 79]. The analysis took into account the high cross-section measured on top of the sharp peaks, a consequence of the high resolution achieved in the measurement (see, for example, the 158 keV resonance) ; this was of great help in eliminating (J,K^{π}) combinations for which the calculated cross-section for compound nucleus formation was smaller than the observed fission cross-section.

Such an analysis is described in detail in [Pla+ 81] and the parameters for three sharp peaks are given in Table VII.A. These three peaks have K = 3 but it appears that the fission penetrability P_f is much smaller for $K^{\pi} = 3^+$ than for $K^{\pi} = 3^-$, implying different barrier parameters for these two sets of quantum numbers.

The small number of sharp peaks which are analysed do no provide evidence for the existence of a third well in terms of two rotational bands of opposite parities. Yet, interpretation of these results can be made consistent with the third well hypothesis as discussed below :

The narrow resonances at 156.7 and 173.3 keV can be considered as caused by two degenerate class-III vibrational levels with opposite parities ($K^{\pi} = 3^+$ and 3^-) and parameters given in Table VII.B. The energy shift of ΔE = 173.3 - 156.7 = 16.6 keV is acceptable. Unfortunately, the rotational levels associated with these vibrational levels as band heads are too difficult to detect. The $J^{\pi} = 4^+$ level has too small a C.N. formation cross-section. The $J^{\pi} = 4^-$ level has a higher value of σ_{CN} but the fission penetrability is too small. The energies of these J = 4 levels were obtained by adding 16 keV to the energy of the band head, as would be obtained with an inertia parameter of 2 keV. Levels with higher J-values correspond to still smaller cross-sections because of the increased effect of the centrifugal barrier and therefore cannot be detected.

In conclusion, high quality fission data have been obtained for ^{231}Pa. A fine structure superimposed on the gross structure is clearly identified in the fission cross-section. Interpretation of these data is consistent with the existence of a third well in the ^{232}Pa fission barrier, though indisputable evidence for such a barrier shape in this nucleus still remains to be found.

II.E - <u>The (^{232}Th+n) system</u>.

Structure in the ^{232}Th near-threshold fission cross-section was studied on many occasions after it was first observed [HS 55], but this study was greatly stimulated by the detection of fine structure in the broad vibrational resonances, interpreted at that time as rotational sequences of levels having a large moment of inertia [BMP 75]. This preliminary analysis of fine structure data was based on the energy spacings only and assumed one-parity sequence of rotational levels.

It is more difficult to obtain accurate data on fine structure for ^{232}Th than for ^{230}Th, essentially because the vibrational resonances are located at higher energy (1.4 - 1.7 MeV as compared to 0.73 MeV for ^{230}Th) where the resolution function is broader. The data are also more difficult to analyse because :

* Fission Fragment Angular Distribution.

i) at higher energy, more angular momentum values of the incident neutron contribute to the compound nucleus formation.

ii) there is a group of vibrational resonances separated by roughly 0.1 MeV with the contribution of several K-values.

More accurate measurements were carried out since the interesting results for ^{232}Th were obtained in order to substantiate more thoroughly their interpretation.

A summary of the ^{232}Th fission data is given in Table VIII.

The fission cross-section was measured with good resolution using either monoenergetic neutrons (ΔE_n = 3 keV around E_n = 1.6 MeV) [Bar 77] or a white source associated with the time of flight method (ΔE_n = 2.3 keV around E_n = 1.4 MeV). The results thus obtained are shown in fig. 33 and 34. They represent the upper limit of accuracy that can be reached by presently-available conventional techniques. As an illustration of the progress accomplished towards measurements of better accuracy, the old data of Henkel and Smith [HS 55] are compared to those of Blons et al [Blo+ 80] in fig. 35. In all these recent σ_{nf} measurements, the fine structure already observed by Blons et al [BMP 75] is confirmed. A more detailed intercomparison of these fine structure data together with a tentative interpretation are given later in the text.

The fission fragment angular distribution was also measured in the best possible conditions but with a broader resolution than for the fission cross-section measurement, as a consequence of the reduced count rate. FFAD data were taken using also either monoenergetic neutrons with fragments detected with Makrofol (ΔE_n = 5 keV) [Bar 77] or a white neutron source associated with the time-of-flight method, the selection of the angle of fragment emission being then achieved with grids (ΔE_n = 7 to 16 keV around E_n = 1.6 MeV [Blo 81] [Auc+ 81]). Illustration of the data thus obtained is given in fig. 33 where it can be seen that there are rapid changes in W(θ) across the region of vibrational resonances.

As for ^{230}Th, it is necessary to fit simultaneously both σ_{nf} and W(θ) data to obtain a meaningful interpretation of the fission process in this energy region.

The gross structure of the vibrational resonances needs to be quantitatively explained first. Attempts were made by the Lucas Heights (L.H.) [BWM 80] and the Bruyères-le-Chatel (BRC) [AC+ 79] groups. Detailed presentation and comparison of their results are given in [Abo+ 79].

The various K contributions determined by both groups for each vibrational resonance are in good agreement with recent determinations [Auc+ 81] illustrated in fig. 36. Therefore, there seems to be a general consensus on the K determinations, except for the 1.7 MeV resonance which should have K = 1/2 according to Blons et al [BMP 75] contrary to all other determinations which give a predominance of K ≥ 3/2.

Since the BRC and L.H. fits are already reviewed in detail elsewhere, there is no need to repeat the same detailed presentation here. The calculations of these two groups are presented in fig. 37 and 38 together with a comparison to the experimental data. In addition to these fission calculations, fits to the radiative capture and scattering cross-sections were also considered

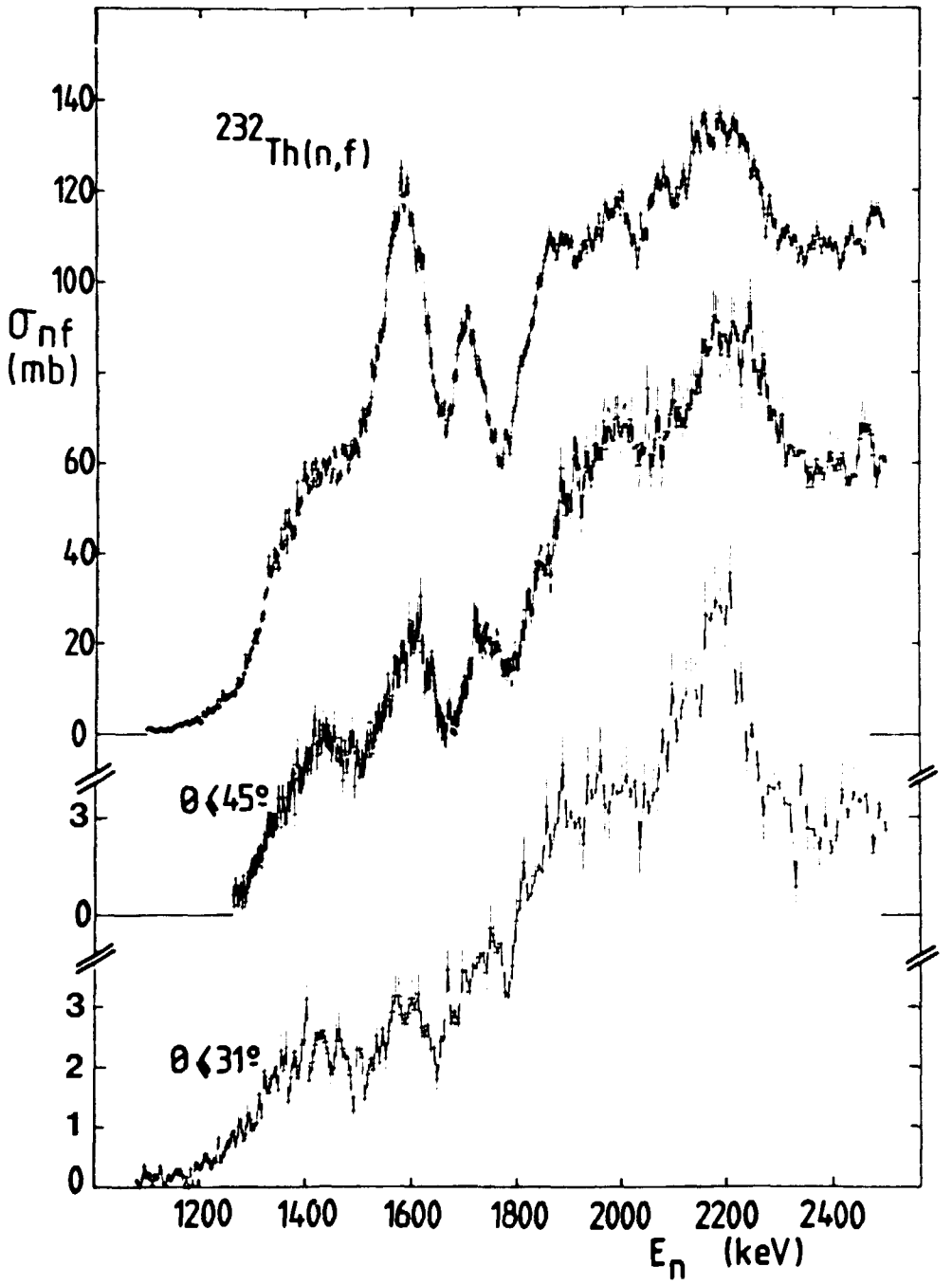

Figure 33

Neutron-induced fission cross-section for ^{232}Th (on top). The cross-sections for fission fragments emitted at $\theta \leqslant 45°$ and $\theta \leqslant 31°$, as measured with grids, are plotted below [Blo+ 80] [BMP 75]. All these results were obtained with the time-of-flight method.

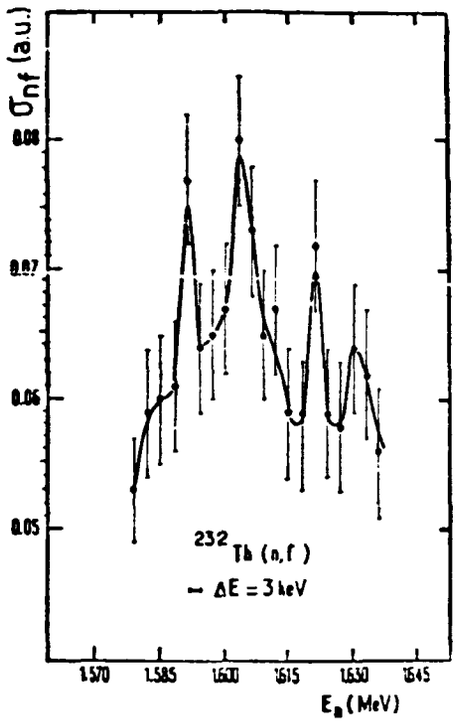

Figure 34 : Neutron-induced fission cross-section for ^{232}Th measured with monoenergetic neutrons [Bar 77].

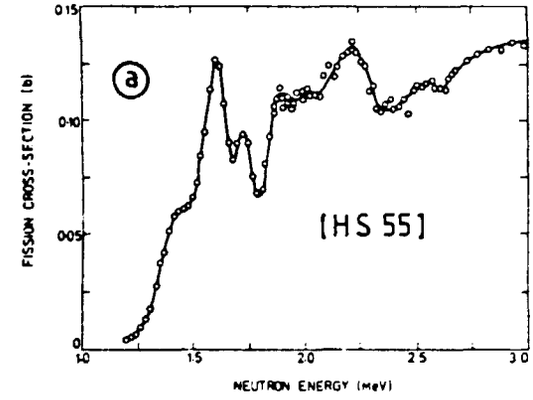

Figure 35 : Comparison of several data for the ^{232}Th neutron-induced fission cross-section :

a) from Henkel and Smith [HS 55]

b) from Blons et al. [Blo+ 80] with insert A.

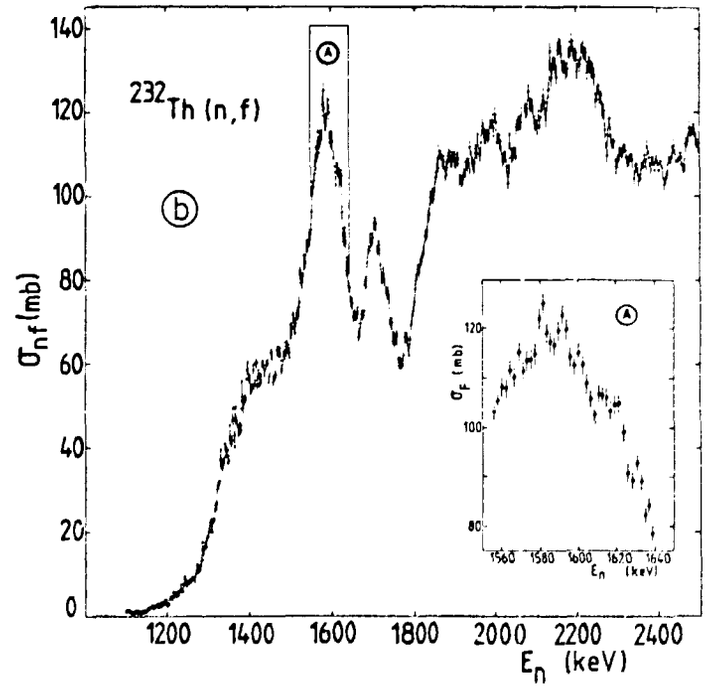

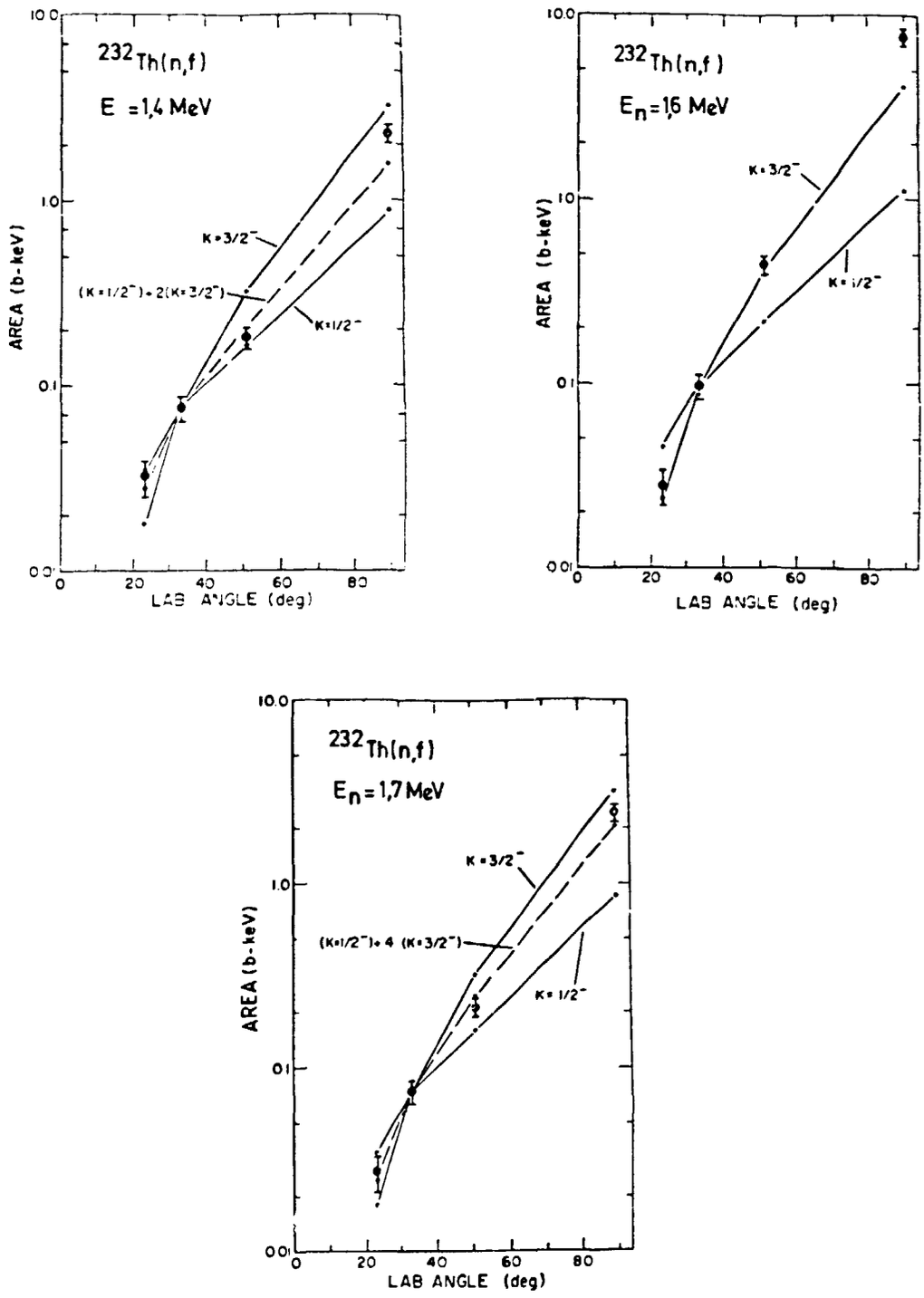

Figure 36

Integral angular distribution of fission fragments (measured with grids) in the ^{232}Th vibrational resonances at E_n = 1.4 MeV, 1.6 MeV and 1.7 MeV. The lines are calculations for various K-contributions [Auc+ 81].

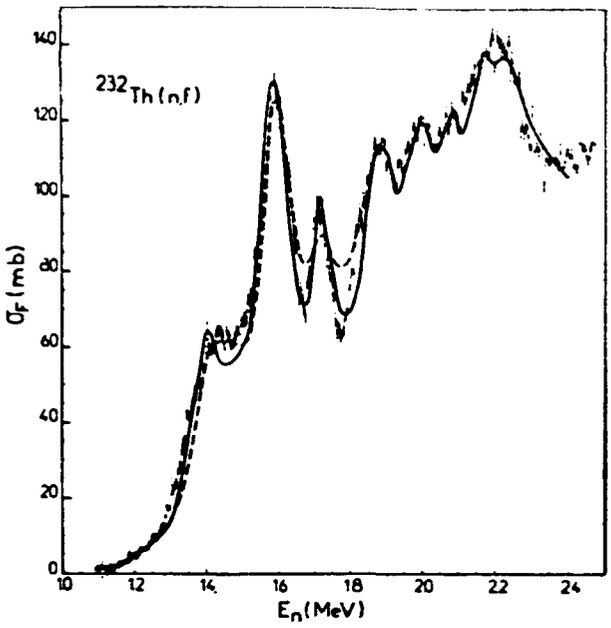

Figure 37 : Fit to the ^{232}Th fission cross-section. The experimental points are from Blons et al. [BMP 75]. The solid line is a fit described in [AJT 79]. The dashed line is the fit from the Lucas Heights group [CBW 77].

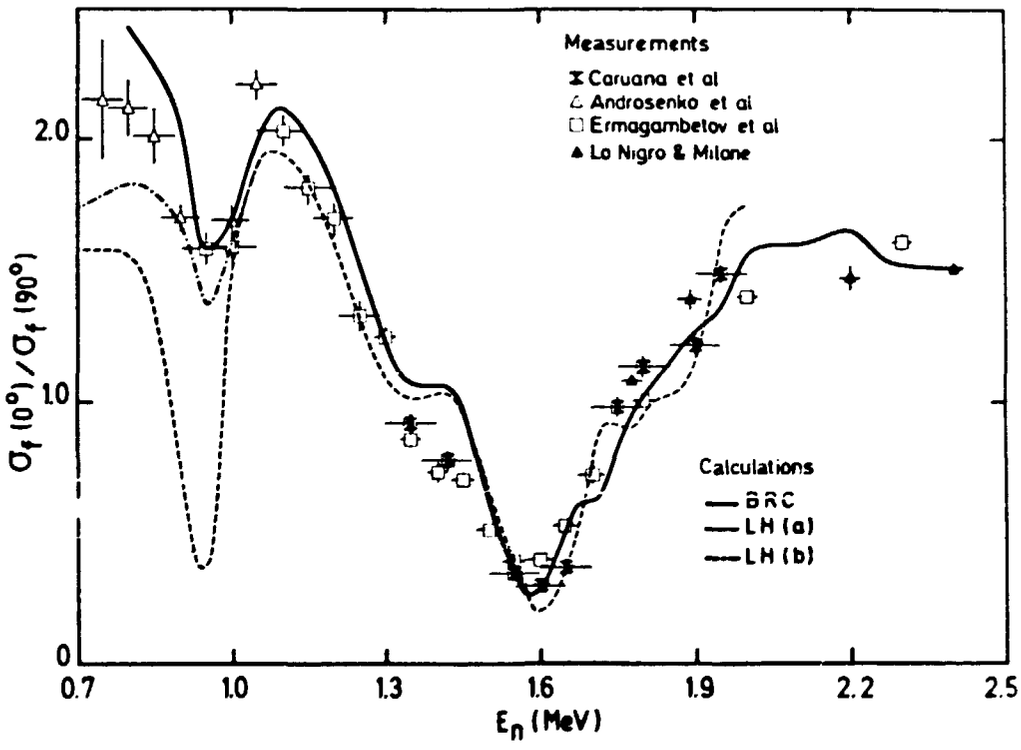

Figure 38

Fit to the ^{232}Th fission fragment anisotropy. The solid line is a fit from the Bruyères-le-Chatel (BRC) group [AJT 79] using the same parameters as those for fig. 37. The other lines (---- and -·-·-) are fits from Lucas Heights (see text).

[Abo+ 79] [AJT 79]. Examination of fig. 37 and 38 shows that it is possible to explain the gross structure in the ^{232}Th fission cross-section together with the anisotropy data. The number of fission channels needed to obtain such fits is impressive as can be seen in Table IX. It must be remarked that, in these analyses, each state in the third well is associated with a fission exit channel. In the BRC fit, most vibrational states were considered as doublets with components of opposite parities (in contrast to the L.H. fit) and as band heads for rotational levels. The lowest K = 1/2 state is not bound in agreement with the predictions of Möller and Nix [MN 76]. The value of the inertia parameter used for the rotational bands is not very important since the sharp peaks of the fine structure do not appear in these calculations, as discussed below.

These fits to the gross structure look satisfactory at first sight but, nevertheless, they present two drawbacks :

i) the calculated fission cross-section above 2.4 MeV (not shown in fig. 37) is above the measured one. This is certainly caused by too many fission channels used to fit the cross-section below this energy,

ii) the fission barrier parameters used in the calculations cannot reproduce the fine structure in the gross structure, as it is illustrated in fig. 39 for the 1.6 MeV vibrational resonance.

Therefore, the analysis reported above is not completely satisfactory and a new set of fission barrier parameters must be found to fit both the gross structure and the fine structure data.

Two trends towards more realistic fission barrier parameters can be suggested :

i) The number of fission exit channels must be reduced in order to yield lower σ_{nf} values above 2.4 MeV. This can be achieved, for example, by assuming more than one vibrational level for each fission channel with, as a consequence, a third well slightly deeper than the one postulated above.

ii) Barriers with smaller penetrability are necessary to reduce the widths of some vibrational states and therefore reproduce the observed widths of the sharp peaks in the fine structure.

It is interesting to have a closer look at the fine structure in the 1.6 MeV vibrational resonances since these sharp peaks, first interpreted as a single-parity rotational band, were at the origin of most of this work. The new results confirm the existence of these sharp peaks whether they are measured with monoenergetic neutrons [Bar 77] or by the time-of-flight method [Blo+ 80]. A comparison of these two data sets is made in fig. 40. But the interpretation is now different for it has to take into account the existence of two bands of opposite parities and also the amplitude of the sharp peaks in terms of neutron and fission penetrabilities. An attempt to fit the fine structure data is under way [Blo 81].

In summary, much work has been achieved in the study of ^{232}Th neutron-induced fission. Satisfactory fits to the gross structure in the fission cross-section have been obtained, in agreement with the results for the angular distribution. But, though the early results of 1975 could be interpreted at that time as the proof of the existence of a third well in the barrier, the more accurate

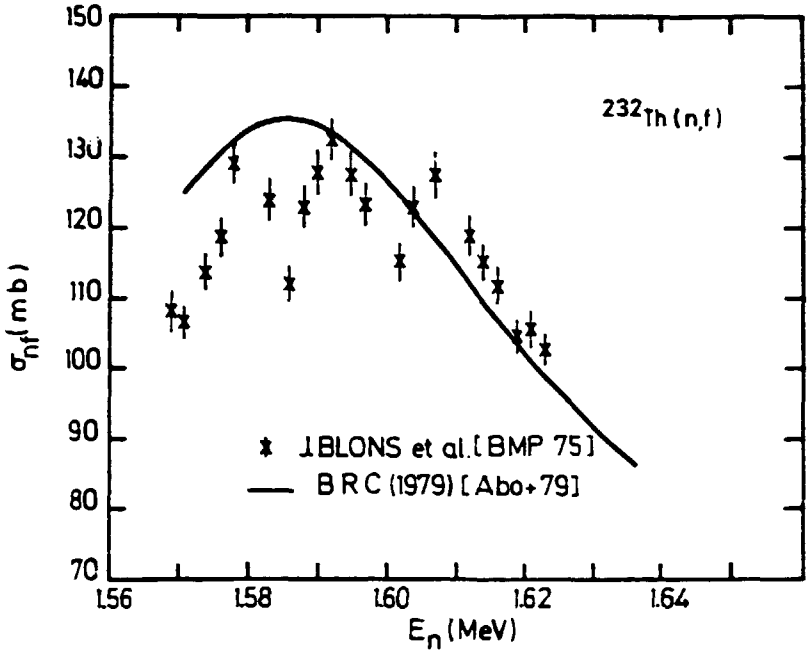

Figure 39

The fine structure (x) in the 1.6 MeV ^{232}Th(n,f) vibrational resonance as obtained in [BMP 75] with portion of the fit (solid line) shown in fig. 37 [AJT 79]. It is obvious that the fine structure is not reproduced by the calculations.

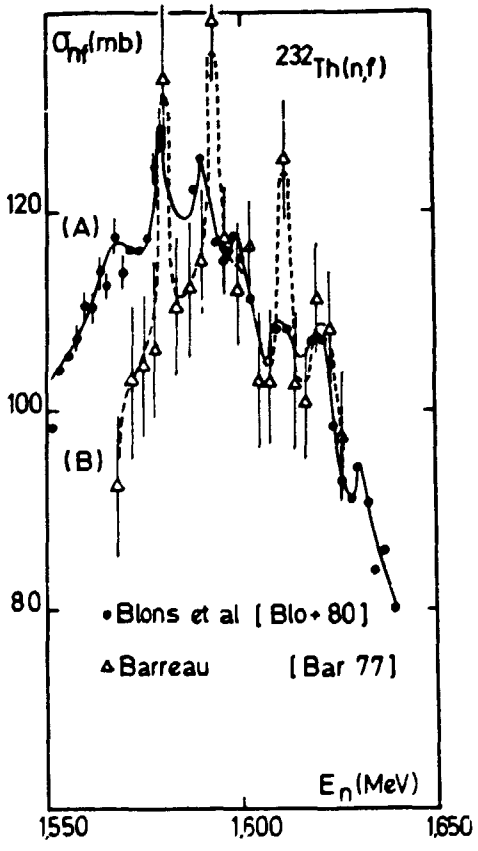

Figure 40 : Comparison of the fine structure data in the 1.6 MeV ^{232}Th(n,f) vibrational resonance, as obtained in high resolution experiments carried out i) by time of flight (A) [Blo+ 80] and ii) with monoenergetic neutrons (B) [Bar 77].

data that have been obtained since then, need to be interpreted with a more sophisticated theoretical approach before one can conclude to the unambiguous existence of a third well in the fission barrier for ^{233}Th.

III - SOME DYNAMICAL ASPECTS IN THE COLD FRAGMENTATION OF ^{234}U AND ^{236}U SYSTEMS.

III.A - General background.

In the preceding chapter, we examined some properties of the fission process that are strongly dependent on the statics of the phenomenon, more specifically on the potential energy surface in the region of the saddle point. This is important, for example, for the determination of the fission probability and, consequently, for the understanding of the behaviour of fission cross-sections. But other properties require a more thorough description of the motion from the formation of the initial state to the scission point.

A complete treatment of fission must include the dynamics of the process, essentially the inertial mass tensor of the system and dissipation. These dynamical aspects influence many properties of the fission fragments such as their yield, kinetic and excitation energies. Measurements of such properties and of their correlations can give a hint to the knowledge of fission dynamics which are still poorly known (see among many other references [VH 73], [Bjö 74], [Blo+ 78b]). For example, the share of the energy available in fission between excitation and kinetic energies of the fission fragments can give some insight into the importance of viscosity in the descent from the saddle point to scission. A large fragment excitation energy, usually determined by neutron evaporation and γ-ray emission, is the indication that the fissioning system has been heated up along the fission path and, therefore, that viscosity plays an important role. Also, the odd-even differences in the fragment yields can tell something about the preservation of superfluidity in the descent to scission. If strong even-odd effects are observed, they may be interpreted as evidence of adiabaticity in the motion along the fission path.

A vast amount of data has been accumulated on the properties of the fission fragments. Yet, the conclusions deduced about the fission dynamics are very controversial. This is because the interpretation of the data is ambiguous. For example, there is usually not a one-to-one correspondence between properties of fission fragments on one hand and fission parameters on the other hand. This can be illustrated by the kinetic energy of the fragments which is the sum of the pre-scission kinetic (E_{sc}) energy and the Coulomb energy at scission (V^c_{sc}) :

$$E^T_K = E_{sc} + V^c_{sc} \qquad \text{(III.1)}$$

Any variation in the fragment kinetic energy can be accounted for either by a change in the former (implying a change in the viscosity) or by the latter (by a modification of the scission configuration), and there is no easy way to disentangle the relative contributions of these two effects.

Another example is provided by the total excitation energy of the fragments which depends on the scission properties. At scission. the fissioning system can be excited, as a consequence of viscosity effects, and the fragments are strongly elongated because of their mutual nuclear interaction. But, after scission, this nuclear interaction is suppressed and the fragments change shape in flight to become more spherical. Therefore, the total fragment excitation energy $E^*(A,Z)$ results from the addition of their excitation energy at scission E^*_{sc} and of their excess deformation energy E^d_{sc} which is transformed into excitation energy.

$$E^*(A,Z) = E^*_{sc}(A,Z) + E^d_{sc}(A,Z) \qquad \text{(III.2)}$$

Again, as for the case of the kinetic energy, there is no direct experimental possibility of separating these two contributions.

A more subtle example is given by odd-even effects in the fragmentation, i.e. differences in the yields of neighbour fragments having even or odd values of Z or N. It is commonly assumed that the existence of such effects can be considered as evidence of preservation of superfluidity between the saddle and scission points and, consequently, of low viscosity during this last phase of fission. But this is far from being obvious. For example, even fragmentations are favoured in terms of the statistical model because they correspond to higher Q-values and, therefore, to larger yields as a consequence of a larger extension in phase space. In such an interpretation odd-even effects can appear though the use of the statistical model implies nuclear viscosity. Conversely, preservation of superfluidity does not automatically lead to even yields for this depends on the necking-in at scission. A slow and adiabatic necking-in preserves pairing in each nascent fragment, but an abrupt necking-in can lead to a breaking of nucleon pairs since pairing is a residual interaction with a long-range correlation. (See Section III.D).

The above examples illustrate the consequences of the fact that, in fission experiments, measurements are made on the secondary fission fragments when they are far apart and after neutron evaporation, if present. It is not possible, through these experiments, to have directly access to the scission configuration where the primary fragments (prior to neutron emission) are still in contact. Therefore, the scission configuration can be pictured only with the help of fission models which can be tested only on the properties of the secondary fragments at infinity. Also, the parameters describing the fragment properties are in large number and not accessible simultaneously, even with the most sophisticated spectrometers.

Various models can be used to interpret the data :

i) The adiabatic model assumes that the collective and internal degrees of freedom are completely decoupled. This implies that the motion of the fissioning nucleus between the saddle and scission points occurs without transfer of energy from the kinetic energy in the fission mode to the intrinsic excitation energy. At scission, all the difference in potential energy between the saddle and scission points appears in the form of pre-scission kinetic energy. There is a kind of internal inconsistency in this model since it implies the maximum possible kinetic energy of the system, whereas the coupling of collective and intrinsic degrees of freedom increases with velocity. Therefore, the adiabatic model can apply to cases having small potential energy changes between the saddle and the scission points. (See Section III.D).

ii) The statistical model relies on physical hypotheses opposite to those of the adiabatic model for it implies a strong coupling between the collective and internal degrees of freedom. Therefore, the descent from the saddle point to scission is viscous and, at each step of the motion, there is equilibrium between all degrees of freedom whether they are collective or intrinsic.

iii) Intermediate models are also used between these two extremes. One of them assumes that the collective degrees of freedom are themselves strongly coupled, but with absence of coupling between the collective degrees of freedom as a whole and the intrinsic ones [Nör 69]. For example, in this model, the energy of the vibrational states can be transformed into pre-scission kinetic energy but not into excitation energy. Therefore, the collective and intrinsic modes are separately in thermal equilibrium at different temperatures T_{coll} and T_{int} respectively.

Also, the dissipation that may occur during the descent from saddle point to scission can be of several types and the calculations can be made with various assumptions. The microscopic approach is used for example in the time-dependent-Hartree-Fock (TDHF) method in which the evolution of the system is obtained given the initial conditions and a two-body effective interaction [Neg+ 78]. Macroscopic approaches have different physical assumptions : i) in the one-body dissipation [Blo+ 78b], the energy transfer occurs through interaction of the nucleons (supposed to have a long mean free path) with the moving boundary of the system and ii) in the two-body dissipation which is more likely to occur when the nucleons have a short mean free path, energy transfer is made through two-body collisions as in classical viscosity of usual macroscopic bodies [DSN 76]. The macroscopic calculations are usually carried out for systems free from shell effects. The relevant fission data are scarce and too much ambiguity is associated with fits to these data. At present, experiments cannot decide which type of viscosity actually occurs in fission.

In the remaining part of this chapter, attention is paid only to low-energy fission of ^{234}U and ^{236}U. Properties of these systems are dominated by shell effects and consequently cannot help clarifying viscosity aspects which are more related to bulk matter properties. Yet, interesting results have been obtained both experimentally and theoretically and these can throw a light on possible mechanisms that occur between saddle point and scission.

First, some properties of fission fragments produced in the thermal-neutron induced fission of ^{235}U are recalled (Section III.B). The ^{236}U fissioning system thus obtained is certainly one of the best studied since very important fission rates can be achieved by irradiating ^{235}U fission foils with intense neutron beams produced in high-flux reactors. In such conditions, it is possible to study fission events with selected and correlated values of some fission parameters. Analysis of these fission data shows the interest of extending the range of selected fission parameters to extreme values in order to have access to fission events for which the primary fragments are only weakly excited, below the neutron emission threshold. This is the so-called "cold fragmentation" which is discussed in Section III.C and for which unexpected results are obtained. An interpretation of these results, in terms of recent Hartree - Fock - Bogolyubov calculations is proposed in Section III.D.

III.B - Some properties of thermal-neutron induced fission of ^{235}U.

A great quantity of data has been accumulated about the properties of this ^{236}U fissioning system. Rather than reviewing all these data, which would be far beyond the scope of this report, the presentation is restricted here to fission results pertinent to possible viscosity effects and obtained with the Lohengrin spectrometer, one of the most sophisticated apparatus used for this type of study.

Results obtained with the Lohengrin spectrometer have been recently presented in an article [Lan+ 80] which, in many aspects, supersedes earlier presentations. It is recalled that Lohengrin is a mass spectrometer combining electrostatic and electromagnetic separations of the secondary fission fragments (i.e. after prompt neutron evaporation), with a resolving power of $A/\Delta A \simeq 400$ [Mol+ 75, Mol+ 77]. At the exit of the spectrometer, mass-separated fission fragments are available with a given ionic charge q and with a given kinetic energy. The nuclear charge distribution of these fragments can be further determined by measuring, by time of flight, their energy loss in a carbon absorber placed behind the spectrometer [Cle+ 75], but charge separation can be obtained only for the light fragment group. Of special interest to our discussion are the yields, as a function of their kinetic energy, of fission fragments having given Z and N values. These yields are presented, for the light fission group, in fig. 41, 42 and 43 for various A-, Z- and N-values respectively.

An odd-even effect in the Z-yields shows up clearly for kinetic energies comprised between 83.6 MeV and 112 MeV, and increases with kinetic energy in this range. The odd-even effect in the A- and N-yields is not as pronounced and shows up clearly only for high kinetic energies. It must be noted that the Z-yields reflect those at scission but not the N- (and A-) yields because of prompt neutron evaporation. Therefore, only the Z-yields can be directly analysed whereas interpretation of the N- and A-yields needs the simulation of neutron evaporation (for example by Monte-Carlo methods as in [Lan+ 80]).

The proton odd-even effect Y^p_{o-e} in the yields, can be defined as :

$$Y^p_{o-e} = \frac{Y^p_e - Y^p_o}{Y^p_e + Y^p_o} \qquad \text{(III.3)}$$

where Y^p_e and Y^p_o are the even-Z and odd-Z yields respectively.

This definition can be used locally, in a narrow range of Z-yields and for a well-defined kinetic energy or, on the contrary globally, when averaged over a wide range of yields or kinetic energies or both.

The increase with excitation energy of the proton odd-even effect for the light fragment group is illustrated in fig. 44.

Globally, from these measurements, the odd-even effect in the Z-yields is found to be (23.7 ± 0.7) % in good agreement with other estimations from other laboratories.

A proton odd-even effect can also be detected in the fragment kinetic energy as is illustrated in fig. 45 where it can be seen that, on the average, even-Z fragments have a kinetic energy 0.4 MeV greater than for odd-Z ones. (This corresponds to a 0.7 MeV difference for both fragments).

Interpretation of these odd-even effects, in terms of moderate viscosity during the motion between saddle point and scission [Lan+ 80], is summarized below.

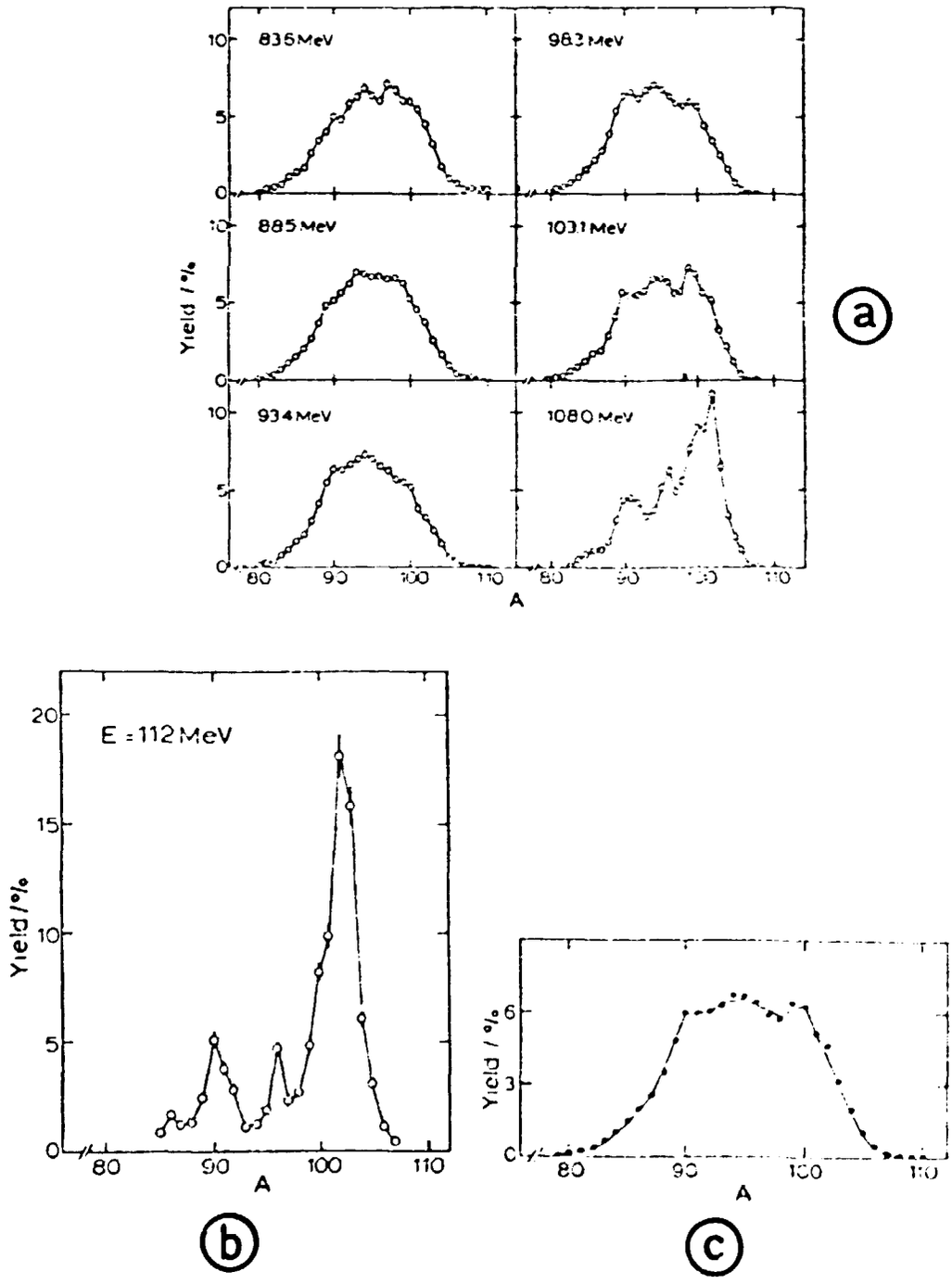

Figure 41

A-yields in the light fragment group for ^{235}U thermal-neutron induced fission [Lan+ 80]

a) For various values of the fragment kinetic energy.

b) For a fragment kinetic energy of 112 MeV.

c) Averaged over all kinetic energies. (The solid line is from [MR 78]).

All distributions are normalized to 100 %.

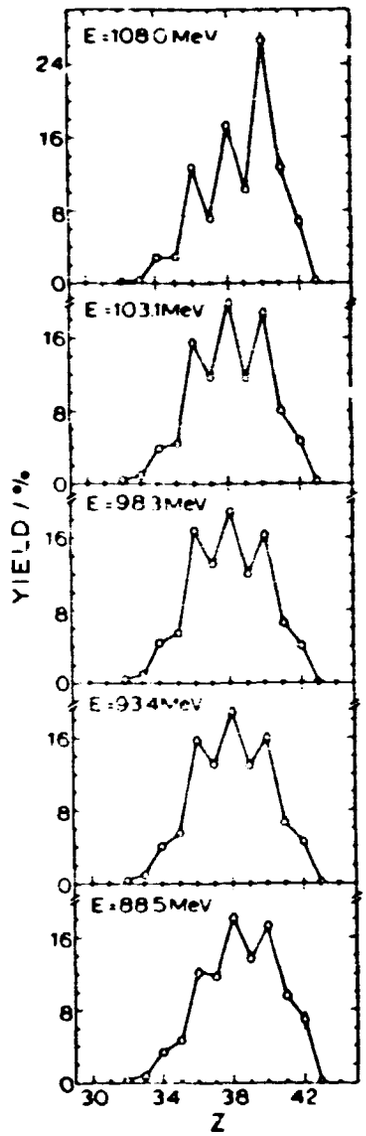

Figure 42

Z-yields in the light fragment group for ^{235}U thermal-neutron induced fission and for various values of the fragment kinetic energy [Lan+ 80]. All distributions are normalized to 100 %.

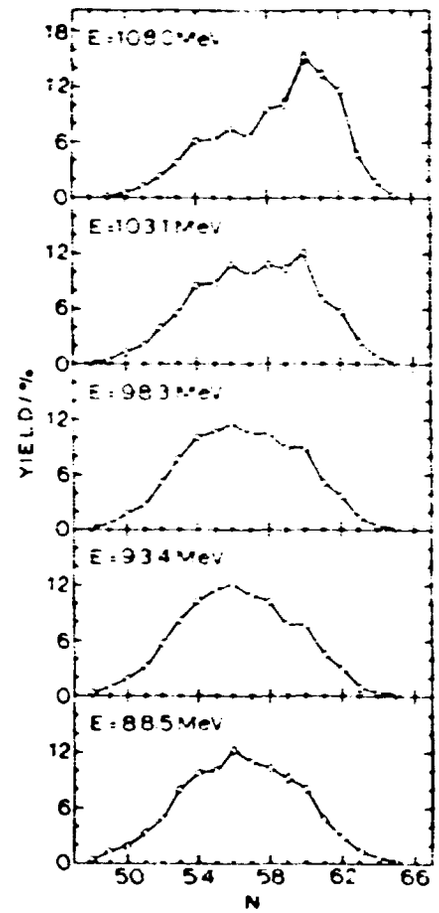

Figure 43

N-yields in the light fragment group for ^{235}U thermal-neutron induced fission and for various values of the fragment kinetic energy [Lan+ 80]. All distributions are normalized to 100 %.

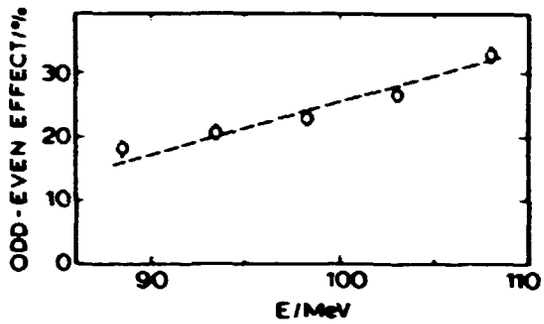

Figure 44

Variation of the odd-even effect in the Z-yields for the light fragment group as a function of fragment kinetic energy (deduced from results shown in fig. 42) [Lan+ 80].

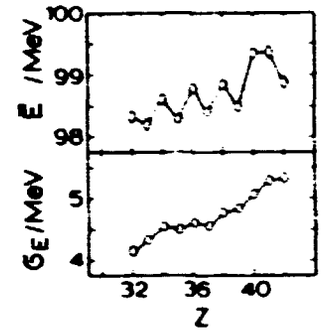

Figure 45

Kinetic energy of the fission fragments (light fragment group) as a function of Z for thermal-neutron induced fission in ^{235}U. On top, average kinetic energy. Below, standard deviation of the distribution [Lan+ 80].

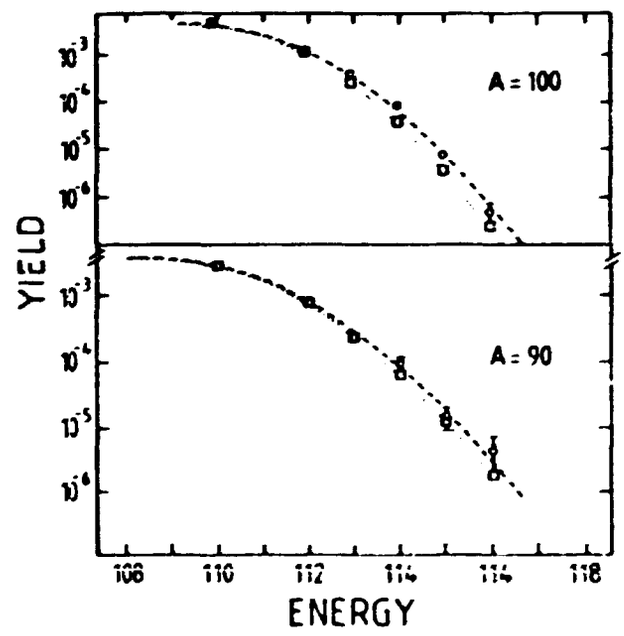

Figure 46

Variation of the A-yields (for A = 100 and A = 90) with kinetic energy (in MeV) for the thermal-neutron induced fission of ^{233}U [Arm 81].

At scission, the system is composed of two components, one which is superfluid despite viscosity and one which contains broken pair(s). Odd-odd fragmentation comes from the broken-pair component only whereas even-even fragmentation is a mixture of superfluid and broken-pair components. This representation explains the odd-even differences in the yields and their increase with fragment kinetic energy as a consequence of a decrease in the viscosity effect. One should also take into account the effect of odd-even differences in Q-values on the yields. This representation can also explain the odd-even differences in fragment kinetic energy. If the motion is superfluid all the way to scission, all the energy available at scission then appears in the form of pre-scission kinetic energy ; this corresponds to the adiabatic model discussed earlier. If pair breaking occurs during the descent from the saddle point, the energy required for pair breaking then comes as a reduction of the pre-scission kinetic energy.

Since the observed odd-even effects increase with fragment kinetic energy, it is interesting to explore these effects up to extreme values of the kinetic energy for which the excitation energy of the fragments is too small for neutron evaporation to occur. This is the so-called "cold fragmentation" discussed in Sections III.C and III.D.

III.C - "Cold fragmentation" in thermal-neutron induced fission of ^{233}U and ^{235}U.

The two systems ^{234}U and ^{236}U formed in the absorption of thermal neutrons by ^{233}U and ^{235}U respectively are in a superfluid state at the saddle point. Since superfluidity seems to be partially destroyed near scission even for fragments of higher kinetic energy, though to a lesser extent, it is interesting to explore the superfluidity properties of primary fragments with the highest possible kinetic energy. Such events are more difficult to study experimentally since the probability of fragmentation decreases very rapidly with increasing kinetic energy as is illustrated in fig. 46. On the other hand, they can be interpreted more easily because these fragments with high kinetic energy are, in fact, the primary fragments since their excitation energy is small, below the neutron emission threshold. In this so-called "cold fragmentation", properties of one fragment are closely linked to properties of the complementary fragment. For example, if Z_L and A_L are respectively the atomic and mass numbers of the light fragment, then the corresponding numbers for the heavy fragment are $Z_H = 92 - Z_L$ and $A_H = 234 - A_L$ (for ^{234}U) or $A_H = 236 - A_H$ (for ^{236}U). Also, if E_K^L is the kinetic energy of the light fragment, then momentum conservation requires that

$$E_K^T = E_L(1 + \frac{A_L}{A_H}) \qquad \text{(III.4)}$$

for the total kinetic energy of both fragments.

Cold fragmentation in the fission yields of ^{234}U and ^{236}U has been recently studied by two groups, one (for ^{234}U) using the Lohengrin facility mentioned earlier ([Arm+ 81], [Arm 81]) and the other (for ^{236}U and ^{234}U) using a pair of solid-state detectors [Sig+ 81]. The results obtained by these two groups are briefly reviewed below.

Among the results obtained by the first group for ^{234}U (with Lohengrin), fig. 47 illustrates the variations in the A-yields for several biases set on the light fragment kinetic energy. The effect of the Q-value is obvious. For high energy biases, only selected events with $Q > E_K^T$ are actually observed. These results demonstrate also that events corresponding to cold fragmentation have been detected with a total kinetic energy very close to the Q-value. Another representation of the results thus obtained is given in fig. 48 where the total kinetic energy is compared to the average Q-value (called $\bar{Q}$), as a function of A, for fission events at the 10^{-5} yield level. The value of $\bar{Q}$ for a given A-fragmentation is obtained by averaging the Q-values over the Z-distribution corresponding to this A-value. Fragments detected in this manner have a total kinetic energy (well defined by the spectrometer for a given A-fragmentation) close to $\bar{Q}$. The excitation energy for both fragments in such events is 3.8 ± 1.2 MeV on the average with an odd-even A difference of about 1 to 2 MeV.

Of special interest to our discussion is the even-odd effect in the Z and N yields in this cold fragmentation. Proton pairing seems to play an important role. For example, even-Z isotopes such as $^{84-86}Se$, $^{88-91}Kr$ and $^{94-96}Sr$ are found with a great abundance in the corresponding A-yields. Also, the proton odd-even effect can be determined directly from the independent yields at E_K^L = 112 MeV and is found to be equal to 46 %. In contrast, the neutron odd-even effect in the yields is much smaller, though the results are not influenced by neutron evaporation. The weak effect of neutron pairing is illustrated by the high yields of many odd-N isotopes such as ^{95}Sr and ^{91}Kr. Generally, odd-N isotopes have yields comparable to those of their even-N neighbours which should be favored by their higher Q-value. In the independent yields at E_K^L = 112 MeV, the neutron odd-even effect is about 10 % only.

In conclusion of this work, no evidence of complete superfluidity is found in the cold fragmentation of ^{234}U since, even at these low excitation energies, broken pair components are important, especially for neutrons.

In the results obtained earlier for ^{234}U and ^{236}U by the second group, the technique used to resolve the yields into well-defined nuclear species is different. The two fragments are detected by two solid-state detectors which give the kinetic energies of these fragments. Moreover, the time-of-flight difference Δt between the two fragments is also recorded and this provides the possibility of resolving the fragment masses [Gue+ 78] by using the following relation :

$$\Delta t = \frac{1}{\sqrt{E_K^1}} \left[\left(1 - \frac{\ell_2}{\ell_1} \frac{m_2}{m_1}\right) \ell_1 \sqrt{m_1} \right] \qquad \text{(III.5)}$$

where E_K^i, ℓ_i, m_i are respectively the kinetic energy, flight length and mass of fragment i (i = 1,2). The quantity in brackets can take a discrete set of values only and, therefore, for a fixed kinetic energy, the Δt spectrum is, in fact, a mass spectrum in as much as no neutron evaporation occurs in flight. With this method, it is easy to identify events caused by cold fragments from those which have emitted neutrons.

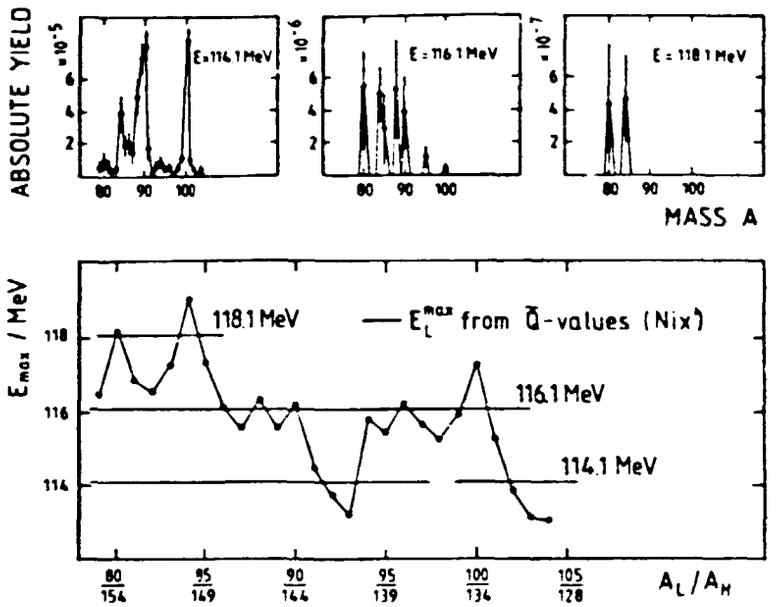

Figure 47 : On top, A-yields for cold fragmentation (light fragment group) in ^{233}U thermal-neutron induced fission for 3 different values of the fragment kinetic energy. Below, maximum possible kinetic energy of the fission fragments (light group) calculated from $\bar{Q}$-values (from [MN 80]) averaged over the Z-distribution for each A-value [Arm 81].

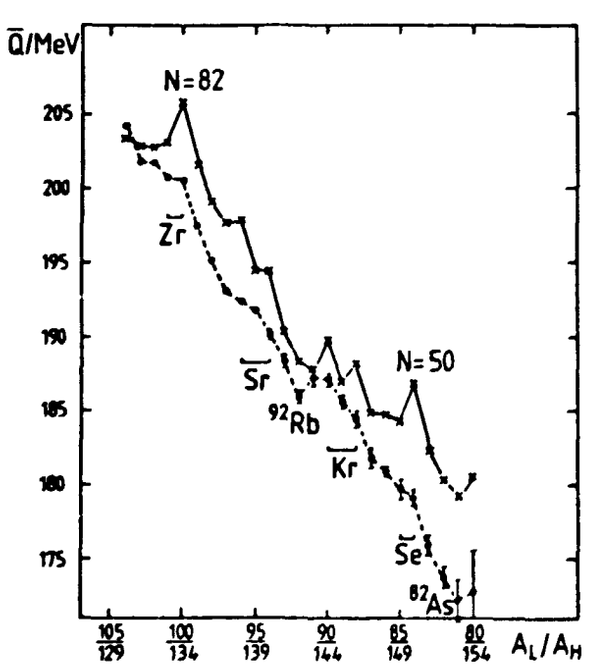

Figure 48 : Total kinetic energy E_K^T(-·-·-), at yields $y(A) = \int_{E_K^T}^{Q} dE \frac{dy}{dE} = 10^{-5}$, compared to the $\bar{Q}$-value as given in [MN 80] (solid line). Isotopes of even elements with independent yields larger than 90 % and odd-odd nuclei with yields larger than 50 % are indicated [Arm 81].

In addition, the behaviour of the Q-values in the region of A_H = 132 gives the possibility of separating the Z-yields by properly setting the total kinetic energy of the system, as is illustrated in fig. 49. In this figure, the maximum Q-values (called Q_{Max}) obtained for each mass ratio by selecting the best Z_L - Z_H combination is plotted as a function of the mass ratio. These Q_{Max} values exhibit the familiar odd-even effect but the general trend shows a rather flat and horizontal portion around A_H = 132 as a consequence of the extreme stability of the Z = 50 - N = 82 configuration. Also plotted on the same figure are the Q-values (called Q_0) closest to Q_{Max} but obtained with a different Z_L - Z_H combination. In the strip between the Q_{Max} and Q_0 lines lie the values of the maximum total kinetic energy detected in this experiment. For each mass ratio, fragments having a total kinetic energy between Q_{Max} and Q_0 have only one Z_L - Z_H combination, that of Q_{Max}. Therefore, by setting E_K^T in the experiment between Q_{Max} and Q_0, it is possible to separate cold fragments having well-defined Z and N numbers. Unfortunately, this method can apply only to a limited number of fragments because of the behaviour of Q with A. The yields for cold fragments selected in this manner are given in fig. 50 for several values of E_K^T.

This experiment though intrinsically limited to a narrow variety of fragments is very clean and can give the following information :

i) There is no observed odd-even Z effect in the kinetic energy of cold fragments in contrast to what is observed at lower kinetic energies (see fig. 45).

ii) There is no significant odd-even effect whether in Z- or N-yields. For example, the yield at Z_L = 41 is comparable if not superior to those at Z_L = 40 and Z_L = 42 for the same neutron numbers.

In conclusion, the results on cold fragmentations for both the ^{234}U and ^{236}U systems do not exhibit a strong enhancement of superfluidity as expected. The reason for this must be found in another mechanism such as the one which is suggested below.

III.D - Mechanism proposed for cold fragmentation.

The apparent paradox that superfluidity seems to be more preserved for fragments of low kinetic energy than for cold fragments having a high kinetic energy can be explained by a better knowledge of the statics of the phenomenon, i.e. by the potential energy surface of the fissioning system.

Recent microscopic calculations of this surface, using the Hartree- Fock - Bogolyubov method with the D1 effective nucleon-nucleon interaction [BGG 81] can indeed shed some light on this problem. The results obtained for ^{240}Pu with this method are displayed in fig. 51 where the surface is plotted as a function of the deformation constraints Q_{20} and Q_{30} imposed on the self-consistent field. The ground state and the isomeric states are easily recognised in P_1 and P_2 respectively. A very flat saddle point appears along the line M_2M_3 for mass-asymmetric deformations (as expected) and the "fission valley" starts to go down slowly beyond M_3 for increasing elongation (or Q_{20}) as can be seen in fig. 52. This valley (called V_1) is supplemented by another surface (called V_2) which is the very steep "fusion valley" corresponding to heavy-ion reactions. These two valleys are separated in the plot of fig. 51, but the introduction of another deformation parameter Q_{40}, accounting

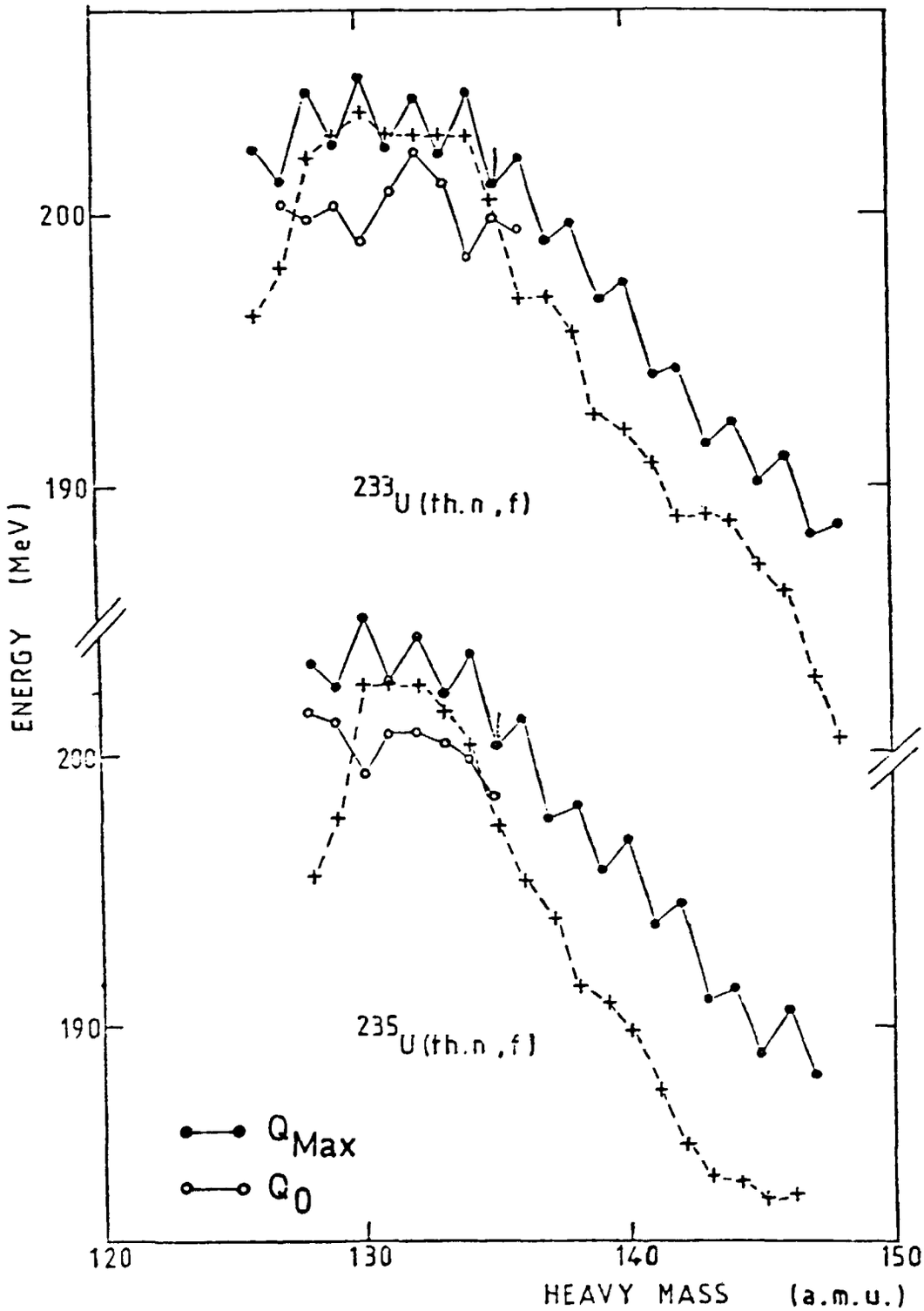

Figure 49 : Highest total kinetic energy (--+--) observed for fragments emitted in thermal-neutron induced fission in ^{233}U (top part) and ^{235}U (bottom part) as a function of the heavy fragment mass number A. For each mass number, the Q values for several Z - N combinations were calculated. The highest one (•) and the one immediately below (○) are indicated [Sig+ 81].

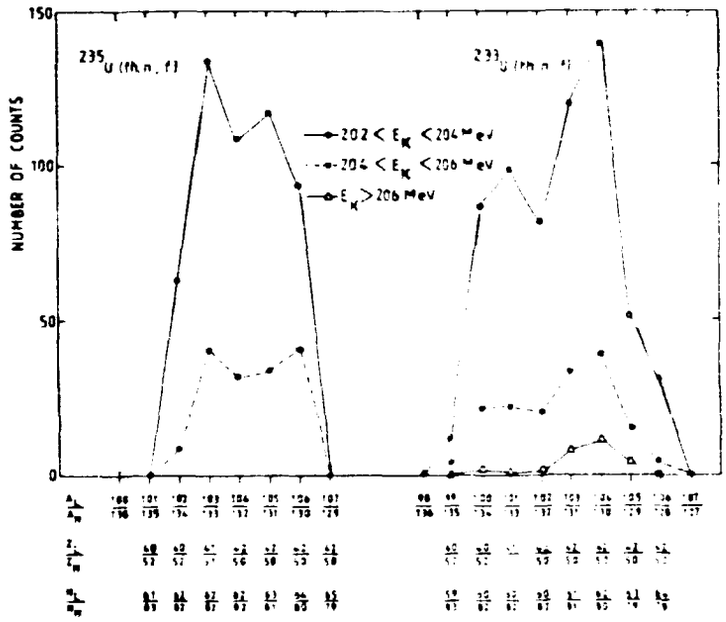

Figure 50

Yields (not normalized) of well-defined primary fragments emitted in the cold fragmentation of ^{234}U and ^{236}U systems, obtained by the absorption of thermal neutrons, for various values of the total kinetic energy [Sig+ 81].

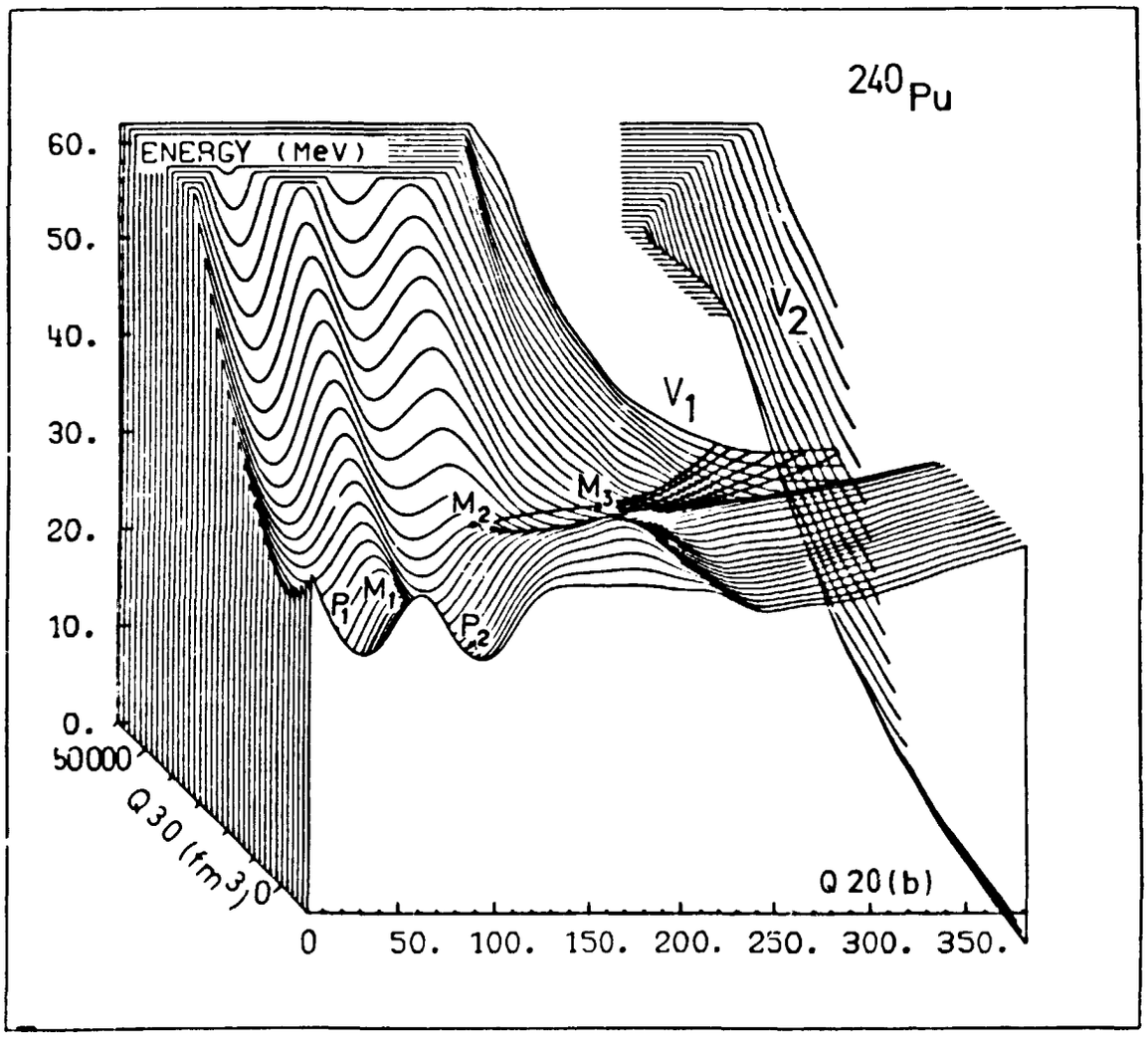

Figure 51

Three-dimensional plot of the ^{240}Pu potential energy as a function of Q_{20} and Q_{30} deformation constraints, as calculated with the Hartree - Fock - Bogolyubov method [BGG 81].

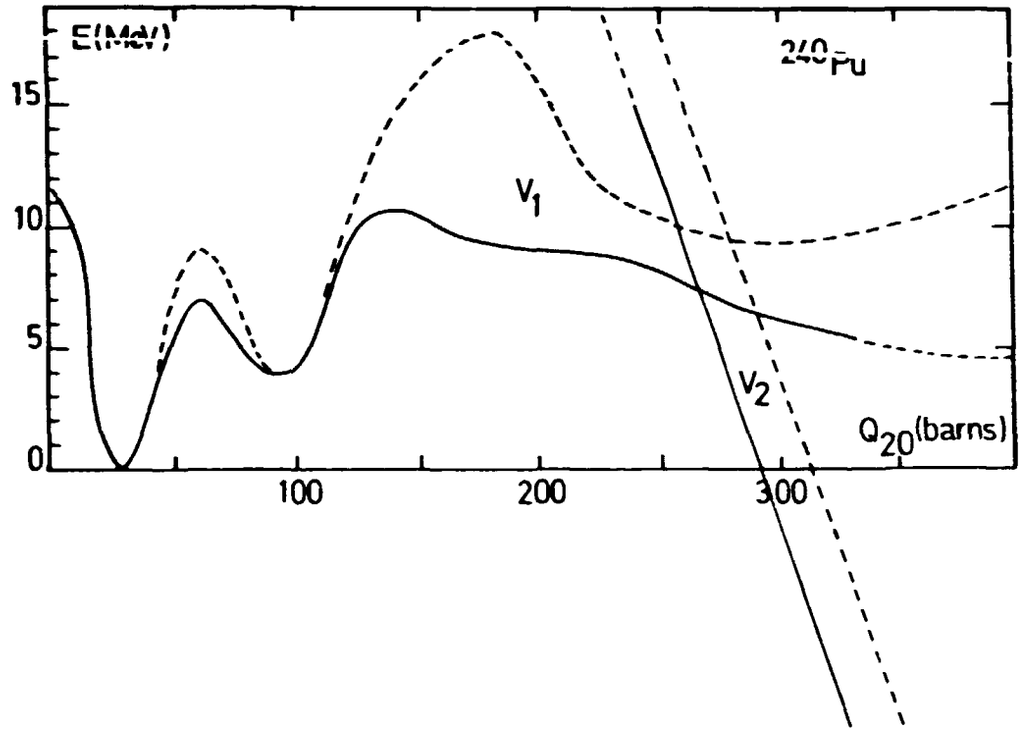

Figure 52

One-dimensional representation of the ^{240}Pu potential energy surface (as shown in fig. 51) as a function of the Q_{20} deformation constraint. V_1 and V_2 represent the fission and the fusion valleys respectively. The dashed line is obtained for a system having mass and axial symmetry whereas the solid line includes axial asymmetry (inner hump of the fission barrier) and mass asymmetry at larger deformations [BGG 81].

for necking-in (or buldging) of the nucleus, makes possible a connection between V_1 and V_2. The potential energy surface can now be represented as a function of Q_{20} and Q_{40}, for a given value of Q_{30}, as in fig. 53 where the Q_{30} value corresponds to the most probable mass division. The fission and fusion valleys appear clearly and are separated along the Q_{40} coordinate by a barrier (called the Q_4 barrier) having a decreasing height for increasing Q_{20}. This height goes to zero for $Q_{20} \simeq 370$ barns. The fusion valley is steeper than the fission one but both have the same potential energy value around $Q_{20} = 260$ barns (see fig. 52). This corresponds, in the fusion valley, to two separated fragments with deformations close to that of their ground state.

Interpretation of the fission results presented in Sections III.B and III.C can easily be explained with such a potential energy surface assuming that its shape is similar for ^{234}U and ^{236}U systems. During its descent in the fission valley, the nuclear system moves slowly as a consequence of the small decrease of potential energy with elongation. Therefore, viscosity should not play an important role and superfluidity should be preserved almost completely during this phase. At the end of the fission valley (around $Q_{20} \simeq 370$ barns), the nascent fragments start to appear and this is very important for the pairing correlations. If the nucleus were spheroidal, there would be only a weak spatial correlation between nucleon pairs. But with some necking-in, the nucleon orbits must be described with a double-centre shell model potential (with some overlap) with the consequence that some spatial correlation starts to appear, in the sense that nucleon pairs tend to be located either in one fragment or the other. If the system could continue to be slowly elongated (i.e. with increasing Q_{20}), then this spatial correlation of the nucleon pairs could become more pronounced. But, in the absence of Q_{40} barrier between the fission and fusion valleys, the system falls down in the fusion valley. This transition is difficult to describe for a rapid necking-in corresponding to a fall down to the bottom of the fusion valley is certainly limited by viscosity effects which are more important for high multipole orders (such as those necessary to account for sudden necking-in). But whatever the detailed nature of the transition is, it is reasonable to assume that it would lead to some pair breaking.

In addition to the conventional descent in the fission valley (described above), another fission mode is possible whereby the system undergoes a shape transition from the fission valley to the fusion valley (even for Q_{40} values smaller than 370 barns) by tunnelling through or passing over the Q_{40} barrier. Such a shape transition is illustrated in fig. 54 where the nuclear shapes are plotted for an intermediate Q_{20} value ($\simeq 300$ barns) when the system is in A (fission valley), in C (fusion valley) and in B (top of the Q_{40} barrier) (the locations of these points are indicated in fig. 53). These fission events coming from the higher portion of the fusion valley are mixed with those from the fission valley though with a much smaller probability because of the tunnelling of the Q_{40} barrier. These "fusion valley" events have a higher kinetic energy than those of the fission valley because they occur at a smaller elongation and, therefore, the fragments are formed in a more compact configuration, hence with a higher Coulomb energy. Setting a high bias for the kinetic energy enhances the proportion of these "fusion valley" events. If the kinetic energy is set high enough, for example near the Q-value, only "fusion valley" events can occur since no scission possibility exists in the fission valley at such an energy. Therefore, the bias on the kinetic energy is equivalent to a filter which favors the "fusion valley" events, the higher the bias, the greater the proportion of these events. Also the height of the Q_{40} barrier increases with kinetic energy ; this explains why the fission yields decrease so rapidly with increasing kinetic energy, as illustrated in fig. 46.

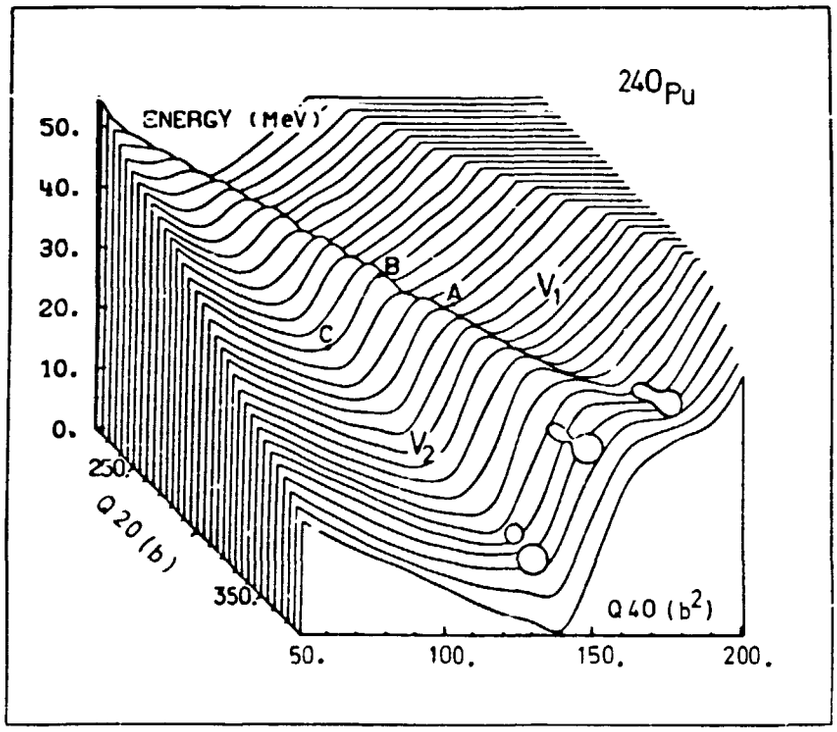

Figure 53

Three-dimensional representation of the ^{240}Pu potential energy as a function of Q_{20} and Q_{40} deformation constraints, as calculated with the Hartree - Fock - Bogolyubov method. The Q_{30} parameter is set to the most probable mass division [BGG 81].

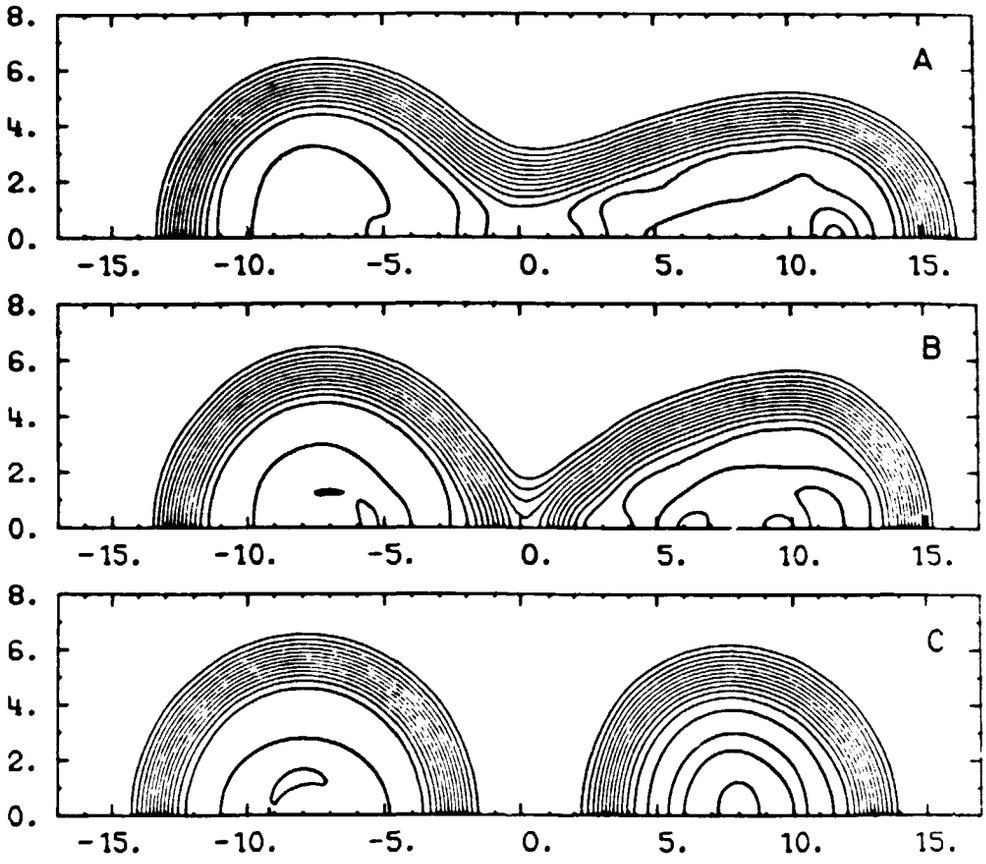

Figure 54

Isodensity contour plot of the deformed ^{240}Pu at the points A, B, C of the potential energy surface plotted in fig. 53 [BGG 81]. Distances are given in fermis.

Therefore, cold fragmentation can result from that particular fission mode whereby a shape transition occurs by penetrating the barrier between the fission and fusion valleys (see fig. 55) as already pointed out in [BGG 81]. The initial state (in the fission valley) has only a weak long-range spatial pair correlation because of the spheroidal deformation without necking-in. It is reasonable to assume that the fast shape transition mentioned above will not greatly modify this pair correlation with the consequence that no odd-even effects are expected in the final state (in the fusion valley) as observed in the experiments.

In conclusion, microscopic H.F.B. calculations of the potential energy surface for a largely deformed heavy nucleus seem to provide the basis for a coherent description of the low-energy fission of ^{234}U and ^{236}U, in agreement with the experiments.

According to this description, most fission events come from the slow and adiabatic motion of the nuclear system down the fission valley. This type of motion continues while preserving superfluidity until some slow necking-in starts to appear implying the appearance of fragment shells associated with pair spatial correlation within those shells. Near the end of this motion, the vanishing height of the barrier between the fission and fusion valleys causes the motion to change character. Instead of pursuing its slow descent in the fission valley, no barrier then prevents the system from falling down into the fusion valley, with a fast neck snapping controlled by viscosity but in an unknown manner. Whatever the detailed rupture of the neck is, some pair breaking is anticipated at that stage but also, some of the pair correlation in the nascent fragments (present at the end of the fission valley) should be preserved. This explains the presence of odd-even effects in the yields of most common fission events.

The rare cold fragmentation events recently studied originate from a different mechanism. The high kinetic energy associated with this fragmentation prevents the system from gently descending the fission valley along the elongation degree of freedom. Rather, the system is forced to find a more compact scission configuration by crossing the barrier between the fission and fusion valleys. In the fusion valley the system consists in two separated and cold fragments having a deformation close to that of their ground state. The Coulomb energy of such a scission configuration is close to the total fission energy release (the Q-value), as observed. The difficulty in crossing the barrier explains the very low yields for such a fragmentation. Also, the shape transition between the two valleys occurs at an early stage where the pair spatial correlation is still very weak, in agreement with the absence of odd-even effects in the observed yields. It is interesting to note that in contrast to conventional fission, cold fragmentation is very close to the inverse process for heavy-ion fusion. It would be exactly the inverse process if scission configuration consisted in two fragments in their ground state. Though this completely-cold fragmentation is not excluded, its yield is far too small to be detected experimentally.

Lastly, one may notice that viscosity seems to play only a minor role in both types of fission, with the possible exception of the fast neck rupture in conventional fission.

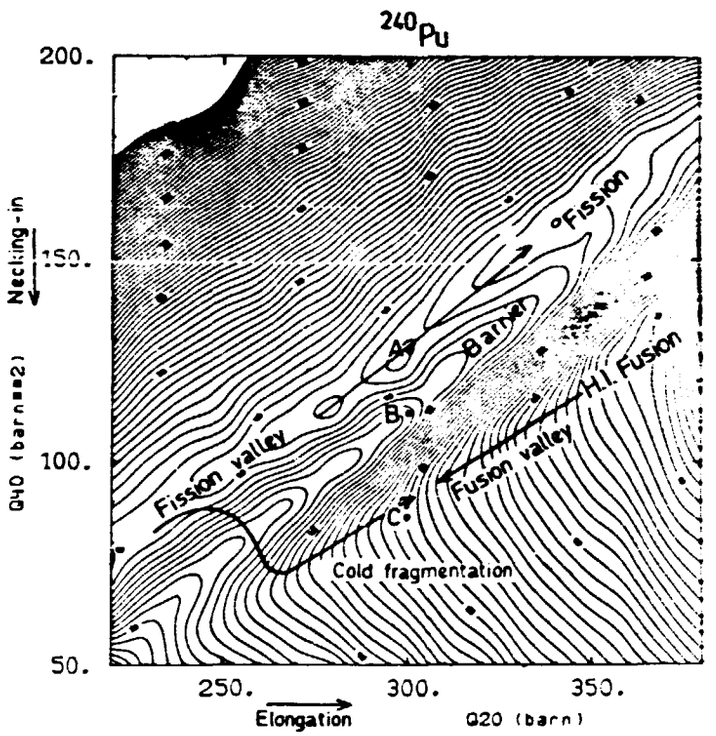

Figure 55

Contour plot of the ^{240}Pu potential energy surface (as displayed in fig. 53) where the paths for fission, cold fragmentation and heavy-ion fusion are indicated.

IV - CONCLUSION

The few selected topics discussed in this talk illustrate the progress accomplished recently in the understanding of some aspects of the fission process.

The fission barrier calculated with the macroscopic-microscopic method gives two humps with heights in good agreement with the data, except for light actinides. For these nuclei (Th and Pa isotopes) a third hump, already predicted by some calculations, is necessary to explain the results. A great effort has been made to find indisputable proof of the existence of such a barrier shape for light actinides. This evidence seems to be provided by the excellent ^{230}Th fission data in the 715 keV vibrational resonance region. The analysis of ^{231}Pa and ^{232}Th data, also of very high quality, is consistent with a triple-humped fission barrier but does not provide evidence for its existence. Progress in this direction now needs more intense neutron sources and more sophisticated detection techniques.

The understanding of fission dynamics from the saddle point to scission is still very poor. Microscopic calculation of the evolution of the system is possible using the time-dependent Hartree-Fock method, but the computer time is very long, even with simplifying assumptions. Also the information contained in TDHF calculations is too rich for the sole purpose of understanding dissipation in fission. Different macroscopic approaches have been studied such as one-body and two-body dissipation but they apply only to hot fissioning systems almost impossible to study experimentally. Comparison of the theory can be made only with scarce and ambiguous experimental data and, when possible, this comparison cannot decide which type of dissipation actually occurs in fission. Fission data of a better quality are available at low energy but then, the dynamics are controlled by a combination of bulk matter properties and shell effects, the latter being predominant. Unraveling these effects in order to have access to viscosity is very difficult at present. Therefore, understanding dissipation in fission still remains a challenge for the future. In this talk, results about low-energy fission of ^{234}U and ^{236}U systems are reported with special emphasis on cold fragmentation. Interpretation of the results is possible qualitatively in terms of static microscopic calculations using the H.F.B. method. A coherent description of the results can be made for conventional fission as well as for cold fragmentation. This description is dominated by shell effects, as expected, and viscosity seems to play but a minor role. Cold fragmentation appears to be not a simple extrapolation of conventional fission towards higher kinetic energy but rather the result of a new mechanism close to the inverse heavy-ion fusion. Further progress towards a more quantitative understanding of these aspects of fission require more specific calculations for the systems being studied together with some test of the accuracy of the H.F.B. method at large deformations ; also, more extensive experimental studies are necessary, if possibly over a wider range of fission fragments.

[illegible]

[illegible]

TABLE I

VALUE OF THE INERTIA PARAMETERS FOR FISSION ISOMERS

Fission isomer	$\hbar^2/2\mathcal{J}$ (keV)	Ref.
^{236}U	3.36 ± 0.01	[Bor+ 77]
^{238}U	3.27 ± 0.03	[Met 79]
^{239}Pu	3.36 ± 0.01	[Bac+ 79]
^{240}Pu	3.343 ± 0.003	[Spe+ 72]

TABLE II

SUMMARY OF ^{230}Th DATA DISCUSSED IN THE TEXT

($E_n \simeq 715$ keV)

Neutron Source	Type of measurement	Resolution (FWHM in keV)	Ref.
VdG Monoenergetic neutrons	σ_{nf} $W(\theta)$	10 to 20	[JLE 72]
Nuclear Detonation + Time of flight	σ_{nf} (100°) σ_{nf} (125°)	a few keV	[MV 71] [VM 81]
Linac + Time of flight	σ_{nf}	1.7	[Blo+ 78a]
VdG Monoenergetic neutrons	σ_{nf} $W(\theta)$	2.5 "	[Bru 80] "
VdG Monoenergetic neutrons	$W(\theta)$	10	[Yue+ 71]
VdG Monoenergetic neutrons	$W(\theta)$	8	[CBW 77]

TABLE III

^{230}Th VIBRATIONAL RESONANCE AROUND 715 keV

Parameters used in the calculation of fission cross-section and fragment anisotropy data with one single-parity band of rotational levels.

K^{π}	$\hbar^2/2J$ (keV)	a	Ref.
$1/2^+$	2.0	- 1.76	[Bru 80]
$1/2^-$	2.628	2.4	[Bru 80]
$1/2^+$	2.4	0.4	[Blo+ 80]
$1/2^-$	2.5	2.4	[Blo+ 80]
$1/2^+$	1.8	0	[Bol+ 81]
$1/2^-$	1.8 to 2.7	- 2 to - 2.4	[JLE 72]

TABLE IV

^{230}Th VIBRATIONAL RESONANCE AROUND E_n = 715 keV

Parameters used to fit simultaneously fission cross-section and fission fragment anisotropy data with two rotational bands of opposite parities

K^{π}	$\hbar^2/2\mathcal{J}$ (keV)	$a_{1/2} = -a_{-1/2}$	$(E_0^- - E_0^+)$ (keV)	Ref.
$\frac{1}{2}^{+,-}$	1.9	- 1.1	3	[Bru 80]
$\frac{1}{2}^{+,-}$	1.85 ± 0.1	- 1.1 ± 0.2	3	[Blo+ 80] (version B)
$\frac{1}{2}^{+,-}$	1.85	- 1	3	[Bol+ 81]
$\frac{1}{2}^{+,-}$	2.0 ± 0.1	0.2 ± 0.2	- 10	[Blo 81] (version C)

TABLE V

SUMMARY OF ^{231}Pa FISSION DATA DISCUSSED IN THE TEXT

Neutron Source	Type of measurement	Resolution at 150 keV (FWHM in keV)	Ref.
VdG Monoenergetic neutrons	σ_{nf}	40	[DS 64]
Nuclear Detonation + Time of flight	σ_{nf}	4	[MV 71]
VdG Monoenergetic neutrons	σ_{nf}	2	[Sic+ 79]
Synchrocyclotron + Time of flight	σ_{nf}	2	[Sym 79]
Linac + Time of flight	σ_{nf}	0.4	[Pla+ 81]
VdG Monoenergetic neutrons	$W(\theta)$	5	[Sic+ 79]

TABLE VI

Energies of the sharp peaks observed below E_n = 450 keV in the ^{231}Pa fission cross-section and indicated by arrows in fig. 32. The peak energies are grouped according to the gross structure in the fission cross-section [Pla+ 81].

E_n (keV)	E_n (keV)
156.7	-
-	312.1
173.3	319.3
182.3	324.2
185.2	328.6
187.4	-
190.2	336.7
193.8	343.3
200.0	350.3
-	358.2
281.9	-
-	371.1
300.6	375.7
304.5	

TABLE VII

A - PROPERTIES OF SOME SHARP PEAKS IN THE ^{231}Pa FISSION CROSS-SECTION [Pla+ 81]

Energy (keV)	Resolution width (FWHM in keV)	Natural width (keV)	Observed peak cross-section (mb)	(K,J^{π})	T_f
156.7	0.4	2.9	83	$(3,3^+)$	≈ 0.2
173.3	0.47		6	$(3,3^-)$	≈ 1
371.1	1.2	6.4	26	$(3,4^-)$	≈ 1

B - SUGGESTED POSSIBILITY OF TWO ROTATIONAL BANDS OF OPPOSITE PARITIES AROUND E_n = 160 - 180 eV

$K^{\pi} = 3^-$				$K^{\pi} = 3^+$			
Energy (keV)	J^{π}	$\sigma_{CN}^{J^{\pi}}$ (mb)	Remarks	Energy (keV)	J^{π}	$\sigma_{CN}^{J^{\pi}}$ (mb)	Remarks
156.7	3^-	20	Observed	173.3	3^+	210	Observed
172.7	4^-	8	Postulated	189.3	4^+	2	Postulated

TABLE VIII

SUMMARY OF ^{232}Th FISSION DATA DISCUSSED IN THE TEXT

Neutron Source	Type of measurement	Resolution (FWHM in keV at E_n = 1.6 MeV)	Ref.
Linac Time of flight	σ_{nf}	7	[BMP 75]
VdG Monoenergetic neutrons	σ_{nf}	3	[Bar 77]
Linac Time of flight	σ_{nf}	2.3	[Blo+ 80]
VdG Monoenergetic neutrons	W(θ)	30 - 50	[ES 70] [And+ 69]
VdG Monoenergetic neutrons	W(θ)	100 - 200	[LM 68]
VdG Monoenergetic neutrons	W(θ)	100	[CBW 77]
Linac Time of flight	W(θ) (θ < 30°) W(θ) (θ < 45°)	16 7	[BMP 75] [Blo+ 80]
Linac Time of flight	W(θ) (θ < 23.4°, θ < 33.7°, θ < 51.7°)	8.4	[Auc+ 81]
VdG Monoenergetic neutrons	W(θ)	5	[Bar 77]
VdG Monoenergetic neutrons	W(θ)	8	[Hol 81]

TABLE IX

Fission-barrier parameters used to
fit ^{232}Th fission cross-section and angular distribution data
(BRC fit shown on fig. 37 and 38) [Abo+ 79]

(All energies in MeV)

(K,π)	E_B	E_{III}	E_C	$\hbar\omega_B$	$\hbar\omega_{III}$	$\hbar\omega_C$
1/2 +	5.49	5.47	6.86	1.30	0.60	1.30
7/2 -	5.70	5.46	6.875	0.74	0.60	1.05
1/2 +	6.27	5.72	6.86	1.20	1.0	1.23
3/2 +	6.29	5.723	6.77	1.40	1.0	1.40
1/2 +	6.22	5.86	7.24	1.40	1.0	1.40
3/2 +	6.35	5.81	6.92	1.40	1.0	1.40
[3/2 +	6.62	5.90	7.01	1.40	1.0	1.40
3/2 -	6.61	5.89	7.00	1.40	1.0	1.40
[5/2 +	6.45	5.90	6.96	1.40	1.0	1.40
5/2 -	6.46	5.91	6.97	1.40	1.0	1.40
[1/2 +	6.73	6.026	7.62	1.40	1.0	1.40
1/2 -	6.74	6.036	7.63	1.40	1.0	1.40
[3/2 +	6.78	6.016	7.29	1.40	1.0	1.40
3/2 -	6.79	6.026	7.30	1.40	1.0	1.40
[1/2 +	6.76	6.19	7.43	1.40	1.0	1.40
1/2 -	6.77	6.20	7.44	1.40	1.0	1.40
[5/2 +	6.85	6.175	7.23	1.40	1.0	1.40
5/2 -	6.86	6.185	7.24	1.40	1.0	1.40
[1/2 +	7.01	6.305	7.54	1.40	1.0	1.40
1/2 -	7.02	6.315	7.55	1.40	1.0	1.40
[1/2 +	7.20	6.38	7.70	1.40	1.0	1.40
1/2 -	7.21	6.39	7.71	1.40	1.0	1.40
[1/2 +	7.20	6.48	7.54	1.40	1.0	1.40
1/2 -	7.21	6.49	7.55	1.40	1.0	1.40
[1/2 +	7.22	6.55	7.57	1.40	1.0	1.40
1/2 -	7.23	6.56	7.58	1.40	1.0	1.40
[1/2 +	7.24	6.625	7.52	1.40	1.0	1.40
1/2 -	7.25	6.735	7.55	1.40	1.0	1.40

[means band heads for rotational levels used in the calculations but not indicated in this table.

REFERENCES

Abo+ 79 H. ABOU YEHIA, J. JARY, J. TROCHON, J.W. BOLDEMAN and A.R. de L. MUSGROVE, Proc. Conf. Nuclear Cross-Sections and Technology, Knoxville (1979) 469.

AJT 79 H. ABOU-YEHIA, J. JARY and J. TROCHON, Report INDC(FR) 34/L - NEANDC(E) 204 "L" (1979).

And+ 69 C.C. ANDROSHENKO, S.B. ERMAGAMBETOV, A.V. IGNATJUK, N.S. RABOTINOV, G.M. SMIRENKIN, A.S. SOLDATOV, L.N. USACHEV, D.L. SPAK, S.P. KAPITZA, J.M. TSIPENJUK and L. KOVAKS, Physics and Chemistry of Fission, IAEA Vienna (1969) 419.

Arm 81 P. ARMBRUSTER, Invited talk given at the Workshop on "Semi-classical Methods in Nuclear Physics", Grenoble (March 18-20, 1981).

Arm+ 81 P. ARMBRUSTER, U. QUADE, K. RUDOLPH, H.G. CLERC, M. MUTTERER, J. PANNICKE, C. SCHMITT, J.P. THEOBALD, W. ENGELHARDT, F. GÖNNENWEIN and H. SCHRADER, to be published.

Auc+ 81 G.F. AUCHAMPAUGH, S. PLATTARD, N.W. HILL, G. de SAUSSURE, R.B. PEREZ and J.A. HARVEY (1981), to be published.

Bac+ 79 H. BACKE, L. RICHTER, D. HABS, V. METAG, J. PEDERSEN, P. SINGER and H.J. SPECHT, Phys. Rev. Lett. 42 (1979) 490.

Bar 77 G. BARREAU, D. Sc. Thesis, Bordeaux (1977).

BGG 81 J.F. BERGER, M. GIROD and D. GOGNY, C.R.A.S., to be published.

Bjö 74 S. BJÖRNHOLM, Physica Scripta 10A (1974) 110

BL 80 S. BJÖRNHOLM and J.E. LYNN, Rev. Mod. Phys. 52, Nb 4 (1980) 725

Blo+ 78a J. BLONS, C. MAZUR, D. PAYA, M. RIBRAG and H. WEIGMANN, Phys. Rev. Let. 41 (1978) 1282.

Blo+ 78b J. BLOCKI, Y. BONEH, J.R. NIX, J. RANDRUP, M. ROBEL, A.J. SIERK and J.W. SWIATECKI, Ann. Phys. 113 (1978) 330

Blo+ 80 J. BLONS, C. MAZUR, D. PAYA, M. RIBRAG and H. WEIGMANN, International Winter Meeting on Nuclear Physics, Bormio (1980), and Journées d'études sur la fission, Alpe d'Huez (1980), unpublished.

Blo 81 J. BLONS, International Winter Meeting on Nuclear Physics, Hirschegg (Jan. 19-23, 1981) and private communication (1981).

BMP 75 J. BLONS, C. MAZUR and D. PAYA, Phys. Rev. Lett. 35 (1975) 1749.

Bol+ 81 J.W. BOLDEMAN, D. GOGNY, A.R. de L. MUSGROVE and R.L. WALSH, Phys. Rev. C 22, Nb 2 (1980) 627

Bor+ 77 J. BORGGREEN, J. PEDERSEN, G. SLETTEN, R. HEFFNER and E. SWANSON, Nucl. Phys. A279 (1977) 189

BPM 77 J. BLONS, D. PAYA and C. MAZUR, Note CEA-N-1959 (1977) 90.

Bra+ 72 M. BRACK, Jens DAMGAARD, A.S. JENSEN, H.C. PAULI, V.M. STRUTINSKY and C.Y. WONG, Rev. Mod. Phys. 44 (1972) 320

Bru 80 B. BRUNEAU, D. Sc. Thesis, Bordeaux (1980).

BWM 80 J.W. BOLDEMAN, R.L. WALSH and A.R. de L. MUSGROVE, Physics and Chemistry of Fission, IAEA Vienna (1980), Paper B13.

CBW 77 J. CARUANA, J.W. BOLDEMAN and R.L. WALSH, Nucl. Phys. A285 (1977) 205

Cle+ 75 H.G. CLERC, W. LANG, H. WOHLFARTH, K.H. SCHMIDT, H. SCHRADER, K.E. PFERDEKÄMPER and R. JUNGMANN, Z. Phys. A274 (1975) 203.

DS 64 S.M. DUBROVINA and V.A. SHIGIN, Dok. Akad Nauk SSSR 157, Nb 3 (1964) 561 (Translation in Sov. Phys. Dokl. 9, Nb 7 (1965) 579.

DSN 76 K.T.R. DAVIES, A.J. SIERK and J.R. NIX, Phys. Rev. C 13, Nb 6 (1976) 2385.

EJ 65 J.E. EVANS and G.A. JONES, Private communication to J.E. LYNN (1965).

ES 70 S.B. ERMAGAMBETOV and G.N. SMIRENKIN, Sov. J. Nucl. Phys. 11 (1970) 646.

Gue+ 78 C. GUET, M. ASGHAR, P. PERRIN and C. SIGNARBIEUX, Nucl Inst. Meth. 150 (1978) 189.

Hol 81 M. HOLMBERG, Internal Report (Research Institute of National Defence, Stockholm), unpublished (1981).

HS 55 R.L. HENKEL and R.K. SMITH, Report BNL 325 edited by D.J. HUGHES and J.A. HARVEY (1955).

JLE 72 G.D. JAMES, J.E. LYNN and L.G. EARWAKER, Nucl. Phys. A189 (1972) 225

Lan+ 80 W. LANG, H.G. CLERC, H. WOHLFARTH, H. SCHRADER and K.H. SCHMIDT, Nucl. Phys. A345 (1980) 34.

LM 68 S. LO NIGRO and C. MILONE, Nucl. Phys. A118 (1968) 461.

Met 79 V. METAG, Physics and Chemistry of Fission, IAEA Vienna (1979), Paper SM-241/B3.

Mic 73 A. MICHAUDON, Advances in Nuclear Physics, Plenum Press, 6 (1973) 1.

Mic 78 A. MICHAUDON, Physics Today (Jan. 1978) 23.

MN 74 P. MÖLLER and J.R. NIX, Physics and Chemistry of Fission, IAEA Vienna (1974), vol. I, 103.

MN 76 P. MÖLLER and J.R. NIX, Private communication (1976)

MN 80 P. MÖLLER and J.R. NIX, Report LA-UR-80-1966, Los Alamos Scientific Laboratory (1980)

Mol+ 75 E. MOLL, H. SCHRADER, G. SIEGERT, M. ASHGAR, J.P. BOCQUET, G. BAILLEUL, J.P. GAUTHERON, J. GREIF, G.I. CRAWFORD, C. CHAUVIN, H. EWALD, H. WOLLNIK, P. ARMBRUSTER, G. FIEBIG, H. LAWIN and K. SISTEMICH, Nucl. Instr. 123 (1975) 615.

Mol+ 77 E. MOLL, H. SCHRADER, G. SIEGERT, M. HAMMERS, M. ASGHAR, J.P. BOCQUET, P. ARMBRUSTER, H. EWALD and H. WOLLNIK, Kerntechnik 19 (1977) 374.

MR 78 M.E. MEEK and B.F. RIDER, Compilation of fission product yields, Vallecitos Nuclear Center, NEDO-12154-2(E) class-1 (1978).

MV 71 D.W. MUIR and L.R. VEESER, Proceedings of the third Conference on Nuclear Cross-Sections and Technology, Knoxville, Conf. 710301, vol. 1 (1971) 292.

Neg+ 78 J.W. NEGELE, S.E. KOONIN, P. MÖLLER, J.R. NIX and A.J. SIERK, Phys. Rev. C 17, Nb 3 (1978) 1098.

Nix 72 J.R. NIX, Annu. Rev. Nucl. Sci. 22 (1972) 65.

Nör 69 W. NÖREMBERG, Physics and Chemistry of Fission, IAEA Vienna (1969) 51.

Pay 80 D. PAYA, Physics and Chemistry of Fission, IAEA Vienna (1980), vol. 1, 207.

Pla+ 81 S. PLATTARD, G.F. AUCHAMPAUGH, N.W. HILL, G. de SAUSSURE, J.A. HARVEY and R.B. PEREZ, Phys. Rev. Let. 46, Nb 10 (1981) 6[illegible].

SBP 73 A. SOBICZEWSKI, S. BJÖRNHOLM and K. POMORSKI, Nucl. Phys. A202 (1973) 274

Sic+ 79 A. SICRE, F. CAÏTUCOLI, G. BARREAU, T.P. DOAN, T. BENFOUGHAL and B. LEROUX, Physics and Chemistry of Fission, Jülich 14-18 May 1979, IAEA Vienna (1980), vol. 1, 187

Sig+ 81 C. SIGNARBIEUX, M. MONTOYA, M. RIBRAG, C. MAZUR, C. GUET, P. PERRIN and M. MAUREL, Journal de Physique 42 (1981) L-437

Spe+ 72 H.J. SPECHT, J. WEBER, E. KONECNY and D. HEUNEMANN, Phys. Lett. 41B (1972) 43

Str 67 V.M. STRUTINSKY, Nucl. Phys. A95 (1967) 420.

Sym 79 D.B. SYME, Neutron Interlab Seminar, Paris (June 1979), unpublished.

VH 73 R. BANDENBOSCH and J.R. HUIZENGA, Nuclear Fission (Academic Press 1973).

VM 81 L.R. VEESER and D.W. MUIR, Report LA-UR-81-1589 (1981), to be published in Phys. Rev. C.

Yue+ 71 G. YUEN, G.T. RIZZO, A.N. BEHKAMI and J.R. HUIZENGA, Nucl. Phys. A171 (1971) 614.

Manuscrit reçu le 19 novembre 1981

Edité par
le Service de Documentation
Centre d'Etudes Nucléaires de Saclay
91191 GIF-sur-YVETTE Cédex (France)